TU WIEN TECHNISCHE UNIVERSITÄT WIEN

Development and Evaluation of an Arterial Pulse Wave Form Analysis Algorithm

carried out for the purpose of obtaining the degree of

Dipl.-Ing.

in

Biomedical Engineering

by

Philipp Chorherr, BSc
Registration number: 1026166
Paulinengasse 4/12-15
A-1180 Vienna

submitted to

Vienna University of Technology

Institute of Electrodynamics, Microwave and Circuit Engineering

under the supervison of

Univ.Lektor Dipl.Ing. Dr.techn. Bernhard Hametner
Univ.Lektor Dipl.Ing. Dr.techn. Christopher Mayer
Ao.Univ.Prof. Dipl.Ing. Dr.techn. Eugenijus Kaniusas

Vienna, April 2019

Statutory Declaration

I hereby declare that I have written this Master Thesis independently, that I have completely specified the utilized sources and resources and that I have definitely marked all parts of the work - including tables and figures - which belong to other works or to the internet, literally or extracted, by referencing the source as borrowed.

_____   _____
Date   Philipp Chorherr

Eidesstattliche Erklärung

Hiermit erkläre ich, dass die vorliegende Arbeit gemäß dem Code of Conduct, insbesondere ohne unzulässige Hilfe Dritter und ohne Benutzung anderer als der angegebenen Hilfsmittel, angefertigt wurde. Die aus anderen Quellen direkt oder indirekt übernommenen Daten und Konzepte sind unter Angabe der Quelle gekennzeichnet. Die Arbeit wurde bisher weder im In– noch im Ausland in gleicher oder in ähnlicher Form in anderen Prüfungsverfahren vorgelegt.

_____   _____
Datum   Philipp Chorherr

Abstract

Relaxation techniques such as yoga or mantra breathing are known to decrease blood pressure. This particularly applies to guided slow breathing which improves the arterial baroflex sensitivity and thus employs a blood pressure lowering effect. Novel wearable sensor technology enables ubiquitous, continuous and non-invasive measurement of the blood pressure's evolution over time by using the pulse transit time as surrogate. To further investigate the potential of pulse waves as indicator for alteration of blood pressure, this thesis deploys a newly devised algorithm using MATLAB$^{©}$ to quantify and evaluate pulse waves.

In an exhaustive literature research, the state of the art quantification methods were collected and described. From this compilation, several methods were selected for implementation. The employed algorithm can be divided into three major parts. In the first part, the data is preprocessed. A central moving average filter is applied to the signals and the pulse waves are separated. Subsequently, a strict artefact annotation filter rejects non-physiological waves. In part two, the Systolic Pressure, the Dicrotic Notch Pressure and the Dicrotic Wave Pressure of all physiological waves are automatically annotated. Initially, existing algorithms were used and the annotated points were visually examined. The examination of the annotated Dicrotic Notch Pressure yielded an unsatisfactory accuracy for the data sets analysed. Thus, a novel algorithm was designed to find the Dicrotic Notch Pressure. Besides the pressure values, their timings were extracted and analysed. Moreover, derived parameters such as amplitude ratios were calculated to further describe the waves.

In the last step, the annotated and derived features were statistically

assessed and their timely evolution were depicted. The algorithm was applied to biosignal recordings of 30 subjects with essential hypertension, each lasting for approximately 15 minutes. During the initial ten minutes, the subjects exercised guided breathing followed by five minutes of unguided breathing.

Exemplarily, the 3-min averaged duration between the wave's onset and the Dicrotic Notch significantly decreased by $5.57\ ms\ (p < 0.01)$ during the entire recording and with respect to the baseline, implying a leftward shift of the Dicrotic Notch. The Total Pulse Duration significantly decreased by $18\ ms\ (p < 0.05)$ during the course of the recording, implying a decline in width.

This thesis presents an algorithm to automatically separate, filter and annotate pulse waves. The obtained results are promising and encourage further investigation.

Kurzfassung

Entspannungstechniken, wie Yoga oder die Mantra-Meditation, sind als blutdrucksenkend anerkannt. Dies trifft besonders auf langsames und tiefes Atmen mit Hilfe einer maschinellen (apparativen) Anleitung zu, welches die Baro-Reflex-Sensitivität verbessert und demnach einen blutdrucksenkenden Effekt hat. Neue, tragbare Sensortechnologie ermöglicht die portable, kontinuierliche und nichtinvasive Messung des Zeitverlaufs des Blutdrucks durch die Verwendung der Pulstransitzeit als Surrogat. Um das Potential der Pulswellen als Indikator für Änderungen des Blutdrucks zu untersuchen, wurde ein neuer Algorithmus, der Pulswellen quantifiziert und evaluiert, in MATLAB$^{©}$ implementiert.

In einer umfassenden Literaturrecherche wurden die State-Of-The-Art-Methoden zur Quantifizierung von Pulsewellen gesammelt und erläutert. Aus dieser Kollektion wurden einige ausgewählt und implementiert. Der benutzte Algorithmus kann in drei Hauptteile gegliedert werden. Im ersten Teil werden die Daten vorverarbeitet. Ein gleitender Mittelwert-Filter wird auf das Signal angewandt und die Pulswellen werden separiert. Anschließend werden durch eine strenge Annotation von Artefakten alle nicht-physiologischen Pulswellen aussortiert. Im zweiten Teil wird der Punkt des systolischen Drucks, der Dicrotic Notch und der Punkt des Dicrotic-Wave-Drucks aller physiologischer Wellen automatisiert annotiert. In einem ersten Schritt wurden hierfür bereits existierende Algorithmen verwendet und die annotierten Punkte wurden anschließened visuell kontrolliert. Die Kontrolle der analysierten Datensätze ergab eine unbefriedigende Genauigkeit der annotierten Dicrotic-Notch-Punkte. Deshalb wurde ein neuer Algorithmus zur Findung des Dicrotic Notches entwickelt. Nebst den Druckwerten wurde auch

das zeitliche Auftreten der Punkte extrahiert und analysiert. Weiters wurden abgeleitete Parameter wie die Amplitudenverhältnisse berechnet, um die Wellen genauer beschreiben zu können. Im letzten Schritt wurden alle annotierten und abgeleiteten Parameter statistisch evaluiert und deren Zeitverläufe dargestellt.

Der Algorithmus wurde auf 15-minütige Biosignalaufnahmen von 30 Patienten mit essentieller Hypertonie angewandt. Während der ersten zehn Minuten wurde die Atemfrequenz vorgegeben, die anschließenden fünf Minuten wurde frei geatmet.

Beispielsweise sinkt die über drei Minuten gemittelte Zeitdauer zwischen Wellenbeginn und Dicrotic Notch signifikant um insgesamt $5.57\ ms$ ($p < 0.01$), während der gesamten Aufzeichnung und relativ zur Basislinie, was eine Linksverschiebung des Dicrotic Notch bedeutet. Des Weiteren sinkt die totale Pulsdauer während der gesamten Aufnahmezeit signifikant um $18\ ms$ ($p < 0.05$), was eine Verringerung der Breite der Pulswelle impliziert.

Diese Diplomarbeit präsentiert einen Algorithmus, der Pulswellen automatisch separiert, filtert und annotiert. Die erhaltenen Resultate sind vielversprechend und rechtfertigen weitere Studien.

Contents

Contents

Contents

1. Introduction

1.1. Motivation

It is widely recognised that blood pressure is a valid indicator for cardiovascular diseases, the worldwide leading cause of death [1, 2]. Until recently, non-invasive, continuous monitoring of blood pressure was not feasible due to the manner of the methods. Monitoring via catheterization is known as the gold standard amongst blood pressure measuring methods, providing data instantaneously by placing a strain gauge in direct blood contact. Inherently, the downside to catheterization is its invasive character. Non-invasive approaches like auscultation, oscillometry and volume clamping on the other hand require either an inflatable cuff which is uncomfortable to wear or specialised staff to execute the measurement [3]. Introducing novel sensor designs as wearable devices using pulse oximetry enables continuous and ubiquitous blood pressure monitoring by analysing the pulse transit time [4]. For hypertension treatment, it was shown that relaxation techniques like mantra breathing can lower blood pressure during application [5]. A topic of interest not yet addressed is the possible alteration of the pulse wave form during aforementioned breathing techniques. Possible changes could provide ground for further investigation regarding the connection of blood pressure and the contour form of pulse waves.

1.2. Objective

Thus, the aim of the thesis was the development of an algorithm for automatic analysis and assessment of the pulse wave form, derived from a photoplethysmographic signal. Existing methods for quantifying pulse waves were collected and described in an exhaustive literature research. Based thereupon, several methods were selected for implementation. The subsequent designed algorithm, using the numerical computing environment MATLAB$^{©}$ 2018b, provides means for the automatic fragmentation of pulse waves and the annotation of selected features. Afterwards, the algorithm is applied to pre-processed pulse wave signals, provided by test subjects undergoing breathing relaxation techniques (i.e. a pre-specified and guided breathing exercise). The extracted features are then evaluated concerning their timely evolution and potential alteration, based upon the averages across subject.

1.3. Structure

The thesis is subdivided in four major parts. In the first part, a comprehensive summary of physiological and technical fundamentals are elaborated. Starting with the cardiovascular system, the function of the human heart, the pathophysiology of blood pressure and methods for measurement are provided in chapter 2.

The foundation of the devised algorithm is presented in chapter 3, displaying the results of an extensive literature research and comprising methods of quantification of pulse waves.

Chapter 4 describes the methodology. Starting with the origin of the evaluated data, the algorithm is thoroughly described and the statistical means are discussed. Lastly, in the final section, the results are displayed and discussed in chapters 5 and 6, concluding the thesis with future prospects.

2. Fundamentals

To correctly analyse pulse waves, a profound understanding of their nature is paramount. Thus, this chapter will provide insight on the physiology of the heart as a pump and its impact on the body. Closely entwined and of likewise importance is the blood pressure. Origin, dynamics and its implication for the human body will be discussed. In the last introductory step the idea behind **Photoplethysmography** as recording tool will be explained.

2.1. Physiology of the Heart

The heart can be described as a displacement pump, using its chambers and valves to suck and eject blood through the contraction of specialized muscle cells. The rhythmic beat guarantees blood flow throughout the vascular system, providing tissue and organs with oxygen and nutrients.

A more detailed description of the electrical activity of the heart as well as the human circulatory system is given below, following the textbooks of Klinke and Silbernagl [6] and Lippert [7].

2.1.1. Electrical Activity of the Heart

Muscular contractions throughout the body are caused by electric impulses. While the muscle cells of the heart are special, the principle of electricity is the same and will be discussed in the following section.

To maintain the heart's steady pumping rhythm a pacemaker is required. This role is fulfilled by the sinus node located in the upper right ventricle, thus making the heart independent of excitation from the outside. The tissue of the sinus node lacks the stabilizing effect of the potassium efflux, resulting in a sinusoidal polarisation and depolarisation of the membrane potential and ultimately in the generation of action potentials. This occurs approximately 70 times per minute during the relaxation period of the myocardium (i.e. heart muscle).

The conduction system of the heart is depicted in figure 2.1. Starting at the sinus node, the action potentials travel over the atria, initiating the atrial contraction which consequently fills the ventricles with blood. To ensure that the ventricular contraction is executed in succession, the atria and ventricles are electrically isolated. The sole conductive tissue connecting the two areas is located in the atrioventricular node, delaying the spread of excitation significantly. From there, the depolarisation propagates towards the bundle of His, situated in the heart's septum where the conductive medium splits up into bundle branches, leading towards the heart apex. The branches merge into countless Purkinje fibres, passing the excitation on to the ventricular myocardium which ultimately leads to the contraction of the ventricles, indicating the start of the systole. In the final stages of the ejection phase and the end of the systole, the working myocardium begins to relax and the heart is repolarised, readying the start of the next cycle.

2.1.2. The Circulatory System

Blood flows in a circulatory system. To keep the blood flowing and consequently the cells oxygenated, a rhythmic pump is required. The function of the pump is provided by the heart and its four chambers and valves as seen in figure 2.2. When the heart muscle contracts, the two upper chambers, called atria, eject the blood into the two lower chambers, the ventricles. The contraction of the left and the right part of the heart takes
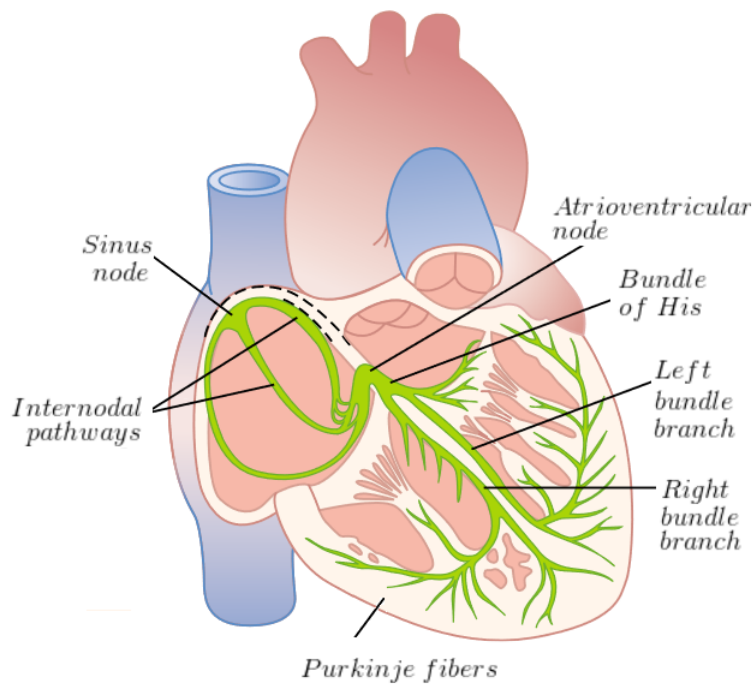
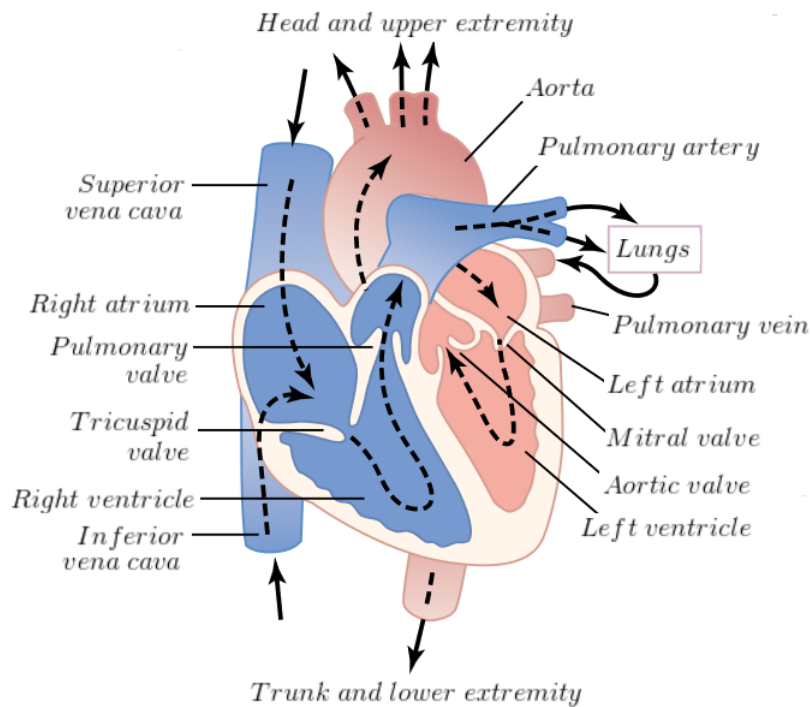Figure 2.1.: Conduction system of the heart. Adapted from [8]

Figure 2.2.: Structure of the heart. Adapted from [8]

place simultaneously. The pumping motion is produced by a rhythmic alternation between contraction (systole) and relaxation (diastole). To avoid ejection into the wrong direction, two sets of valves, namely the atrioventricular valves and the semilunar valves, close and open accordingly. The function of an "inlet valve" between atria and ventricles is represented by the mitral valve and the tricuspid valve. The "outlet valves" closing off the ventricles are called aortic valve and the pulmonary valve. The opening and closure of the valves which allow unidirectional flow takes place purely passively through the blood flow, following the pressure gradient in the heart.

The circulatory system itself consists of the high pressure system, also called systemic circulation, the low pressure system or pulmonary circulation and the venous system. Oxygenated blood is ejected by the right

ventricle and travels along the arterial blood vessels to the peripheral areas of the body. At the capillaries, oxygen and nutrients diffuse into the surrounding tissue and the blood flows through the venous system back to the heart where it reaches the right atrium and consequently the right ventricle. The deoxygenated blood is then pumped into the second circulatory system, the pulmonary circulation. The vessels lead into the lungs where the blood cells are enriched with oxygen, diffusing from the alveoli into the blood stream. Finally the blood travels back to the left atrium and ventricle, starting the circulation anew. Due to the higher blood pressure in the arteries (systolic pressure around 120 mmHg), the left ventricle exhibits a larger muscular force compared to the right ventricle which has to overcome the low blood pressure of the pulmonary artery (systolic pressure about 20 mmHg). The average human body holds about $4-5$ litres of blood, thus at an average heart rate of 70 beats per minute and an average stroke volume of 75 ml, blood takes about 1 minute for a whole circulation [8].

2.2. Blood Pressure

2.2.1. Fundamentals

The heart pumps blood against the total vascular resistance, also called impedance, of the arterial tree. With declining diameter of the vessels the resistance rises, consequently, a higher force is needed to keep the blood flowing. Blood pressure is defined as the force per area which is applied by the blood onto the vessel walls and is measured in millimetres of mercury (mmHG) [9]. As the heart contracts, blood is released into the arteries in the form of a pulse wave which travels into the periphery. Amongst other features, the pulse can be described by its amplitude and its base line. The point of highest blood pressure is caused by the contraction of the heart and called systolic blood pressure. Under normal conditions a systolic blood pressure of about 120 mmHg is considered healthy. As the heart relaxes, the blood pressure drops to its lowest value, the diastolic blood pressure, usually measured to be around 80 mmHg in a healthy
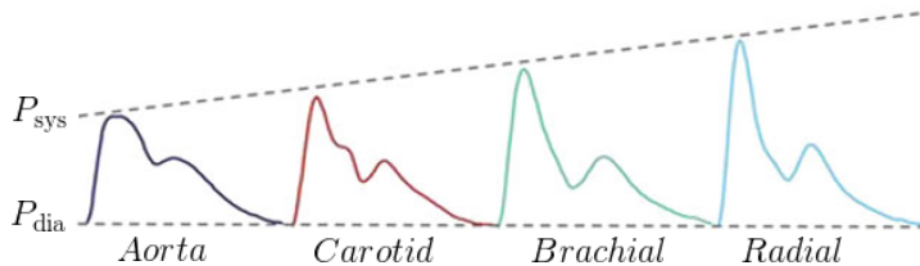
Figure 2.3.: Evolution of the pulse wave throughout the arterial tree. Adapted from [10]

individual. Due to the pulsatile motion of the heart, the blood pressure oscillates between the diastolic and systolic pressure level.

As the blood progresses in the arterial tree, the mean pressure declines with increasing distance from the heart, measuring about 0 mmHg at the termination of the venae cavae, thus making a statement on blood pressure a matter of definition. Without further specification, blood pressure refers to the systemic arterial blood pressure [8]. Similarly to the blood pressure, the shape of the pulse wave changes while moving towards the periphery as seen in figure 2.3. A phenomenon only visible in close proximity to the heart is the sharp cut in the wave form shown in figure 2.4. Due to its nature called incisura, the sudden drop in blood pressure is thought to be caused by the closure of the aortic valve, accompanied by a short reflux of the blood into the heart [11]. Attenuating with increasing distance from the heart, the incisura is overlapped by a more prominent feature, the dicrotic notch. The dicrotic notch manifests as trough between the pressure peaks and is caused by wave reflections at sites of impedance mismatch.

2.2.2. Pathology

Classification of blood pressure is done in four stages: normal, elevated, hypertension stage 1 and hypertension stage 2 [12]. Office Blood pressure is considered optimal when determined to be below $120/80$ mmHg, normal
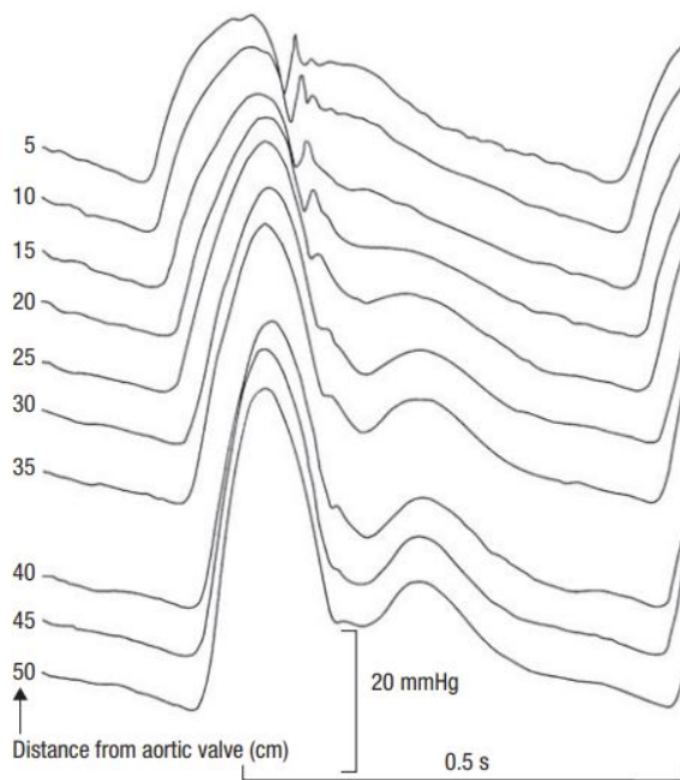
Figure 2.4.: Pressure waves recorded in a wombat. The incisura vanishes with increasing distance to the aortic valve. Taken from [11]

in the range of $120 - 129/80 - 84$ mmHg, high normal in the range of $130 - 139/85 - 89$ and hypertensive when above. The specification "office" blood pressure is necessary, because the classification thresholds differ when the measurement is performed in the office, out of office or in ambulatory monitoring. High blood pressure is recognized as a significant risk factor for various cardiovascular diseases such as arteriosclerosis, heart failure, myocardial infarction, stroke and chronic kidney disease. According to a modification of Ohm's law for hemodynamics, blood pressure can be interpreted as proportional to blood flow, dependent on cardiac output and blood volume, and peripheral resistance, affected by the contractile state of the vessels. Alongside various pathologies of the heart, an increase in peripheral resistance is the primal cause of hypertension [13].

A large variety of measuring methods exist to assess blood pressure and the wave morphology of the pulse. In the following, the most important approaches will be outlined shortly while photoplethysmography will be discussed separately.

2.2.3. Methods of Measurement

Auscultatory Sphygmomanometer

Considered as non-invasive gold standard, the underlying principle of the auscultatory sphygomanometer is the evaluation of the Korotkoff sounds. By inflating a cuff which is wrapped around the upper arm at heart level, the blood flow through the brachial artery is stopped as soon as the applied pressure exceeds the systolic blood pressure. As the blood flow is re-established by continuously lowering the pressure induced by the cuff on the artery, the turbulent flow is audible as first Korotkoff sound through a stethoscope. This pressure level is acknowledged to be the systolic blood pressure. Further reducing the cuff pressure changes the quality of the sounds. The initially heard tapping sound is replaced by a more rhythmical and harsher sound. As the cuff pressure reaches the diastolic pressure level, the artery is no longer occluded during diastole. Consequently, the main acoustic source is gone leaving only muffled

noise which also vanishes after slightly lowering the pressure further. The pressure level at the point of muffled sound is considered to be the diastolic blood pressure. To correctly interpret the sounds and operate the cuff, medical training is required.

Factors affecting the measurement are cuff size, cuff position and cuff deflation rate. Auscultatory sphygomanometer provides blood pressure values in a range of ± 5 percent of the values directly measured within the arteries [8, 10, 14].

Oscillometric Method

In contrast to auscultatory sphygomanometer, the oscillometric method does not require special training. Similarly, it is based on the occlusion of the brachial artery via an inflatable cuff and the subsequent, gradual reopening by reduction of the applied pressure. The pressure oscillations in the cuff during the deflation caused by changes in blood flow are evaluated by an eletric transducer. As shown in figure 2.5, the oscillations increase in amplitude with decreasing cuff pressure, reaching their maximum close to the mean aterial pressure and starting to decrease below. The onset and halt of the pressure oscillations do not correspond with systolic and diastolic blood pressure. These parameters can be derived by using empirically found algorithms.

Independence of medical staff and robustness to external noise are the strengths of the oscillometric method. The downside of the easy use is that the amplitude of the oscillations is strongly influenced by other factors, mainly the mechanical properties of the arteries. This may lead to underestimation of mean arterial pressure in subjects with higher arterial stiffness, such as old people. The comparsion with other blood pressure measurement techniques show the validity of the oscillometric sphygomanometer [10, 16].
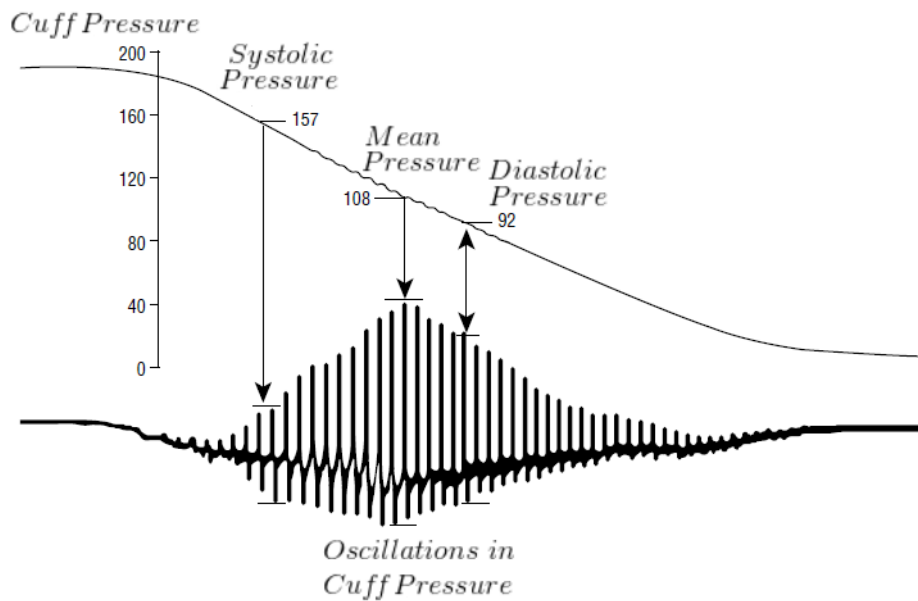
Figure 2.5.: Illustration of the oscillometric method. Adapted from [15]

Tonometry

Tonometry is a non-invasive technique to assess the morphology of blood pressure waves. The idea is to distort a superficial artery by pressing it against an underlying bone structure with a transducer, often used on the radial artery at wrist level. In this configuration the blood pressure in the vessel is approximately equal to the normal contact stress applied by the tonometer onto the skin. The stress is thereafter transformed into an electrical signal by a surface sensor, providing the morphology of the pulse wave rather than absolute pressure values. By calibrating the wave form using systolic and diastolic pressure evaluated by conventional cuff measurement, absolute pressure values can be derived.

Even though this method enables continuous, non-invasive blood pressure measurement, the sensitivity to exact placement and the need for recalibration for every patient prove to be major drawbacks. The introduction of transducer arrays placed across the artery provided a remedy but the recalibration issue remains making tonometry not suitable for

routine check-ups in clinics [10, 17].

2.3. Photoplethysmography

The data used in this thesis were recorded using photoplethysmography, thus a more thorough explanation of its functionality is provided.

2.3.1. Fundamentals

Briefly, photoplethysmography is the principle of measuring changes in blood volume by using light. A ray of light is emitted by a source, most commonly a diode, and passes through the tissue under test where it is gradually attenuated or reflected. The remaining light is then detected by a photodiode, transduced into an electrical signal and further processed. In its most basic form only one light source and a detector are required making photoplethysmography a simple and cost efficient method. A typical photoplethysmographic signal consists of a pseudo constant offset, usually denoted as DC (direct current) component and a changing AC (alternating current) component. The offset is introduced by tissue such as bone, fat, muscle and average blood volume which absorbs light at a steady rate. There is a slight variation due to breathing activities and thermoregulation [18, 19]. The AC component mirrors the instantaneous blood volume change in the artery between diastole and systole. It is evident that the fundamental frequency of the AC component is defined by the heart rate, making photoplethysmography useful for clinical monitoring of the same.

2.3.2. Technical Aspect

As light interacts with tissue through absorption, scattering and reflection an appropriate choice of wavelength is paramount. Studies on the optics of human skin show that within the visible range the main absorption is attributed to blue light followed by the green-yellow region. Wavelengths
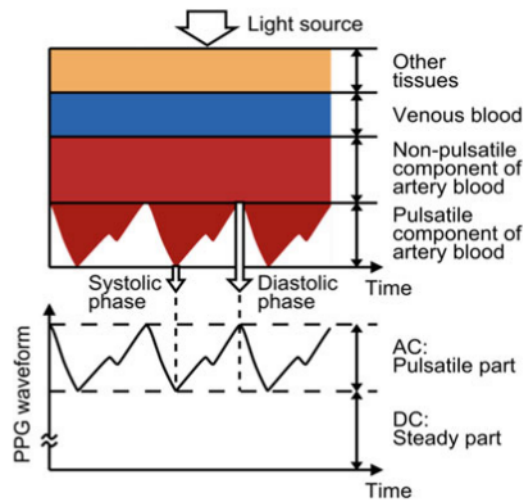
Figure 2.6.: Path of incident light in photoplethysmography. Taken from [10]

in the ultraviolet range are absorbed by melanin as well as water which also absorbs light in the longer infrared region. Luckily, red and near infrared light passes through, making it ideal for photoplethysmography [20]. The main contributor to infrared light absorption is blood. Thus, an increase in intravascular blood volume results in increased absorption and consequently in a decrease in intensity detected by the photo diode as depicted in figure 2.6. Aside from infrared light other wavelengths are used to probe different depths. The low penetration depth of green light makes it suitable to assess superficial blood flow wile red light is used for deeper lying tissue [10]. Dependent on the oxygenation level of the blood its colour changes. Blood enriched with oxygen appears brighter while oxygen depleted blood has a darker colour. Consequently, this behaviour affects light absorption, making it possible to assess the blood oxygenation through photoplethysmography. This method is called Pulse Oximetry and is widely used in clinical applications.

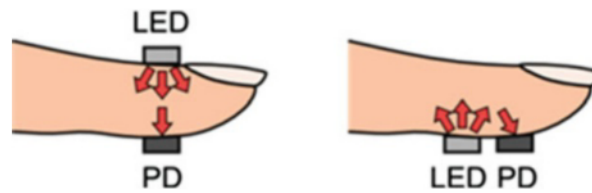Basically there are two methods of photoplethysmography: transmission and reflection.

Figure 2.7.: Basic methods of photoplethysmography: transmission (left) and reflection (right). Taken from [10]

2.3.3. Mode of Operation

The main difference between transmission and reflection mode is the relative position of the photodiode and detector as depicted in figure 2.7. In transmission mode the light source is located on the opposite side of the tissue under test, measuring the light's intensity after travelling through the tissue. While the obtained signal is meaningful, the number of relevant measurement sites is limited. The requirement of being readily accessible while still delivering a distinct signal is not easily met. Locations usually used are fingertips and earlobes, having the drawback that they are sites of limited blood perfusion and their sensitivity to cold, possibly limiting the signal [10, 21].

The issue of sensor placement is solved by using reflection photoplethysmography. By placing the detector on the same side as the light source a variety of measurement sites become accessible. In contrast to transmission mode, the photodiode uses the light reflected or backscattered from the tissue and blood to produce its signal. However, this mode introduces new problems such as the signal's susceptibility to motion and pressure acting on the sensor, making it unqualified as measuring device in sports [10].

3. Quantification of a Pulse Wave

Up to date, there is a wide range of methods to quantify pulse waves. Different descriptions starting from the simple identification of specific points, over the calculation of the area beneath the curves, up to more sophisticated methods like analysis in the frequency domain via Fourier transform are available. Depending on the recorded wave form some characteristic points may be inaccessible. The present chapter will provide a compact overview of the various strategies without claim to completeness.

3.1. Characteristic Points

A fairly straight forward way to characterize a wave form is the description by specific points on the curve. In principle, these points can be chosen arbitrarily. However, they have to be detectable throughout the dataset which proves to be difficult. Consequently, few exceptional points are chosen to quantify a curve. The most frequently used points will be described in the following; if not stated otherwise, the points are measured from the zero line.

3.1.1. Systolic Pressure

The maximum value of a periodic function is a widespread means of quantification. In the case of pulse pressure waves we encounter the **Systolic Pressure** which is visible as the first prominent peak of the

photoplethysmographic signal and denoted by P_{sys}. The Systolic Pressure is caused by the local maximal extension of the arteria during systole, resulting in maximal light attenuation by arterial blood. Arterial extension is linked to the heart's stroke volume and is proportional to the elasticity of the arteries. The Systolic Pressure provides valuable information about the cardiovascular system and is therefore a paramount measure of pulse waves. Additionally, various algorithms exist which determine the maximum of an arbitrary signal [22, 23].

3.1.2. Dicrotic Wave Pressure

The measured signal is the sum of the wave propagating from the heart to the peripheral vessels and the pressure waves travelling from the periphery to the heart. The **Dicrotic Wave Pressure** represents this behaviour. It is defined as the second prominent peak of the photoplethysmographic signal and denoted by P_{dwp}. The location and shape is heavily dependent on the elasticity and stiffness of the arteries, respectively. Since the mechanical properties of the vessels deteriorate and get stiffer with age, the pulse wave velocity increases. The higher velocity shifts the Dicrotic Wave Pressure's location horizontally towards the Systolic Pressure. In extreme examples, the maximum of the returning pulse wave overlaps with the Systolic Pressure, resulting in an amplification of arterial pressure. This amplification is expressed by the **Augmentation Index** as the ratio

$$AIx = \frac{P_{\text{sys}} - P_{\text{i}}}{P_{\text{p}}}$$

where P_{sys} is the Systolic Pressure, P_{i} the pressure at a defined inflection point that indicates the beginning overlap with the reflected wave and P_{p} the pulse pressure. In turn, the pulse pressure is defined as $P_{\text{p}} = P_{\text{sys}} - P_{\text{dia}}$, where P_{dia} denotes the diastolic pressure shown as the wave's onset in figure 3.1 [25, 11].

Systolic and Dicrotic Wave Pressure are widely used in research and found in the work of [26, 27, 23], to name a few.
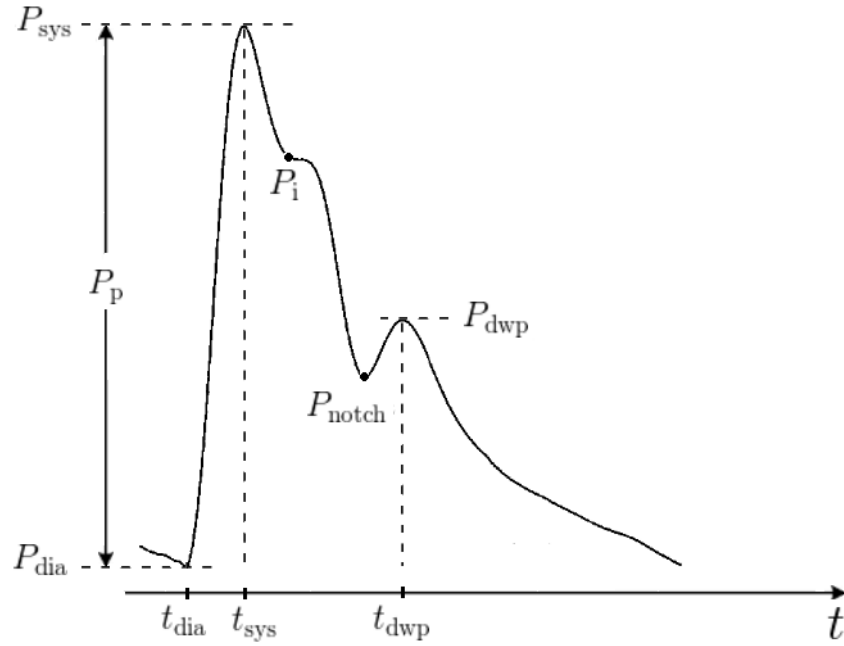
Figure 3.1.: A typical peripheral pulse wave adapted from [24]. P_{sys} and P_{dwp} denote the Systolic Pressure and Dicrotic Wave Pressure, respectively. The wave's onset is marked by P_{dia} and known as Diastolic Pressure. $P_{\mathrm{p}} = P_{\mathrm{sys}} - P_{\mathrm{dia}}$ is commonly referred to as pulse pressure. Visible as points on the curve are the point of inflection P_{i} where the reflected pulse wave augments the wave form and P_{notch}, denoting the position of the dicrotic notch. The crest time t_{C} is defined by $t_{\mathrm{C}} := t_{\mathrm{sys}} - t_{\mathrm{dia}}$ as the time frame between the onset and the Systolic Pressure of the pulse wave. The Dicrotic Wave Time t_{D}, describing the position of the Dicrotic Wave Pressure with respect to the onset is defined as $t_{\mathrm{D}} := t_{\mathrm{dwp}} - t_{\mathrm{dia}}$.

3.1.3. Dicrotic Notch

As already indicated in section 2.2.1 the dicrotic notch is the result of positive wave interference of the incident and reflected waves, visible as trough between the peaks in figure 3.1. According to [28], the position of the dicrotic notch can be seen as an indicator for vasomotor tone. Increased compliance of the arterial tree, for example induced by anesthetics, causes the dicrotic notch to move downwards to the diastolic pressure baseline P_{dia} while an increase in vascular tone results in an earlier occurence and upward shift of the notch [29].

3.2. Width

As already mentioned, the extraction of specific points via algorithms can prove to be tedious. Another method to quantify a wave form is the description by its width. In the case of blood pressure waves, the widths correlate with certain time frames which will be discussed in this section.

3.2.1. Crest Time

The **Crest Time** t_{C} or Rise Time is defined as the time frame between the pulse wave's nadir and the Systolic Pressure. A low Crest Time, and thus a steep rise of the pulse wave, is conditioned by a higher stiffness of the arterial walls and thus higher Youngs Modulus [30]. Therefore, this parameter was found to be a useful feature to classify cardiovascular diseases. Its association to the contractile force as well as the heart's ventricular functions makes it a valuable physiological parameter to observe [26, 31, 32].

3.2.2. Dicrotic Wave Time

The **Dicrotic Wave Time** t_{D} describes the position of the Dicrotic Wave Pressure with respect to the wave's onset. Another parameter found in literature, describing the position of the diastolic peak is the **time delay parameter** also known as **stiffness index**, defined as $t_{\mathrm{DP}} = SIx = t_{\mathrm{D}} - t_{\mathrm{C}}$. The stiffness index specifies the location of the diastolic peak with respect to the systolic peak or, in case of a lacking peak, the point of inflection [33]. As its name implies, SIx is linked to the mechanical properties of arteries. The velocity of a propagating wave is related to arterial stiffness as found in [11] by

$$PWV = \sqrt{\frac{E_{\mathrm{inc}}h}{2r\rho}},$$

where E_{inc} is the incremental Young's Modulus of the arterial wall, h the wall's thickness, r the arterial radius and ρ the blood's density. A higher elastic modulus, synonymously a stiffer vessel, yields a higher pulse wave velocity PWV. Consequently, the reflected wave moves faster, decreasing the stiffness index and bringing the systolic and diastolic peak closer together as represented by figure 3.2. Pulse wave velocity is subject to ongoing research and is thought to be a precursor of cardiovascular diseases [31, 33, 34].

3.2.3. Total Pulse Duration

The **Total Pulse Duration** t_{T} is easily defined as the time difference between the pressure wave's onset and its cessation [34].

3.2.4. Full Width at x-% of Maximum

Linked to the Total Pulse Duration and a rather pragmatic way to describe a curve is the measurement of its width at a specific percentage
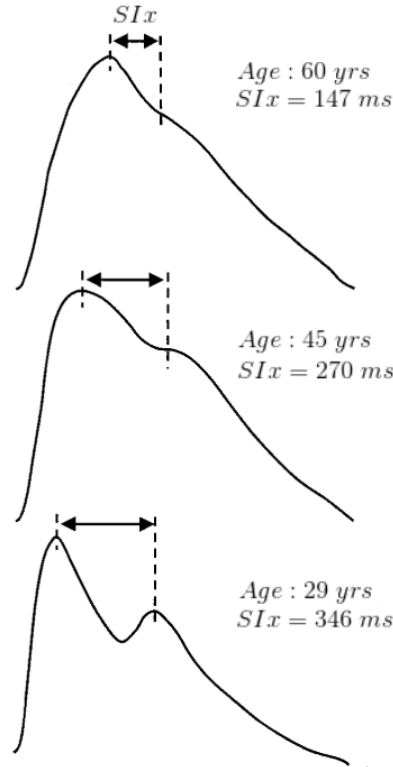
Figure 3.2.: Effect of ageing on the pulse wave's form. Stiffer vessels yield a higher pulse wave velocity and followingly a decreased arrival time of the returning wave, reflected by SIx. Adapted from [33]

of the Systolic Pressure as done in [35]. It is suggested that ratios of different widths at x-% of the maximum could provide information about the subject's cardiovascular system. According to [27, 36], the pulse width at half the maximum shows a correlation with the systemic vascular resistance.

Besides the aforementioned basic time parameters, there are numerous derived parameters of minor importance which shall not be described in this thesis. Several can be found in [23, 34].

3.3. Area

Another commonly used description is the area under the curve. As already mentioned, the AC component of the PPG signal follows the pulsatile blood flow, consequently providing useful information regarding blood flow. A study concluded that the area under the curve is capable of measuring local blood flow and arterial tone [32].

3.3.1. Split Area

Closely related to the total area is the method of splitting the curve at the dicrotic notch and using the resulting parts as parameters as seen in figure 3.3. The origin of the pulse wave's shape can be explained by the wave reflection theory: the initial wave is produced by the heart's activity while the second returning wave is produced by wave reflections at sites of impedance mismatch between different parts of the arterial tree. Hence, it is possible to introduce the inflection point area ratio as

$$IPA = \frac{A_2}{A_1},$$

where A_1 and A_2 are the areas beneath the curve, bordered by the baseline, before and after the dicrotic notch, respectively. As the IPA is primarily influenced by the reflected wave it proves to be a consistent measure for the total peripheral resistance of the system [26, 37, 38].

3.4. Derivatives

Further information about the contour of the wave form can be extracted by analysing the first and second derivative of the signal. By using the first derivative, peaks can be detected directly making it capable of real-time processing. The downside of both methods is the limitation to pulse signals with high signal to noise ratio [40].
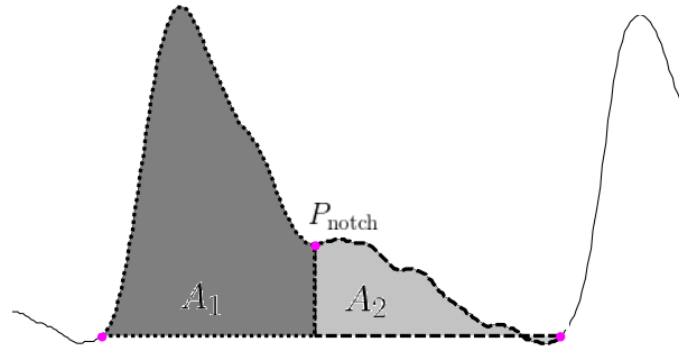
Figure 3.3.: Area beneath a PPG signal split at the dicrotic notch P_{notch}, adapted from [39].

3.4.1. First Derivative

Opposed to the second derivative, the first derivative is rarely used as describing parameter but rather as a tool to extract further information about the signal. For example, in absence of a distinct Dicrotic Wave Pressure the point of inflection can be defined as the point where the first derivative is closest to zero [31, 41]. In [27], the maximum (Upstroke) and minimum (Downslope) of the first derivative were used to assess the wave form of signals recorded via plethysmography at the fingertip and the ear lobe during cold immersion tests. Thorough literature research did not provide further applications.

3.4.2. Second Derivative

The second derivative, also referred to as acceleration plethysmography due to its connection to blood acceleration, is more commonly found in literature. Its specific wave form is used to derive several ratios which are found to be related to, among other things, mechanical properties of the system. The ratios are calculated from the following parts of the wave, measured from the second derivative's baseline:
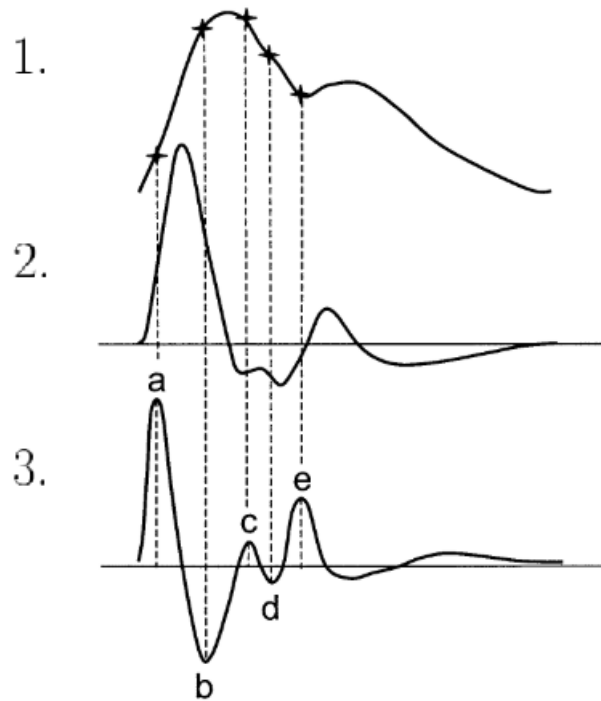
Figure 3.4.: (1.) Original pulse wave, (2.) first derivative, (3.) second derivative including marked waves, taken from [41].

- initial positive (marked as "a" in figure 3.4)
- early negative (b)
- re-increasing (c)
- late re-decreasing (d)
- diastolic positive (e).

Several studies investigated following ratios with respect to their relevance to vascular ageing, heart rate, blood pressure and age in general.

- Ratio of early negative to initial positive $\frac{b}{a}$
  As suggested in [42], the ratio may mark distensibility of large arteries and synonymously stiffness. Thus, $\frac{b}{a}$ could prove to be a valuable marker for arteriosclerosis.
- Ratio of re-increasing to initial positive $\frac{c}{a}$

Takazawa et al. reported the ratio's decrease with arterial stiffness. [43]

- Ratio of late re-decreasing to initial positive $\frac{d}{a}$
  According to [42], $\frac{d}{a}$ could indicate the intensity of the reflected wave from the periphery and arterial stiffness.

- Ratio of diastolic positive to initial positive $\frac{e}{a}$
  Similarily, $\frac{e}{a}$ correlates with decreased arterial stiffness [42].

- Age index (AGI) $\frac{b-c-d-e}{a}$
  The age index was introduced by Takazawa et al. as marker for vascular ageing [43].

3.4.3. Third Derivative

Lastly, for the sake of completeness, the third derivative should be mentioned. It is used by Charlton et al. [44] to determine the early and late systolic component of the pulse wave, initially defined in [45], denoted in figure 3.5 as $p1$ and $p2$, respectively.

3.5. Fourier Transform

Until now, all quantification methods described so far have taken place in the time domain. By utilizing the Fourier Transform, it is possible to convert a signal from the time to the frequency domain, where the frequency spectrum can by analysed. The Fourier Transform is defined as

$$\mathcal{X}(j\omega) = \mathcal{F}\{x(t)\} = \int\limits_{-\infty}^{\infty} x(t)e^{-j\omega t}\mathrm{d}t,$$

where $\mathcal{X}$ denotes the arbitrary signal x in the frequency domain, t the time, ω the angular frequency and j the imaginary unit as defined by $j^2 = -1$. Furthermore, a periodic signal, respectively its wave form, can

3. Quantification of a Pulse Wave
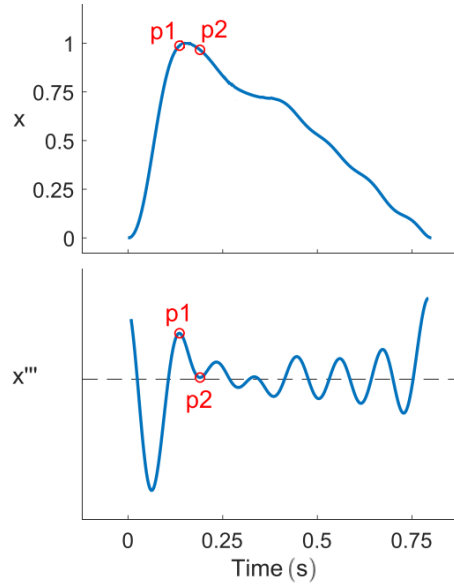
Figure 3.5.: Early and late systolic component and the corresponding points in the third derivative, adapted from [44].

be represented by a Fourier series. A Fourier series consists of sinusoidal wave components whose frequencies are integral multiples of the frequency of repetition of the original wave [11]:

$$x(t) = \frac{a_0}{2} + \sum_{n=1}^{\infty}(a_n \cos(n\omega t) + b_n \sin(n\omega t))$$

with

$$a_n = \frac{1}{\pi} \int_0^{2\pi} x(t) \cos(n\omega t)\mathrm{d}t$$

$$b_n = \frac{1}{\pi} \int_0^{2\pi} x(t) \sin(n\omega t)\mathrm{d}t.$$

In this context, ω denotes the fundamental frequency and $n\omega$ the nth harmonic of the signal.
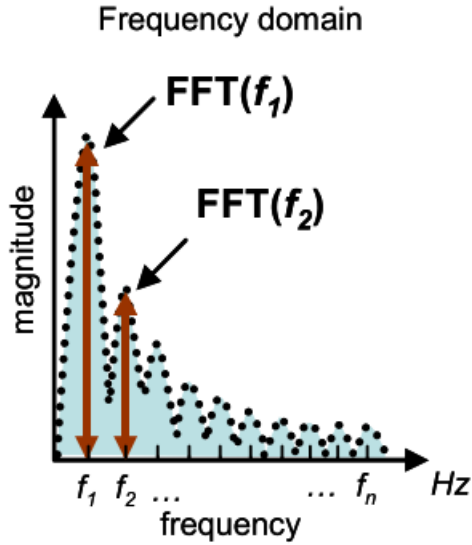
Frequency domain

Figure 3.6.: An arbitrary signal in the frequency domain, adapted from [37]

Sherebrin et al. [46] analysed the harmonics, normalized to the fundamental frequency, in different age groups. The youngest group showed a higher power in the second harmonic compared to the others. The power decrease with age may thus be an indicator of vascular ageing and diseases. Similarily, Olafiranye et al. [47] used the ratio of the nth individual harmonic amplitude to the total harmonic amplitude to investigate the correlation between the arterial wave form and various cardiological parameters in bonnet macaques.

Another parameter derived from frequency domain analysis is the normalized harmonic area (NHA) described in [48] and refined in [37]. It is defined as

$$NHA = \frac{\sum_{n=2}^{N} FFT^2(f_{\text{n}})}{\sum_{n=1}^{N} FFT^2(f_{\text{n}})},$$

where $FFT(f_{\text{n}})$ denotes the amplitude of the nth harmonic of the photoplethysmographic signal as depicted in 3.6. The NHA shows potential

as estimator for arterial blood pressure. Aforementioned development introduced the inflection and harmonic area ratio as

$$IHAR = \frac{1 - \frac{\sum_{n=2}^{N} FFT^2(f_n)}{\sum_{n=1}^{N} FFT^2(f_n)}}{\frac{A_2}{A_1}}.$$

The denominator was already mentioned in 3.3.1 as inflection point area ratio. It was found that IHAR correlates with cardiac output which is an important parameter to monitor the perfusion status of the cardiovascular system [37].

3.6. Curve fitting

The procedure of approximating a given curve, respectively a series of data points, by finding the best fit through a mathematical equation is called **curve fitting** and is a frequent task in every aspect of the engineering field. With respect to pulse wave analysis, the most used approach is curve fitting by Gaussian functions. Various studies describe the approximation of the pressure pulse's wave form by superposing several Gaussian waves. Liu et al. [49] modelled the pulse wave by combining three Gaussian waves in the form of

$$f(n, x) = \sum_{k=1}^{3} f_k(n)$$

with

$$f_k(n) = H_k \cdot e^{\frac{-2(n - C_k)^2}{W_k^2}},$$

where $k \in \{1, 2, 3\}$, $x = (H_k, W_k, C_k)$, H_k denotes the height of the peak, W_k the half width and C_k the peak's position. The optimization criterion used to find the parameters in x is given by
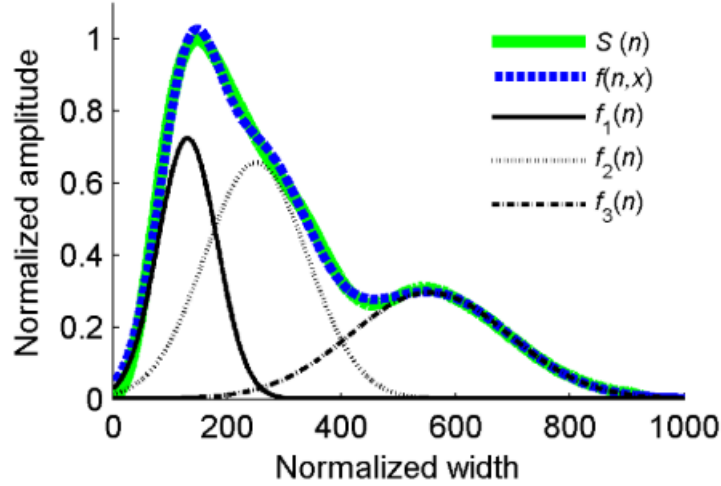
Figure 3.7.: A pulse wave S_{n} approximated by curve fitting using the sum of three Gaussian waves $f(n, x) = f_1 + f_2 + f_3$. Adapted from [49].

$$Min\, f(x) = [S(n) - f(n, x)]^2,$$

where $S(n)$ is the recorded, normalized pulse wave as seen in figure 3.7. This approach was taken to examine the effect of blood pressure and sex on the change of wave reflection. The number of Gaussian waves needed to approximate a physiological signal depends on its morphological features. Wang et al. [50] analysed the effect of increasing wave numbers on the accuracy of the fit and found that the normalized root-mean-square deviation stagnates beyond more than nine Gaussian waves. Curve fitting enables the quantification of pulse waves by the parameters in x, found through the optimization process.

3.7. Empirical Mode Decomposition

Related to but still fundamentally different than the Fourier Transform, **Empirical Mode Decomposition** (EMD) is used to disassemble signals

and was initially introduced by Huang et al.[51]. In contrast to the Fourier Transform, EMD does not specify its basic set of functions as the Fourier Transform does with sinusoids, making the method adaptive. Through continuous spline interpolation the algorithm reduces the signals to its so called intrinsic mode functions (IMF). Two requirements must be met to classify as IMF, : (1) throughout the data series the number of extrema and zero crossings must be the same or vary by a maximum of one and (2) the mean of the envelopes constructed by the local maxima and local minima equals zero.

With the so-called sifting process the following steps are necessary to determine the IMF:

1. local minima and maxima throughout the data series $x(t)$ are determined
2. all minima and maxima are interpolated with a cubic spline curve, constructing an upper envelope $x_u(t)$ and lower envelope $x_l(t)$
3. the average envelope signal $m(t)$ is calculated as the mean of upper and lower envelope as $m(t) = (x_u(t) + x_l(t))/2$
4. the mean is subtracted from the original data series $x(t)$ to generate a new signal $d(t) = x(t) - m(t)$
5. this procedure is repeated iteratively until $d(t)$ meets the requirements to be classified as IMF, denoted by c_1
6. the algorithm is applied to $x(t) - c_1$ to acquire the remaining intrinsic mode functions c_k

The original data series can ultimately be written as

$$x(t) = \sum_{k=1}^{n} c_k + r(t),$$

where $r(t)$ denotes a residue function which acts as stopping condition for the algorithm as soon as it reaches a specific threshold.

The goal of EMD is the identification of different time scales in the signal to analyse their possible physical meaning or background. Cutting the recorded pulse wave train, enables the application of EMD to single pulse waves. Thus, quantification and comparison of pulse waves through their

individual intrinsic mode functions c_k is possible. Further improvement is achieved by combining EMD with the Hilbert transform, thus enabling the representation of the signal's amplitude and its instantaneous frequency as a function of time [52, 53]. Liu et al. [54] used the combination of EMD and Hilbert transform, known as Hilbert-Huang transform (HHT) and an extreme learning machine to detect hypertension. They compared the IMFs and Hilbert spectra of subjects with hypertension to a control group and correctly predicted with an accuracy of 93%, making HHT a valuable tool for pulse wave analysis.

3.8. Attractor Reconstruction

In non-linear dynamic system theory an attractor is a state, respectively a set of states, towards which the considered system strives asymptotically with progressing time regardless of its starting conditions [55]. Naturally occurring systems are to a large degree non-linear and dynamic, a mathematical description or model unknown. Attractor reconstruction allows the restoring of the system's phase space through recorded signals to analyse its behaviour [56]. Aston et al. [57, 58] described in their study the application of attractor reconstruction to cardiovascular wave form data in order to extract its features. A short review of their method will be provided below.

The attractor reconstruction can be broken up into four consecutive steps:

1. **Introduction of delay coordinates**
   The initial step in the reconstruction of an attractor is the definition of delay coordinates following Takens et al. [59]. The idea is that a trajectory in phase space cannot be created from a single signal due to lack of information. It was shown that the introduction of delay coordinates based on the original signal $x(t)$ in the manner of

$$[x(t), \;\; x(t - \tau), \;\; x(t - 2\tau), \ldots, \;\; x(t - (n-1)\tau)],$$

where $\tau \geq 0$ is the time delay and $n \geq 2$ the embedding dimension enables the reconstruction of the attractor. To be able to visualize the phase space properly, the number of dimensions was chosen to be $n = 3$, thus it is necessary to define two variables, $y(t)$ and $z(t)$. Takens et al. showed, that for a periodic signal the time delay τ is well chosen to be a third of the cycle length, the detailed proof can be found in [57]. The two new variables can now be defined as

$$y(t) = x(t - \tau), \quad z(t) = x(t - 2\tau)$$

and the attractor can be plotted in three dimensional space.

2. **Removal of baseline wander**
   The newly introduced signals $y(t)$ and $z(t)$ are directly derived from the original recorded signal $x(t)$. Consequently, a constant offset in form of $x(t) \to x(t) + c$ with $c \in \mathcal{R}$ obviously affects the derived signals as well $y(t) \to y(t) + c$, $z(t) \to z(t) + c$. Considering the phase space this offset leads to $(x(t), y(t), z(t)) \to (x(t), y(t), z(t)) + c(1, 1, 1)$, implying a shift in the direction $(1, 1, 1)$. By projecting the reconstructed attractor on a plane perpendicular to the vector $(1, 1, 1)$ this disturbance can be omitted. Hence, Aston et al. defined a new set of variables

$$u(t) = \frac{1}{3}(x + y + z), \quad v(t) = \frac{1}{\sqrt{6}}(x + y - 2z)), \quad w(t) = \frac{1}{\sqrt{2}}(x - y),$$

   making the attractor invariant to translation in the (v, w) plane.

3. **Density**
   With progressing time, the plot of the attractor tends to become an obscure knot of lines with few outstanding features. To counteract this malevolent behaviour, a way of visualisation is the derivation of a density from the attractor projected on the (v, w) plane. A density plot displays areas which are frequented more often, i.e. have a higher density, in a different color than regions of lower density as seen in figure 3.8.

4. **Time traces**
   After constructing the attractor density, it is possible to extract specific features from it. By recording the attractor trajectory during different time frames, a series of density plots can be created. Extracting the density's maximum or another arbitrary property for each dataset shows its evolution over time which subsequently can be used as diagnostic marker.

The complex shape of the attractor allows quantification of the pulse waves through its variety of features. Obvious choices are the attractors size, linked to the pulse pressure value $P_\mathrm{p} = P_\mathrm{sys} - P_\mathrm{dia}$, varying densities due to wave form variability, or the degree of the attractor's rotation as depicted in figure 3.9. Further research is required to identify other elements and their physiological background. Analysis using attractor reconstruction has two major advantages. Firstly, the unwanted baseline wander is suppressed efficiently with the projection on the (v, w) plane. However, the main advantage lies in the evaluation of the whole data set without discarding any information. While many methods focus solely on specific points like maxima or minima, observing data as a whole may provide deeper understanding of the cardiovascular system and its pathologies.
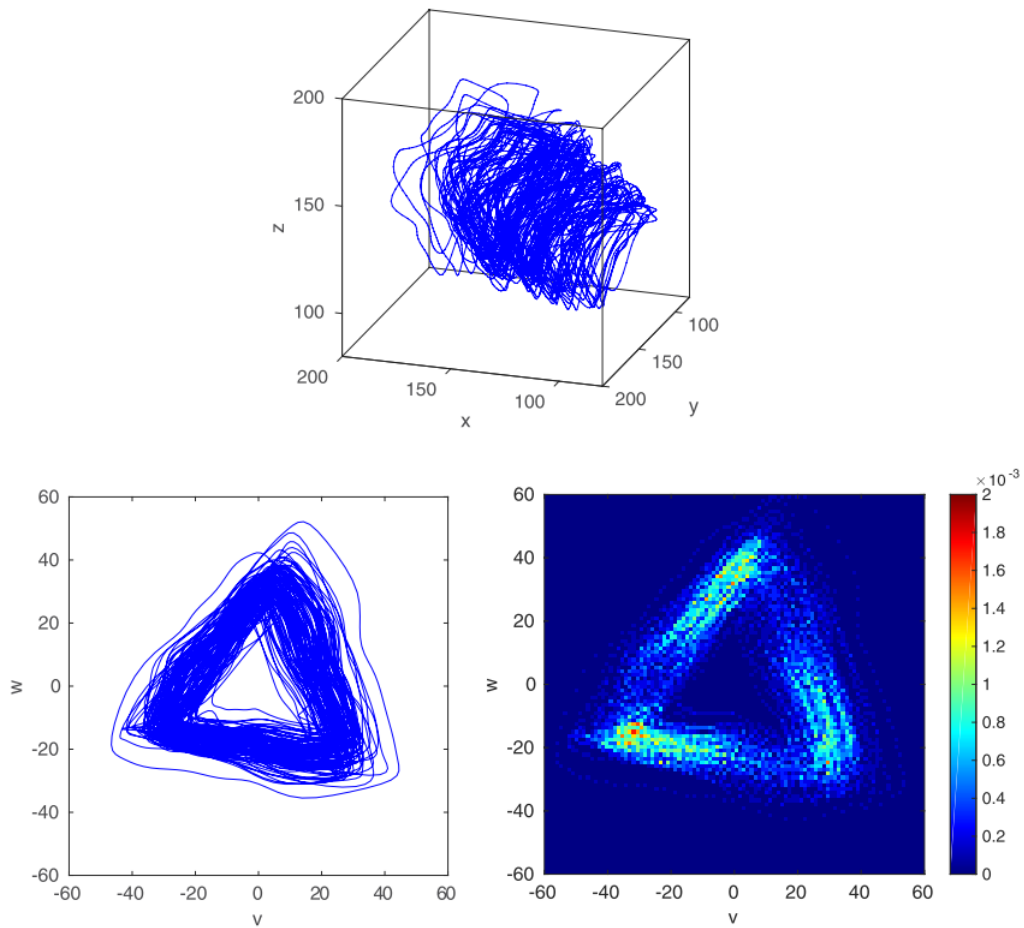
Figure 3.8.: Top: reconstructed attractor of a mouse's blood pressure recording.
Left: the projection of the attractor in the (v, w) plane.
Right: density plot of the trajectory in the (v, w) plane. Adapted from [57]
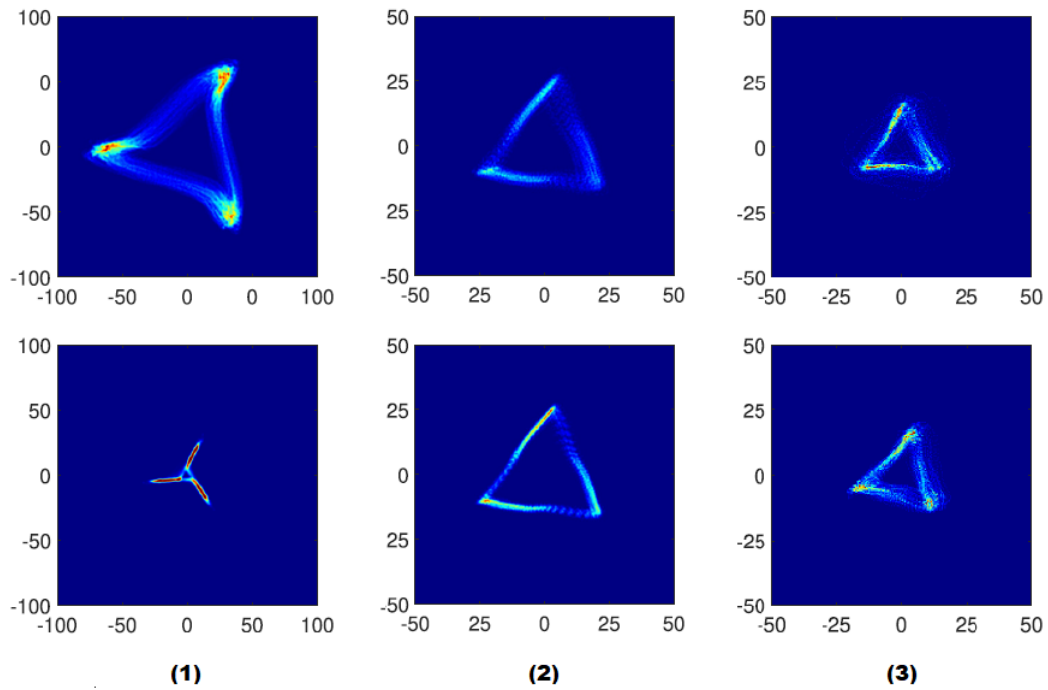
Figure 3.9.: Changes in attractor features, adapted from [58].
(1) large attractor (high P_p) vs. small attractor (low P_p)
(2) high variability (diffuse sides, low density) vs. low variability (distinct sides, high density)
(3) visible rotation of the (lower) attractor due to higher curvature in the downstroke of the pulse waves

4. Methodology

This chapter contains the aggregation of methods applied to acquire, process and present the data used in the thesis.

4.1. Data

A pilot study conducted by the AIT Austrian Institute of Technology in partnership with the Clinical Research Institute in Dortmund, ines mikisek coaching and the Kerckhoff Clinic, deployed a biofeedback procedure, where the sympathetic tone, and therefore the blood pressure, was influenced through modification of respiration. As respiration and relaxation techniques, like mantra breathing or yoga, are known to affect blood pressure, its effect on the pulse wave velocity was examined [60, 61, 62]. The pulse wave data used in this thesis were acquired through photoplethysmography at the fingertips of 30 subjects with treated arterial hypertension. The baseline characteristics of enrolled patients are summarized in table 4.1.

The examination was carried out in a comfortable sitting position, allowing non-restrictive abdominal breathing. A ready-to-use "Biosignal Explorer" system (biosignalsplux, Lisbon, Portugal) was used for recording. The breathing guidance was performed through a custom-made application for Android smartphones and tablets as seen in figure 4.1. The used datasets were acquired during ten minutes of constant, guided respiration, where the pre-specified duration of expiration and inspiration

N (#)	30
Age (years)	62.9 (7.7)
Gender (#/#)	11 females / 19 males
Body height (cm)	174.4 (10.4)
Body weight (kg)	87.6 (18.9)
BMI (kg/m^2)	28.6 (4.7)
Arterial hypertension since (years)	11.4 (10.2)
Systolic blood pressure (mmHg)	133.0 (17.1)
Diastolic blood pressure (mmHg)	83.8 (10.6)
Spontaneaus breathing rate ($1/min$)	13.6 (1.9)

Table 4.1.: Baseline characteristics of enrolled subjects. Data are expressed as mean (standard deviation) or in absolute numbers

varied among the subjects. The guided breathing phase was followed by a five minute cooling down phase. During this phase, the balloon indicating the breathing rhythm was hidden and the subjects tried to continue their constant respiration. Afterwards, the recorded data were gathered for further analysis.

While the data quality was overall high, pre-processing was required to satisfy the needs of post-hoc analysis by the applied algorithm. The methods of pre-processing will be discussed in the section 4.2.

4.1.1. Introducing the Algorithm

To assess the evolution of pulse waves during the course of relaxation techniques, the quantification of pulse waves is necessary. A thorough literature research about existing methods of quantification was conducted and its results were summarized in chapter 3, thus providing the foundation of the applied algorithm. The algorithm per se consists of three major parts, as depicted in figure 4.2. In the first step, the pulse wave data is filtered, separated in single waves and then evaluated by a strict artefact filter (pre-processing). The detailed description is found in section 4.2. Subsequently, relevant features are extracted from the pre-processed pulse waves (section 4.3) and in the third step, statistical
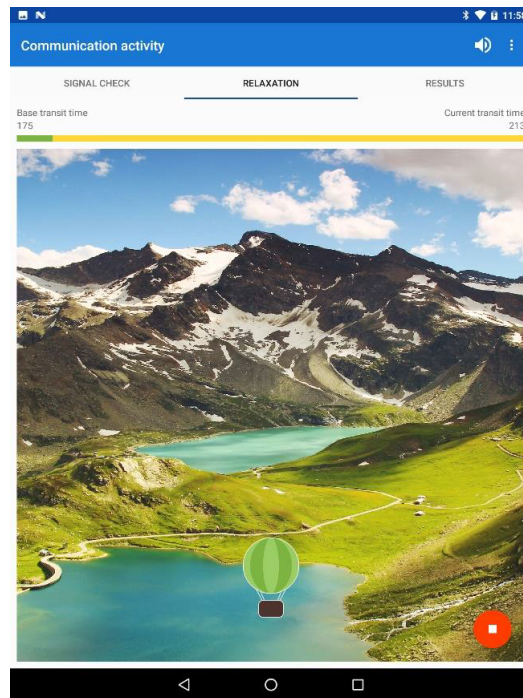
Figure 4.1.: Custom-made Android App guiding the slow breathing exercise. The balloon rises and falls with the individual rhythm, the rise indicating inspiration and the fall indicating expiration

Figure 4.2.: Flowchart representation of the applied algorithm

means are applied to evaluate obtained data (section 4.4).

4.2. Pre-Processing

In section 4.2, the pre-processing procedure is described as illustrated in figure 4.3. In the first step, a low pass filter is applied to the raw data. Subsequently, the processed signal is separated into single pulse waves. The final step in the pre-processing sequence is the annotation of artefacts.
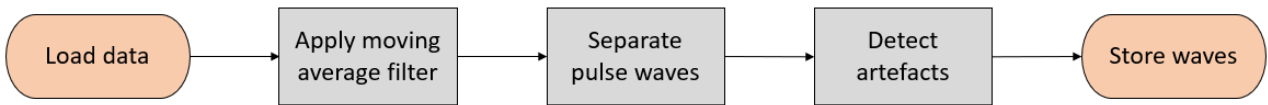
Figure 4.3.: Flowchart representation of the pre-processing procedure

4.2.1. Low-Pass Filter

In order to smooth the raw pulse wave data, i.e. to remove the high frequency components in the signal, a low-pass filter was applied. Therefore, a five-point central moving average filter in the form of

$$P^{\mathrm{i}}(t) = \frac{1}{5} \sum_{j=-2}^{2} P^{\mathrm{i}}_{RAW}(t_{\mathrm{j}}),$$

where i denotes the individual waves and j denotes the running index of points within the waves, was chosen. The processed signal showed a sufficient suppression of high frequency noise, as exemplarily seen in figure 4.4.

(a) Unfiltered pulse wave

(b) Pulse wave after applying a five-point central moving average filter
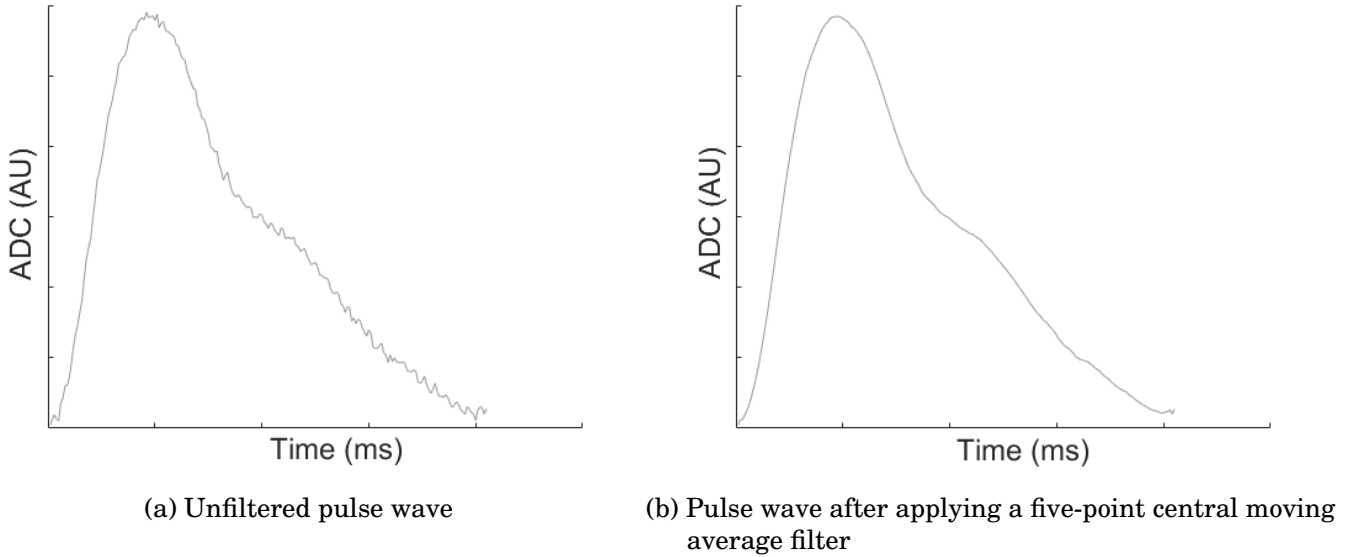
Figure 4.4.: Pulse wave before and after filtering.

4.2.2. Fragmentation

The extraction algorithm was devised to enable automatic annotation on single pulse waves. Thus, the pulse wave signal was separated into single heart beats by detecting the waves' onsets. The algorithm was applied to moving windows with a fixed frame of five seconds, starting with the last identified onset point to guarantee robust, dynamic and thorough detection. Within the window, the most prominent peaks, indicating the Systolic Pressure points, are found by using the function *findpeaks* and its specifiers *MinPeakDistance* and *MinPeakProminence*. The requirement for the minimum distance between two adjacent peaks was set to $300\ ms$ and the minimum prominence of the peak was chosen as $4 \cdot |mean(P_W(t)) -$

$median(P_W(t))|$, where $P_W(t)$ denotes the pulse wave data of the current window. The extracted data window was then further limited by finding the intervals between neighbouring peaks (figure 4.5b).

$$P_{\text{loc}}^{i}(t) = P(t), \qquad t \in [t_{\text{sys}}^{i}, t_{\text{sys}}^{i+1}],$$

where t_{sys}^{i} denotes the timing of the Systolic Pressure of the ith wave.

(a) Finding relevant peaks in the current window and determine P_{loc}

(b) Determine point of maximum perpendicular distance in P_{loc}
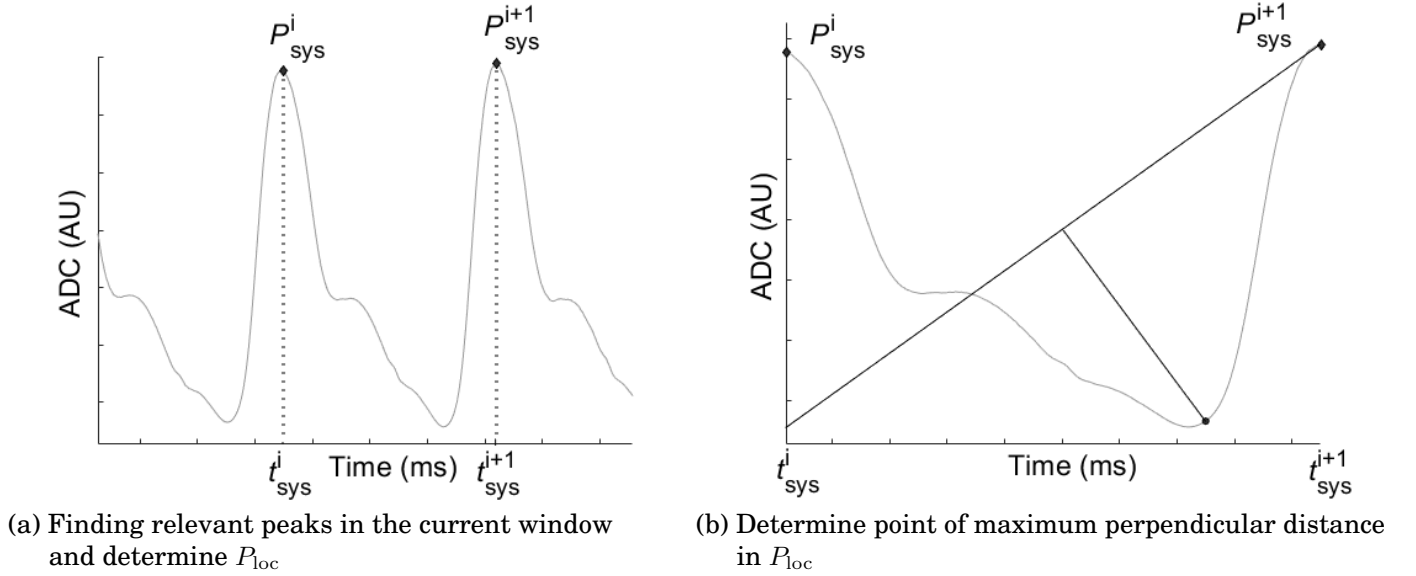
Figure 4.5.: Process of finding the wave's onset

In a first attempt, the minimum P_{min} found in the aforementioned intervals was evaluated for its qualification as onset point and found to be unsatisfactory. In order to improve the quality of fit, a different approach was pursued:

- Draw a line $y(t)$, connecting the interval's left border t_{sys}^{i} at the level of the interval's minimum P_{min} and the interval's right border t_{sys}^{i+1}

at the level of the interval's maximum P_{sys}^{i+1} as seen in figure 4.5a,

$$y(t) = \frac{P_{\mathrm{min}} - P_{\mathrm{sys}}^{i+1}}{t_{\mathrm{sys}}^{i} - t_{\mathrm{sys}}^{i+1}}(t - t_{\mathrm{sys}}^{i+1}) + P_{\mathrm{sys}}^{i+1} \quad t \in [t_{\mathrm{sys}}^{i}, t_{\mathrm{sys}}^{i+1}]$$

- Find the point displaying the maximal perpendicular distance to $y(t)$ (figure 4.5b), representing the wave's onset, as

$$t_{\mathrm{onset}} = \{t \in [t_{\mathrm{sys}}^{i}, t_{\mathrm{sys}}^{i+1}] \mid P_{\mathrm{loc}}^{i}(t) - y(t) \ is \ minimum\}$$

The obtained points were used to cut the continuous data set into its individual blood pressure waves. To remove the effects introduced by the subject's respiration and facilitate comparability, the waves were finally moved to the zero-line. This was done by subtracting the newly found point of onset P_{onset} from the individual waves

$$\widetilde{P}^{\mathrm{i}} = P^{\mathrm{i}} - P_{\mathrm{onset}}^{\mathrm{i}},$$

where $\widetilde{P}^{\mathrm{i}}$ denotes the pulse wave which was moved to the zero-line. In the following, to acknowledge the physiological implications, P_{onset} is further denoted by P_{dia}.

4.2.3. Artefact Removal

Through movement of the subject or poor sensor adhesion, including loss of contact, data can be distorted. These so called "artefacts" have to be removed before further processing. The examined data set classifies as biosignal, meaning it originates from a biological system. A biological system like the human body takes time to adapt to change. As a result and under normal conditions, the magnitude of a biosignal can only vary minimally between two events, e.g. between two succeeding heart beats for pulse wave signals. The provided figures in section 4.2.3, exemplarily showing the detected artefacts, are taken from the original, unmoved signal.

4. Methodology

Artefacts introduced by movement or loss of contact are often visible as instantaneous increase or decrease of the biosignal. Thus, the first attempt to remove artefacts was the classification into physiological and non-physiological respectively abnormal waves according to the individual wave's maximum, represented by P_{sys}. It was assumed that a pulse wave can only increase or decrease by no more than 30% between two succeeding beats which can be described as

$$
\widetilde{P}^{\text{i}} = \begin{cases} \widetilde{P}^{\text{i}}, & \left| 1 - \frac{\widetilde{P}^{\text{i}}_{\text{sys}}}{\widetilde{P}^{i-1}_{\text{sys}}} \right| \leq 0.3 \\ NaN, & \text{otherwise} \end{cases}, i = 2, \ldots, N \tag{1}
$$

where $\widetilde{P}^{\text{i}}$ is the ith individual moved pulse wave, $\widetilde{P}^{\text{i}}_{\text{sys}}$ represents the maximum value of the ith moved pulse wave and $\widetilde{P}^{i-1}_{\text{sys}}$ denotes the maximum value of the preceding moved pulse wave.
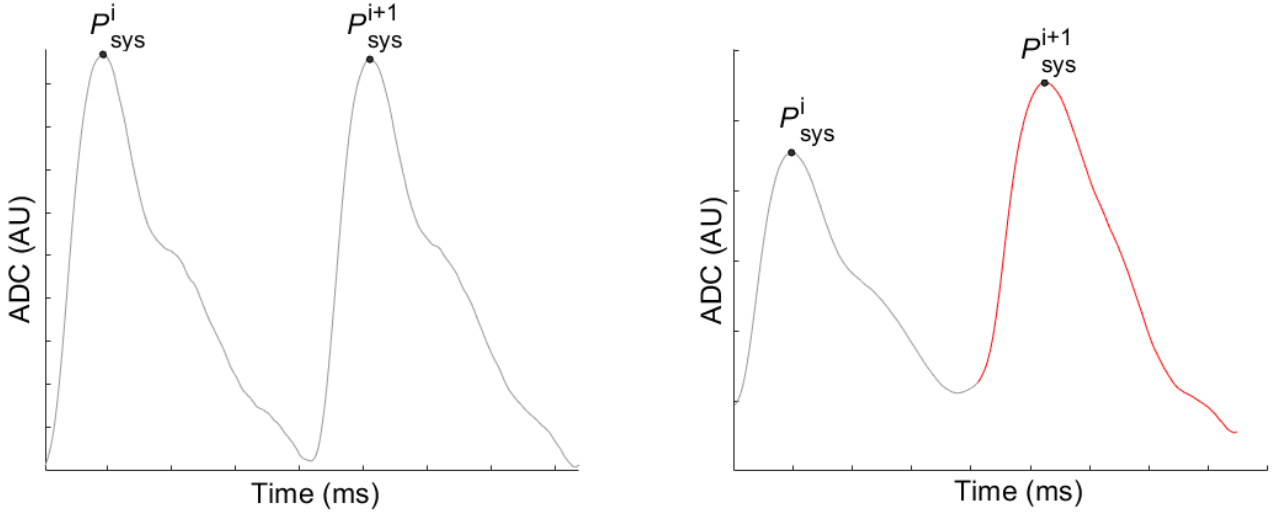
(a) Regular pulse waves with annotated maximum

(b) Pulse wave with visibly greater maximum compared to the preceding wave

Figure 4.6.: Comparison of a regular wave and an artefact wave, annotated due to abnormal increase of its maximum.

If a wave exceeds the 30% limit it is classified as non-physiological and removed from the data set, as seen in figure 4.6.

Similarly, the Pulse Pressure $P_\mathrm{p} = P_\mathrm{sys} - P_\mathrm{dia}$ is also restricted to changes within the range of 30%. Figure 4.7 depicts a rejected wave, where this condition is not satisfied.

$$\widetilde{P}^\mathrm{i} = \begin{cases} \widetilde{P}^\mathrm{i}, & \left| 1 - \frac{\widetilde{P}_p^\mathrm{i}}{\widetilde{P}_p^{i-1}} \right| \leq 0.3 \\ NaN, & \text{otherwise} \end{cases} \quad , i = 2, \dots, N \tag{2}$$
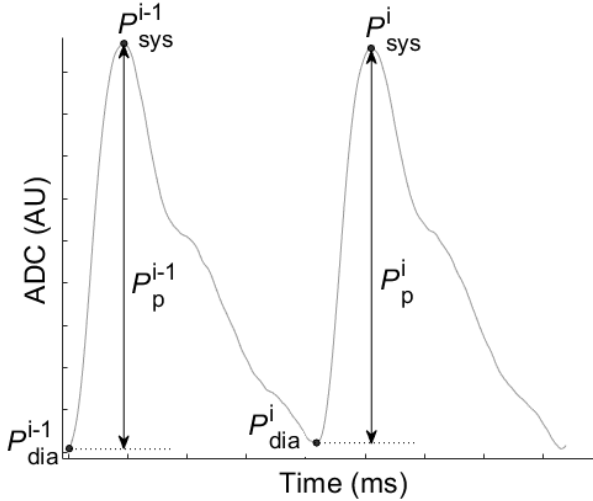
(a) Regular pulse waves with annotated pulse pressure P_p
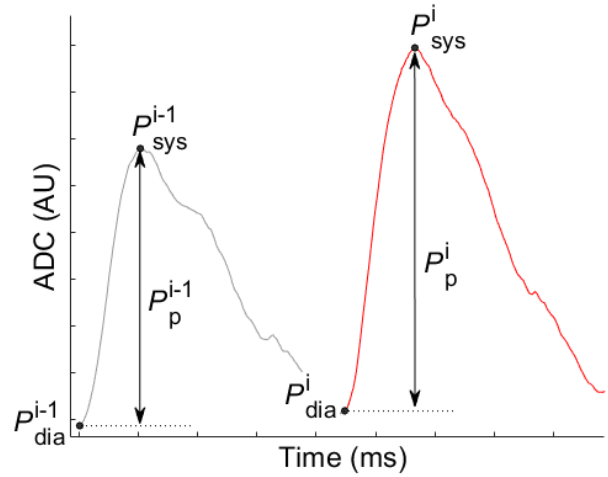
(b) Pulse wave with visibly greater pulse pressure compared to the preceding wave

Figure 4.7.: Comparison of a regular wave and an artefact wave, annotated due to abnormal increase of its pulse pressure.

With the same reasoning, succeeding waves with a change in Total Pulse Duration t_T of more than 30% are eliminated from the data set, as seen in figure 4.8.

$$\widetilde{P}^{\mathrm{i}} = \begin{cases} \widetilde{P}^{\mathrm{i}}, & \left| 1 - \frac{t_T^{\mathrm{i}}}{t_T^{i-1}} \right| \leq 0.3 \\ NaN, & \text{otherwise} \end{cases} \quad , i = 2, \ldots, N \qquad (3)$$
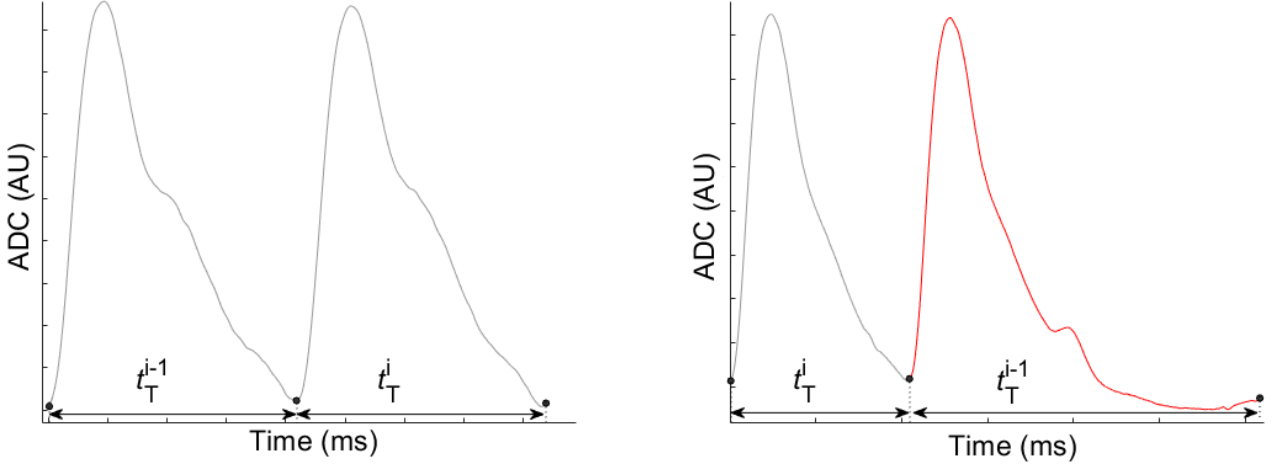
(a) Regular pulse waves with annotated total pulse duration t_{T}

(b) Pulse wave with visibly higher pules duration compared to the preceding wave

Figure 4.8.: Comparison of a regular wave and an artefact wave, annotated due to abnormal increase of its total pulse duration.

Complete loss of contact of the sensor is visible as constant offset, superposed with noise as seen in 4.9a. Spikes in the noise floor are classified as individual waves by the fragmentation algorithm. To remove these artefacts, a filter in the form of

$$\widetilde{P}^{\mathrm{i}} = \begin{cases} \widetilde{P}^{\mathrm{i}}, & \frac{\widetilde{P}_{\mathrm{sys}}^{\mathrm{i}}}{\widetilde{P}_{\mathrm{max}}} \leq 0.1 \\ NaN, & \text{otherwise} \end{cases} \quad , i = 2, \ldots, N \qquad (4)$$

where $\widetilde{P}_{\mathrm{max}}$ denotes the overall maximum of the remaining pulse wave data set, is applied.

45

(a) Loss of sensor contact visible as noisy flat line

(b) Pulse wave with significant level difference between onset and end
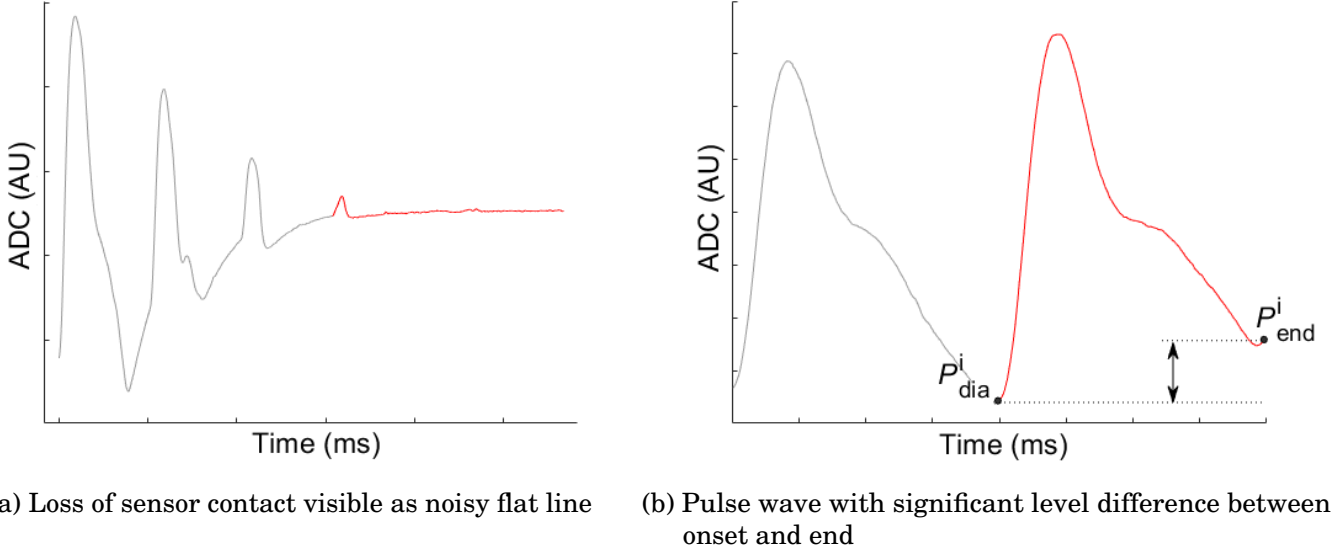
Figure 4.9.: Artefact waves annotated due to abnormal events

Furthermore, the value of the onset point is compared to the value at the wave's cessation. If the values differ by more than 10% of the current wave's maximum, the wave is discarded to prevent the distortion of pressure values during the feature extraction process, as depicted in 4.9b.

$$\widetilde{P}^{\mathrm{i}} = \begin{cases} \widetilde{P}^{\mathrm{i}}, & \left| \frac{\widetilde{P}^{\mathrm{i}}_{\mathrm{dia}} - \widetilde{P}^{\mathrm{i}}_{\mathrm{end}}}{\widetilde{P}^{\mathrm{i}}_{\mathrm{sys}}} \right| \leq 0.1 \\ NaN, & \text{otherwise} \end{cases}, i = 2, \dots, N \tag{5}$$

Lastly, to detect saturation effects, the flatness of the peak is evaluated. Hence, the absolute difference between the peak and the adjacent points is calculated by

$$P_{\mathrm{j}} = max(\widetilde{P}^{\mathrm{i}})$$
$$delta_1 = |P_{\mathrm{j}} - P_{\mathrm{j}-2}| + |P_{\mathrm{j}} - P_{\mathrm{j}+2}|$$
$$delta_2 = |P_{\mathrm{j}+10} - P_{\mathrm{j}+8}| + |P_{\mathrm{j}+10} - P_{\mathrm{j}+12}|$$
$$delta_3 = |P_{\mathrm{j}-10} - P_{\mathrm{j}-12}| + |P_{\mathrm{j}-10} - P_{\mathrm{j}-8}|.$$
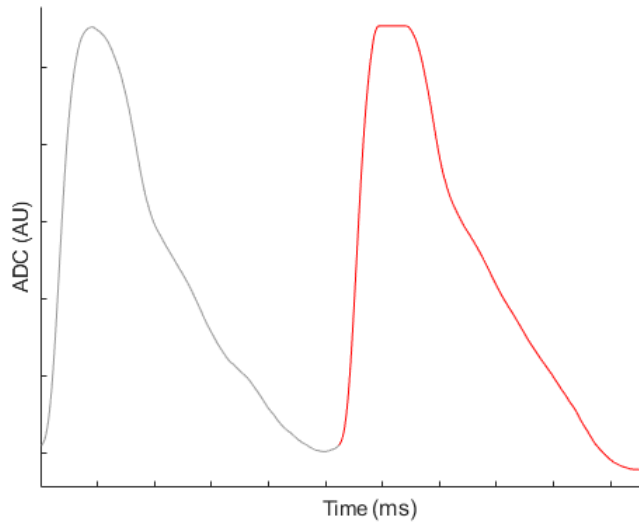
Figure 4.10.: Pulse wave with visible saturation effect

If saturation effects occur, the peak is cut off and thus pseudo constant, as seen in figure 4.10. The difference between adjacent points is therefore small:

$$\widetilde{P}^{\mathrm{i}} = \begin{cases} \widetilde{P}^{\mathrm{i}}, & delta_1 \wedge delta_2 \wedge delta_3 > 10 \\ NaN, & \text{otherwise} \end{cases} \tag{6}$$

The placement of P_{sys} on a pulse wave experiencing saturation effects is arbitrary. If the maximum is found directly at the rising or falling edge,

47

the condition $delta > 10$ is satisfied and the pulse wave is incorrectly accepted. The two additionally evaluated differences $delta_2$ and $delta_3$ guarantee that clipped waves are rejected. After refining the data set, the pre-processing is completed and the extraction algorithm can be applied.

4.3. Feature Extraction

The implemented algorithm extracts the Systolic Pressure P_{sys}, the Dicrotic Wave Pressure P_{dwp} and the Dicrotic Notch P_{notch} from the individual unmoved pulse waves. The process is illustrated as flowchart in figure 4.11. The following algorithms assess single pulse waves, therefore the superscripted running index i is omitted.
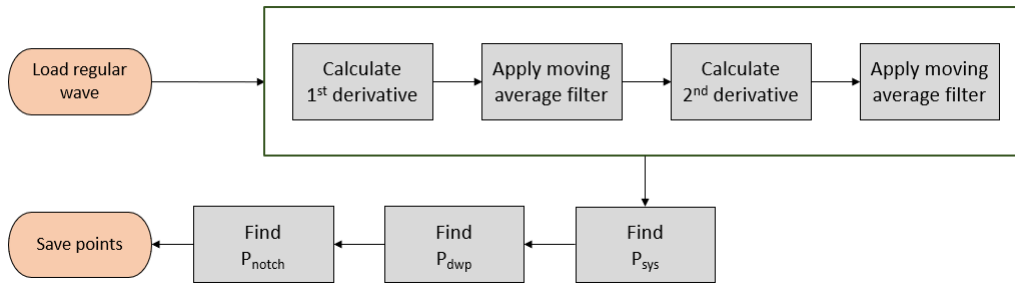
Figure 4.11.: Flowchart representation of the feature extraction procedure

To determine named points, the first derivative of the pulse wave in the form of

$$\dot{P} = P_{j} - P_{j-1},$$

is calculated, approximating the derivative with the difference of adjacent data points. This method introduces additional noise, originating from the finite sample frequency used to convert the analogous signal into a digital one. To counteract, a central moving average filter is applied:

$$\dot{P}_{f}(t) = \frac{1}{5} \sum_{j=-2}^{2} \dot{P}(t_{j})$$

Afterwards, the second derivative is calculated by

$$\ddot{P} = \dot{P}_{f,j} - \dot{P}_{f,j-1}$$

and thereafter filtered

$$\ddot{P}_{f}(t) = \frac{1}{5} \sum_{j=-2}^{2} \ddot{P}(t_{j}).$$

4.3.1. Systolic Pressure

As the Systolic Pressure is defined as the maximum value of the pulse wave, P_{sys} was identified by

$$P_{sys} = max(P(t)), \quad t \in [0, t_{T}].$$

The timing of P_{sys} is denoted by t_{sys}.

4.3.2. Dicrotic Wave Pressure

Dependent on the mechanical properties of the subject's arteries, the Dicrotic Wave Pressure is either visible as the pulse wave's second prominent peak (high elasticity) or overlapped by the falling edge of the forward travelling wave (high stiffness) [25, 11]. In the first case, the Dicrotic Wave Pressure classifies as local maximum. Followingly, it can be be found by examining the roots of the first derivative. In the other case, the Dicrotic Wave Pressure does not manifest as distinct peak. The slope only
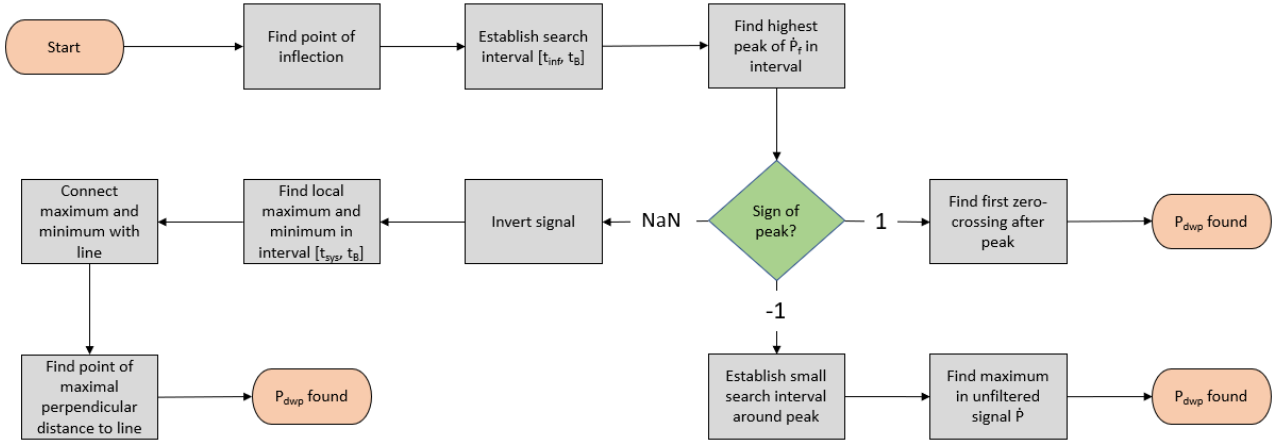
Figure 4.12.: Flowchart representation of the determination of P_{dwp} (Block P_{dwp} in figure 4.11)

approaches zero without actually reaching it. In this instance, the Dicrotic Wave Pressure can be defined as the point where the first derivative is closest to zero. This approach is commonly used in literature, for example in [44], and was thus deployed in a first attempt. To distinguish the cases, the algorithm applies the following steps which are depicted in figure 4.12.

- Establish the search interval containing P_{dwp}. For this, calculate the current heart rate by

$$f_{\mathrm{HR}} = \frac{1}{t_{\mathrm{T}}} \cdot 60 \ bpm,$$

where t_{T} denotes the total beat duration. The ratio of systole to diastole changes with varying heart rate. Thus, the right border t_{B} of the search interval containing P_{dwp} is determined by

$$t_{\mathrm{B}} = \begin{cases} t_{\mathrm{sys}} + \frac{1}{3} \cdot t_{\mathrm{T}}, & f_{\mathrm{HR}} \leq 75 & (systole : diastole \sim 1 : 2) \\ t_{\mathrm{sys}} + \frac{3}{8} \cdot t_{\mathrm{T}}, & 75 < f_{\mathrm{HR}} \leq 120 & (systole : diastole \sim 1 : 1) \\ t_{\mathrm{sys}} + \frac{5}{12} \cdot t_{\mathrm{T}}, & 120 < f_{\mathrm{HR}} & (systole : diastole \sim 2 : 1) \end{cases}$$

50

(a) Find peak with highest value in $\dot{P}$ in $[t_{\mathrm{inf}}, t_{\mathrm{B}}]$

(b) Annotated P_{dwp} in the pulse wave
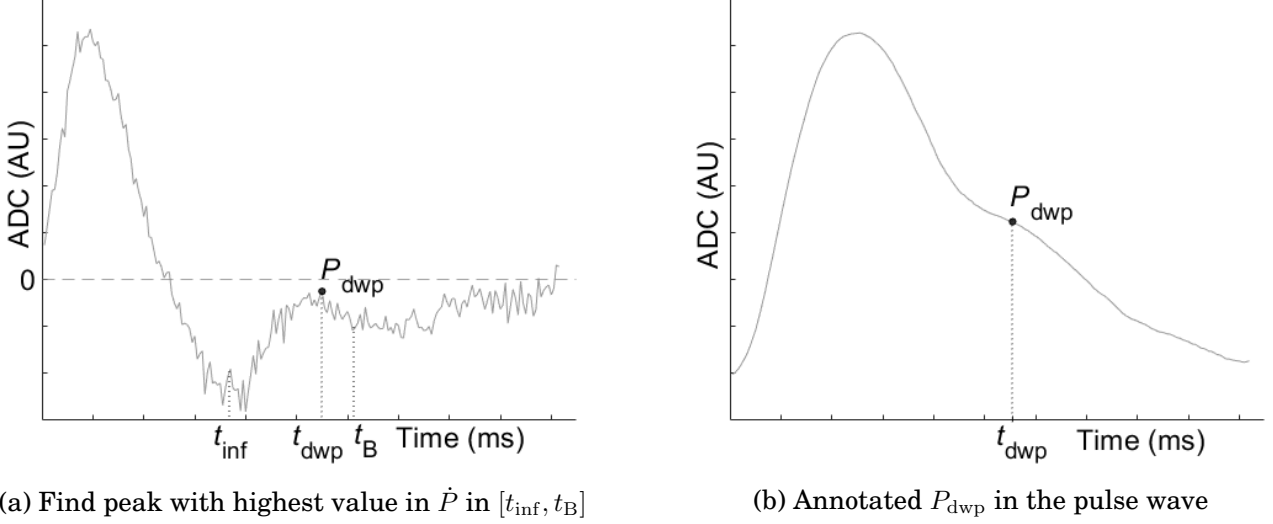
Figure 4.13.: Process of finding P_{dwp}.

- Determine the left border of the search interval by finding the timing of the point of inflection t_{inf} as first root of the second derivative $\ddot{P}_{\mathrm{f}}$ after t_{sys}.
- Find the highest valued peak of $\dot{P}_{\mathrm{f}}$ in the interval $[t_{\mathrm{inf}}, t_{\mathrm{B}}]$, as seen in figure 4.13a, and determine its sign.
- If $sign(peak) = 1$, a local maximum is found:
  - Find the first point pair defining a zero crossing of $\dot{P}_{\mathrm{f}}$ in the interval $[t_{\mathrm{peak}}, t_{\mathrm{B}}]$

$$(\dot{P}_{0,1}, \dot{P}_{0,2}) = (\dot{P}_{\mathrm{f,j}}, \dot{P}_{f,j-1}) : sign(\dot{P}_{\mathrm{f,j}}) - sign(\dot{P}_{\mathrm{f,j-1}}) \neq 0, \quad j = 1, \ldots, N$$

  - Define root from the point pair so that

$$\dot{P}_0 = min(|\dot{P}_{0,\mathrm{n}}|), \quad n = 1, 2$$

  - Starting from the root, respectively the time-wise corresponding point in the original Pulse Wave P, find the maximum in the interval $[t_{0,1}, t_{0,1} + 20ms]$

$$P_{\mathrm{dwp}} = max(P(t)) \quad t \in [t_{0,1}, t_{0,1} + 20ms]$$

since P_{dwp} may differ by a few index points, due to the applied central moving average filter.

- If $sign(peak) = -1$, no local maximum is found:
    - Determine the maximum of the unfiltered first derivative in the interval $[t_{\mathrm{peak}} - 20ms, t_{\mathrm{peak}} + 20ms]$

$$P_{\mathrm{dwp}} = max(\dot{P}(t)), \quad t \in [t_{\mathrm{peak}} - 20ms, t_{\mathrm{peak}} + 20ms],$$

    since P_{dwp} may again differ, due to the filtering process.

- If no peak is found:
    - Find the location of the minimum of $\dot{P}_{\mathrm{f}}$ in the interval $[0, t_{\mathrm{B}}]$,

$$t_{\mathrm{min}} = \{t \in [0, t_{\mathrm{B}}] \mid \dot{P}_{\mathrm{f}}(t) \ is \ minimum\}$$

    - Draw a line $y(t)$, connecting the interval's left border t_{min} at the level of the interval's minimum $\dot{P}_{f,min}$ and the interval's right border t_{B} at the level of the interval's maximum $\dot{P}_{f,max}$

$$y(t) = \frac{\dot{P}_{f,min} - \dot{P}_{f,max}}{t_{\mathrm{min}} - t_B}(t - t_B) + \dot{P}_{f,max} \quad t \in [t_{\mathrm{min}}, t_{\mathrm{B}}],$$

    - Find the Dicrotic Wave Pressure P_{dwp} as the point displaying the maximal perpendicular distance to $y(t)$

$$t_{\mathrm{dwp}} = \{t \in [t_{\mathrm{min}}, t_{\mathrm{B}}] \mid \dot{P}(t) - y(t) \ is \ minimum\}$$

4.3.3. Dicrotic Notch

Whether the Dicrotic Wave Pressure is a local maximum or not defines the process of finding the Dicrotic Notch P_{notch}, as seen in figure 4.14. If it is a local maximum, the Dicrotic Notch is found by determining the minimum of the unfiltered signal in the interval $[t_{\mathrm{sys}}, t_{\mathrm{dwp}}]$:

$$P_{\mathrm{notch}} = min(P(t)), \quad t \in [t_{\mathrm{sys}}, t_{\mathrm{dwp}}]$$
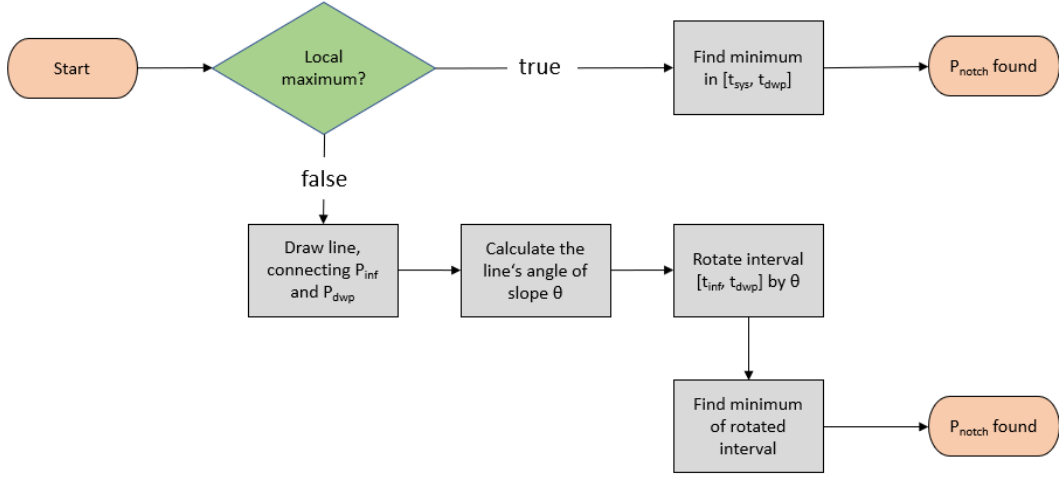
Figure 4.14.: Flowchart representation of the determination of P_{notch} (Block P_{notch} in figure 4.11)

In the opposite case, a wide-spread method of finding the Dicrotic Notch is determining the pulse wave's point of maximum curvature in the interval $[t_{\text{sys}}, t_{\text{dwp}}]$ [44]. The implementation and subsequent assessment proved to be unsatisfactory. Consequently, a new algorithm was sought:

- Consider the pulse wave in the interval $[t_{\text{inf}}, t_{\text{dwp}}]$ as seen in figure 4.15a

$$P_{\text{loc}} = P_{\text{f}}(t), \qquad t \in [t_{\text{inf}}, t_{\text{dwp}}]$$

- Calculate the angle of the line's slope connecting $P(t_{\text{inf}})$ and $P(t_{\text{dwp}})$

$$\theta = \arctan \frac{P_{\text{loc}}(t_{\text{inf}}) - P_{\text{loc}}(t_{\text{dwp}})}{t_{\text{dwp}} - t_{\text{inf}}}$$

- Rotate the considered interval counter-clockwise by θ, horizontally aligning $P_{\text{loc}}(t_{\text{min}})$ and $P_{\text{loc}}(t_{\text{dwp}})$ as seen in figure 4.15b

$$\begin{bmatrix} t' \\ P'_{\text{loc}} \end{bmatrix} = R \cdot \begin{bmatrix} t \\ P_{\text{loc}} \end{bmatrix}, \qquad R = \begin{bmatrix} cos\theta & -sin\theta \\ sin\theta & cos\theta \end{bmatrix}$$

- Find the Dicrotic Notch as minimum of P'_{loc}

$$P_{\text{notch}} = min(P'_{\text{loc}}).$$

53

(a) Localised pulse wave P_{loc} and angle of rotation θ (b) Rotatet localised pulse wave P'_{loc}. The minimum is P_{notch}
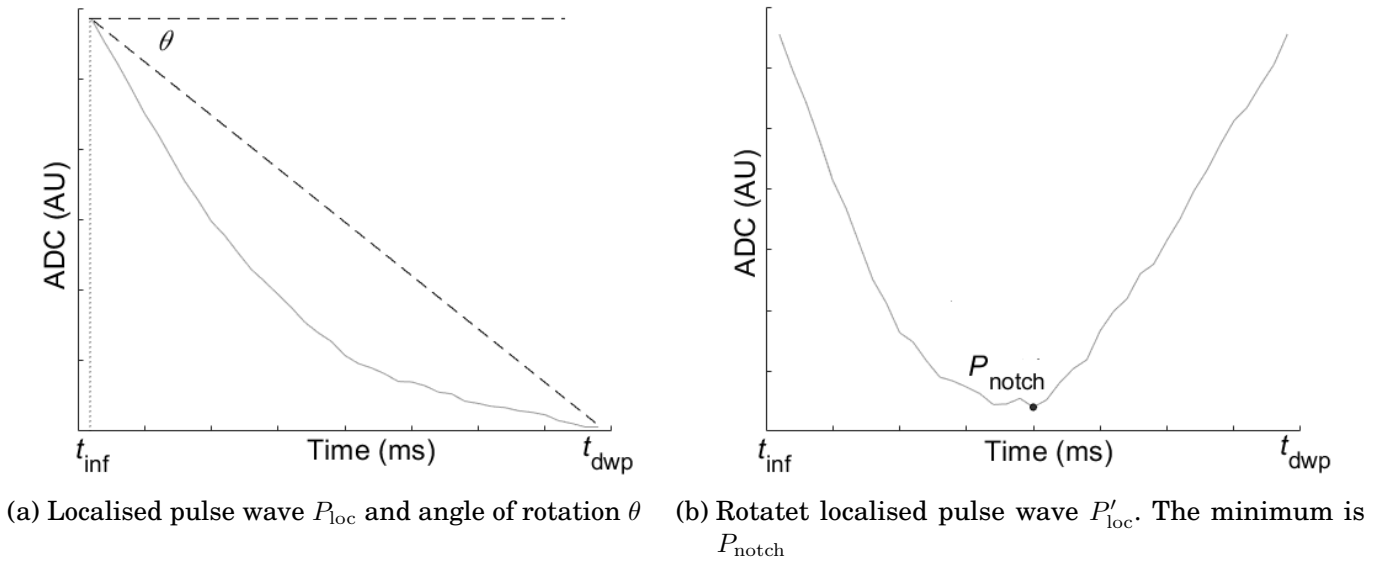
Figure 4.15.: Process of finding P_{notch}.

4.4. Statistics

Up until now, P_{sys}, P_{notch} and P_{dwp} denoted the absolute pressure value, measured from the zero line. However, the absolute values change significantly due to the signal beat introduced by the respiration, falsifying the results, as seen in figure 4.16.
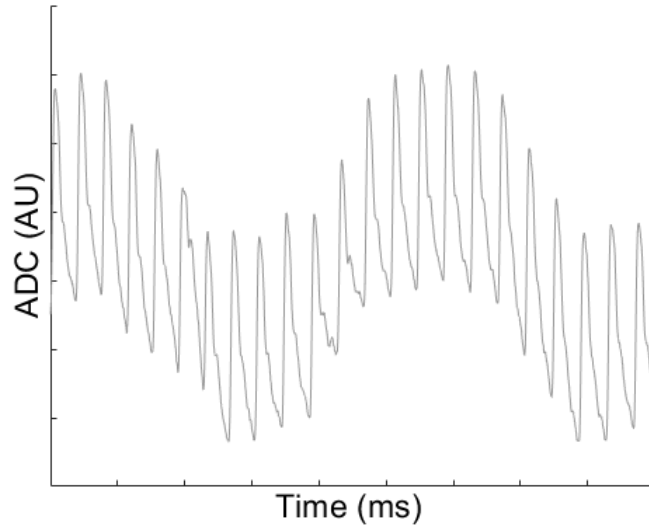
Figure 4.16.: Signal beat introduced by the respiration.

To assess the changes of the pulse waves per se, it was deemed more sound to evaluate the amplitudes, i.e. the points' difference to the baseline P_{dia}. Thus, in the following, P_{sys}, P_{notch} and P_{dwp} denote the respective amplitudes. To assess the pulse waves' contour, various parameters as seen in figure 4.17 were extracted.

The amplitudes P_{sys}, P_{notch} and P_{dwp}, their timings with respect to the waves' onset, as well as their mutual differences schematically denoted by $t_{\text{xy}} = t_{\text{y}} - t_{\text{x}}$ with $x, y \in S, N, D, E$ are depicted. While assessing the pulse wave data, a sudden, non-physiological increase or decrease in magnification was visible in few sections, as seen in figure 4.18.
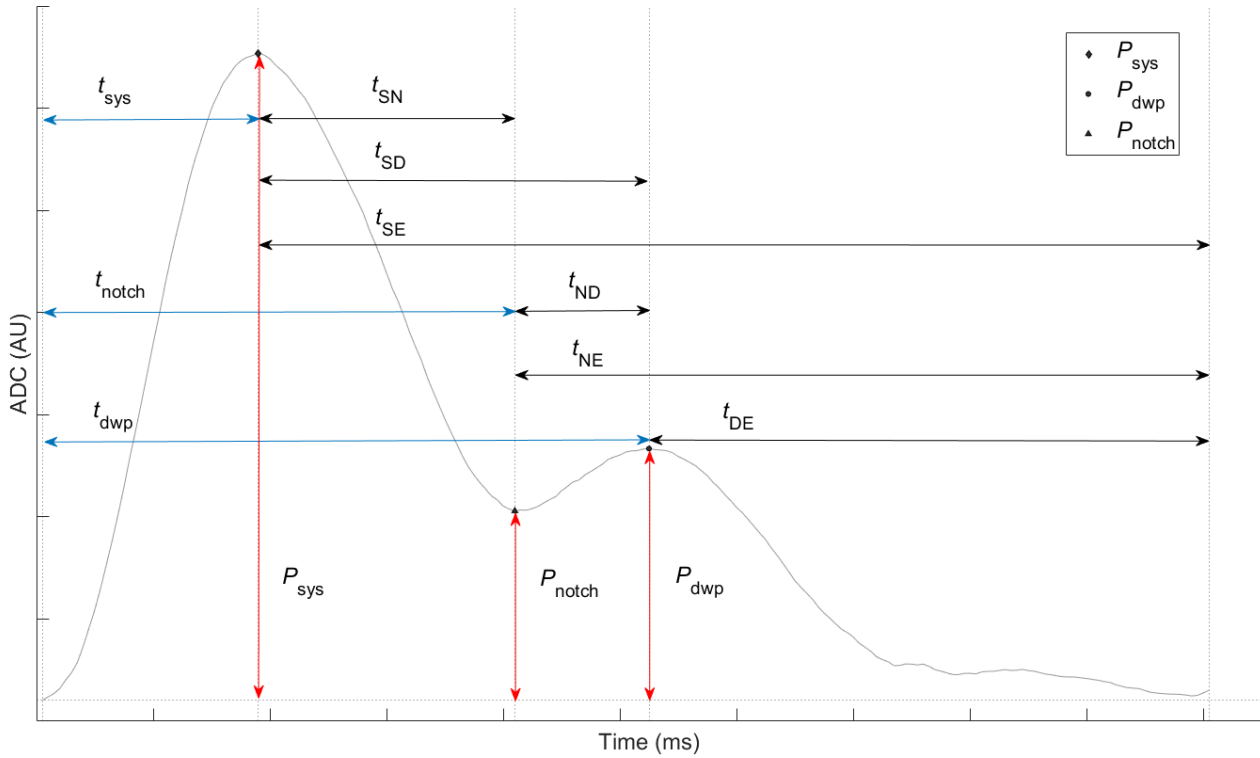
Figure 4.17.: Annotated pulse wave with marked amplitudes and timings.

The reason for these effects is unknown but thought to be originated from the used metrological instrument. To eliminate the possibility that these effects affect the overall evolution of the amplitudes, the following ratios were introduced:

$$P'_{\text{notch}} = \frac{P_{\text{notch}}}{P_{\text{sys}}}$$

$$P'_{\text{dwp}} = \frac{P_{\text{dwp}}}{P_{\text{sys}}}$$

$$P'_{\text{ND}} = \frac{P_{\text{notch}}}{P_{\text{dwp}}}.$$

56
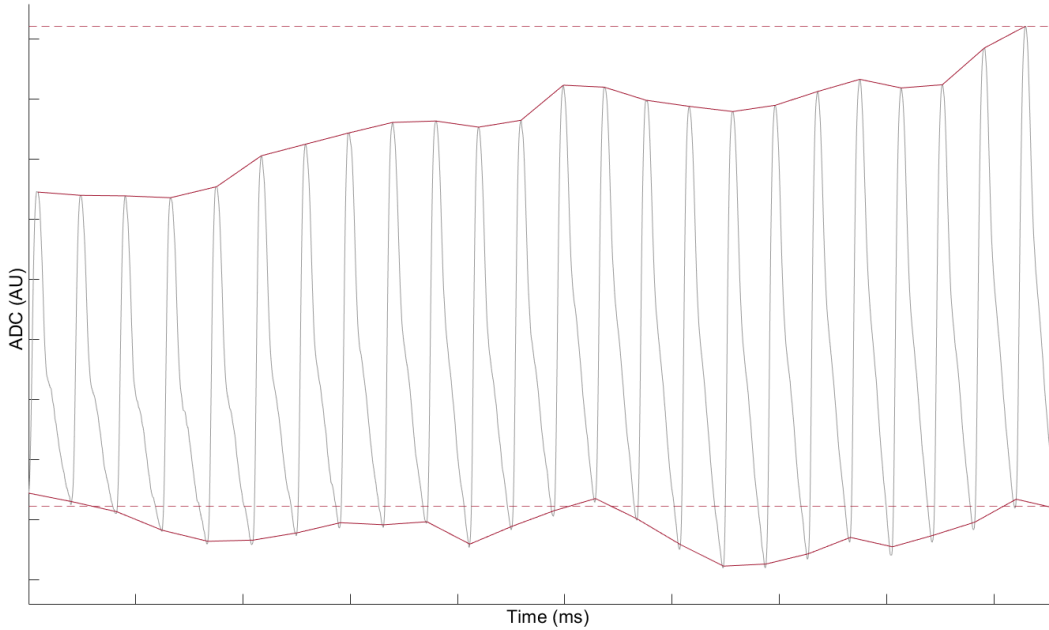
Figure 4.18.: Visible change in magnification, presumably originated from the used metrological instrument

Furthermore, every timing in figure 4.17 was also assessed with respect to the total pulse duration t_T in the form of

$$t' = \frac{t}{t_\text{T}}.$$

To assess the evolution of the pulse waves' contour over time, a moving average was applied to all parameters. The extracted features were averaged per subject in a retrospective window of 180 seconds with a shift of 10 seconds, starting at minute three. The averaging process removes short-term fluctuations as well as outliers and thus smooths the signal. Pulse waves which were annotated as artefact were excluded from the data set and therefore treated as missing values. Subsequently, the mean across all subjects was calculated and depicted along with the 95% confidential interval. Additionally, the data set was divided in three subsets for direct statistical comparison. In order to remove the transition

phases, the length of each subset was set to three minutes. The first subset spanned the first three minutes, representing the baseline. The second subset covered minute seven to minute ten, representing the end of the guided breathing phase. The last subset contained the features of minute twelve to fifteen, representing the end of the cooling phase. The extracted values were averaged within the subsets, as well as displayed as boxplots. To assess the overall difference between the subsets, a repeated measure ANOVA for paired samples was performed. To further specify between which frames the differences occur, the Bonfferoni post hoc test was applied. The resulting p-values indicate the significance of differences between the subsets, where a low p-value corresponds to a high significance. The level of significance α is assumed to be 5%, thus, the null-hypothesis of the test can be rejected when $p < 0.05$.

5. Results

Chapter 5 is divided in two parts. In section 5.1, the algorithm itself is evaluated based upon visual examinations of the annotated features. The actual outcome of the application to the data sets is presented in section 5.2. The results are displayed by absolute values, by the features' function over time and by a boxplot representation.
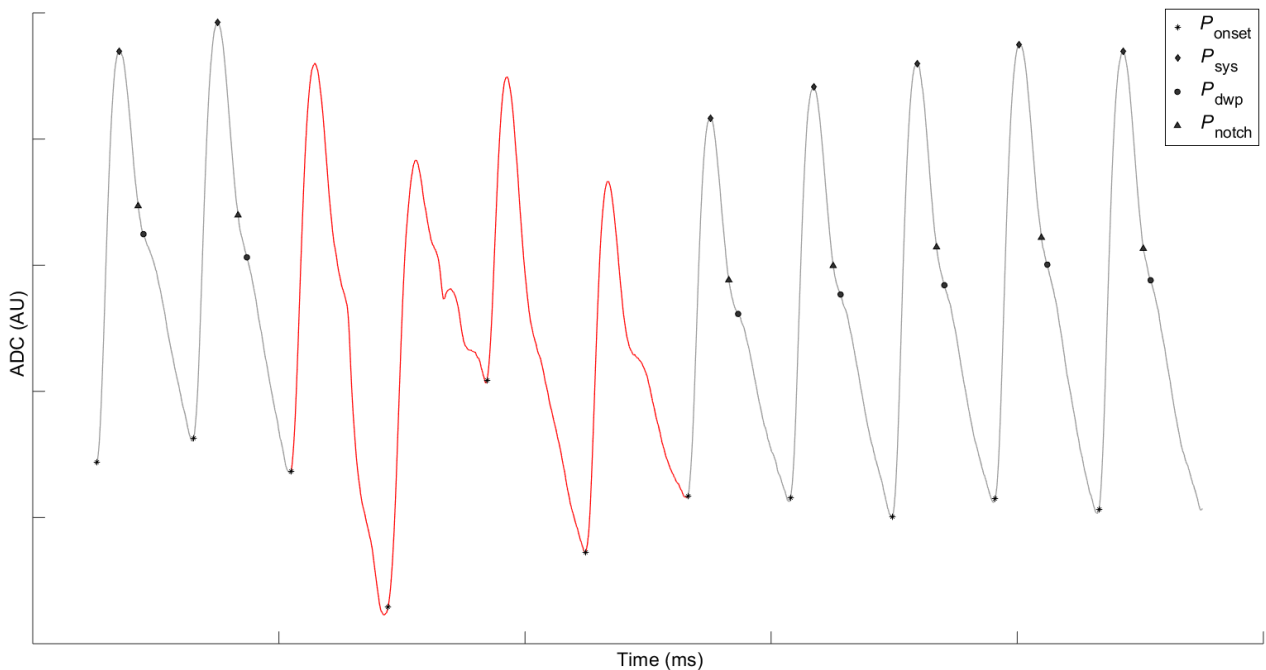
Figure 5.1.: Segment of pulse wave data with annotated points. Waves, identified as artefacts, are plotted in red and excluded from the annotation algorithm.

5.1. Algorithm

The algorithm robustly detects the wave onset points, enabling the fragmentation into singular pulse waves. Overall, 33000 pulse waves were detected and separated. Through a strict pulse selection process, the data is initially prepared for the feature extraction algorithm. Detected artefacts were annotated and excluded, an example is given in figure 5.1. The measure taking effect in shown segment is the exclusion of waves with an apparent difference between the values of onset point and point of cessation. Table 5.1 shows the on average annotated waves per subjects due to the deployed filter, separated by criterion found in section 4.2.3.

Criterion	Annotated waves	Percentage (total waves)
1	3.77 (3.64)	0.34 % (113)
2	8.93 (9.72)	0.81 % (268)
3	1.9 (2.07)	0.17 % (57)
4	3.97 (18.15)	0.36 % (119)
5	168.07 (122.66)	15.28 % (5042)
6	22.33 (34.59)	2.03 % (670)
Σ	208.97 (129.16)	19.00 % (6269)

Table 5.1.: Results of the artefact annotation filter. The results are presented as mean (standard deviation) per filter criterion and in percentage of the 33000 overall extracted waves. The criteria are described in section 4.2.3

The remaining pulse waves were analysed, relevant features were annotated and saved, as examplarily seen in figure 5.2a. Visual examination of a magnitude of waves revealed a high accuracy, even though few samples were found to be unsatisfactory, for example in figure 5.2b. In the depicted case a distinct elevation of the curve is visible where one would assume the location of P_{dwp}, as indicated by the manual annotation $P_{dwp,m}$. The Dicrotic Notch was marked accurately while P_{dwp} slid down to the right.
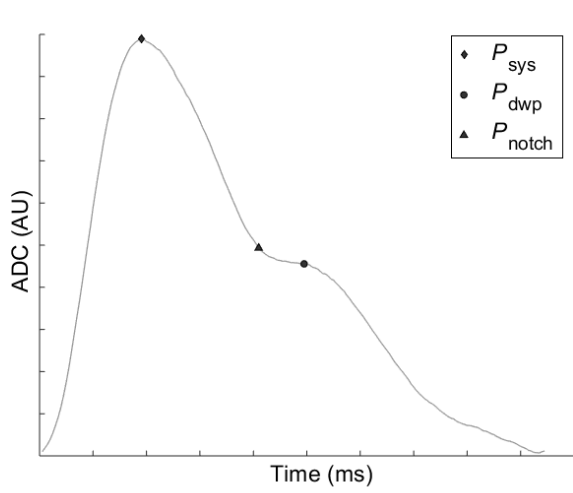
(a) Exemplaric pulse wave with correctly annotated points of interest
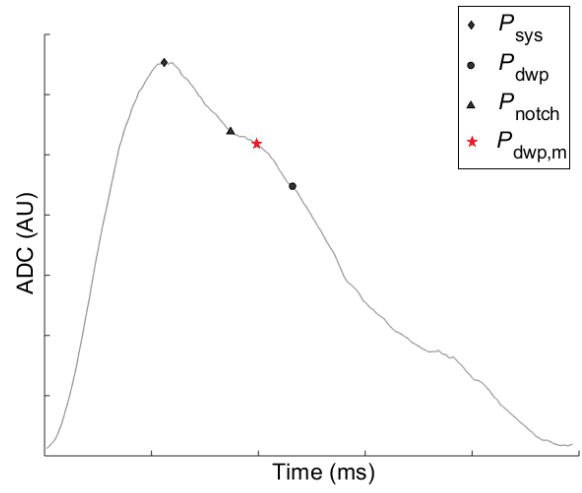
(b) Pulse wave with inaccurately annotated point P_{dwp} and the actual location as indicated by $P_{dwp,m}$

Figure 5.2.: Results of the annotation algorithm.
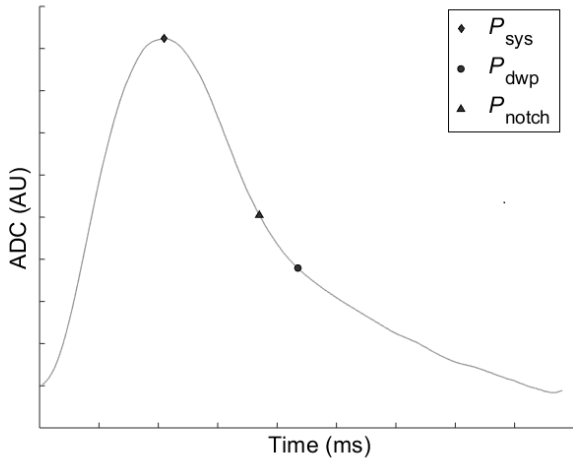
(a) Featureless pulse wave
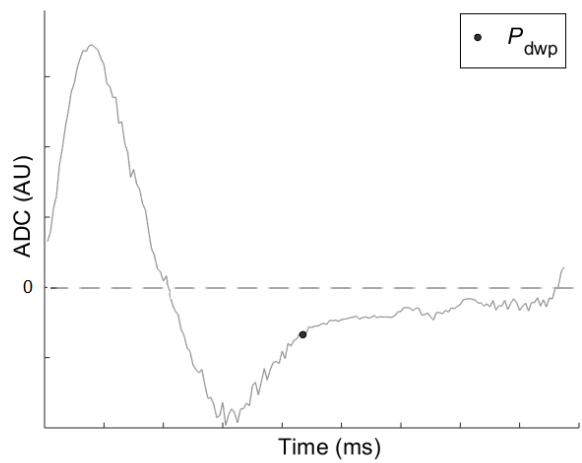
(b) First derivative of a featureless pulse wave with estimated P_{dwp}

Figure 5.3.: To determine the points of interest of depicted featureless pulse waves, a workaround algorithm was implemented.

Additionally, two data sets displayed a high amount of pulse waves which could be described as featureless. Beside the ever dominant Systolic Pressure peak shown in figure 5.3a, no other distinguishable features catch the eye. The concave falling flank of the pulse exhibits no remarkable change in slope and therefore no peak in its first derivative 5.3b, rendering manual and automatic annotation arbitrary. To estimate P_{dwp}, a workaround algorithm was deployed which is deemed sufficient and described in section 4.3.2.

5.2. Features

Section 5.2 presents the results of the applied extraction algorithm by value. Table 5.2 and 5.3 contain collectively the results as described in section 4.4.

5.2.1. Amplitudes and Amplitude Ratios

The evolution of the 3-min average of amplitudes pictured in figure 5.4 shows a steady decline in value. The 3-min averaged Systolic Pressure Amplitude drops by a total of 3701.10 AU (-19.19%), the Dicrotic Notch Amplitude by $1957, 83$ AU (-17.61%) and the Dicrotic Wave Amplitude by 1651.04 AU (-17.12%) (table 5.2). The same decrease is visible in the boxplot representation in figures 5.6 - 5.8. Considering the first and second window, only P_{sys} shows a significant difference in amplitude ($p = 0.036$). In contrast, all amplitudes show significant differences between the first and the last window ($P_{\text{sys}} : p = 0.007, P_{\text{notch}} : p = 0.011, P_{\text{dwp}} : p = 0.013$).

The evolution of the amplitude ratios is depicted in figure 5.5. While P'_{ND} shows a rather steady decline from 1.15 to 1.13 (-1.50%), P'_{notch} and P'_{dwp} drop from 0.58 and 0.50 to their minimum of 0.56 (-2.70%) and 0.49 (-2.03%), subsequently increasing again to their final values of 0.59 $(+1.49\%)$ and 0.52 $(+2.79\%)$. The application of the repeated measurement ANOVA yields non-significance throughout the different time

	3-min averaged Parameters							
Parameter	0 - 3 minutes	7 - 10 minutes	12 - 15 minutes	ANOVA	p-value 1-2	p-value 2-3	p-value 1-3	Unit
Amplitudes								
P_{sys}	19289.84 (7224.35)	17066.80 (8653.80)	15588.74 (9553.15)	0.0065	0.036	0.150	0.007	AU
P_{notch}	11116.64 (4968.28)	9965.74(5634.27)	9158.81 (5734.04)	0.0123	0.089	0.195	0.011	AU
P_{dwp}	9640.51 (4050.34)	8659.53 (4619.52)	7989.47 (4800.39)	0.0169	0.101	0.232	0.013	AU
Amplitude Ratios								
$P_{\text{notch}}/P_{\text{sys}}$	0.5751 (0.1450)	0.5745 (0.1462)	0.5837 (0.1469)	0.3509	1.000	0.238	1.000	1
$P_{\text{dwp}}/P_{\text{sys}}$	0.5041 (0.1114)	0.5089 (0.1152)	0.5182 (0.1161)	0.1762	1.000	0.214	0.357	1
$P_{\text{notch}}/P_{\text{dwp}}$	1.1479 (0.1560)	1.1342 (0.1460)	1.1306 (0.1311)	0.0997	0.188	1.000	0.257	1
Absolute Timings								
t_{sys}	187.37 (32.68)	183.14 (32.14)	185.59 (34.14)	0.2319	0.213	0.536	1.000	ms
t_{notch}	339.33 (17.86)	333.34 (20.06)	333.76 (19.31)	0.0009	<0.001	1.000	0.002	ms
t_{dwp}	398.78 (24.82)	392.19 (21.85)	392.13 (18.89)	0.0328	0.028	1.000	0.118	ms
t_{T}	894.63 (137.25)	868.06 (144.78)	876.16 (140.35)	0.0022	<0.001	0.118	0.042	ms
f_{HR}	68.67 (9.73)	71.00 (10.99)	70.23 (10.48)	0.0025	0.001	0.086	0.045	bpm

Table 5.2.: 3-min average of extracted and derived Parameters. Data are expressed as mean (standard deviation). Column ANOVA comprises the p-value result of the ANOVA itself, whereas the numbered p-value columns contain the result of the post-hoc test, where the numbers indicate which time frames were compared.

Parameter	0 - 3 minutes	7 - 10 minutes	12 - 15 minutes	ANOVA	p-value 1-2	p-value 2-3	p-value 1-3	Unit
			3-min averaged Parameters					
			Mutual Timings					
t_SN	151.96 (33.03)	150.20 (33.27)	148.17 (34.34)	0.2402	1.000	0.966	0.534	ms
t_SD	211.42 (32.97)	209.05 (34.56)	206.54 (35.27)	0.1978	0.940	0.818	0.412	ms
t_SE	707.27 (126.17)	684.92 (136.17)	690.57 (130.67)	0.0088	0.003	0.474	0.080	ms
t_ND	59.45 (19.51)	58.85 (16.60)	58.37 (14.08)	0.6458	1.000	1.000	1.000	ms
t_NE	555.31 (128.88)	534.72 (134.83)	542.40 (130.60)	0.0072	0.001	0.073	0.161	ms
t_DE	495.85 (126.21)	475.87 (135.13)	484.03 (131.72)	0.0082	0.002	0.035	0.196	ms
			Timing Ratios					
$t_\mathrm{sys}/t_\mathrm{T}$	0.2118 (0.0338)	0.2142 (0.0370)	0.2144 (0.0364)	0.4752	1.000	1.000	1.000	1
$t_\mathrm{notch}/t_\mathrm{T}$	0.3866 (0.0471)	0.3921 (0.0503)	0.3884 (0.0472)	0.0669	0.045	0.026	1.000	1
$t_\mathrm{dwp}/t_\mathrm{T}$	0.4542 (0.0551)	0.4618 (0.0625)	0.4569 (0.0594)	0.0858	0.093	0.024	1.000	1
$t_\mathrm{SN}/t_\mathrm{T}$	0.1748 (0.0482)	0.1780 (0.0487)	0.1740 (0.0496)	0.2672	0.410	0.245	1.000	1
$t_\mathrm{SD}/t_\mathrm{T}$	0.2424 (0.0536)	0.2477 (0.0587)	0.2425 (0.0591)	0.1766	0.217	0.117	1.000	1
$t_\mathrm{SE}/t_\mathrm{T}$	0.7882 (0.0338)	0.7858 (0.370)	0.7856 (0.0364)	0.4752	1.000	1.000	1.000	1
$t_\mathrm{ND}/t_\mathrm{T}$	0.0676 (0.0217)	0.0697 (0.0231)	0.0685 (0.0206)	0.6458	0.690	1.000	1.000	1
$t_\mathrm{NE}/t_\mathrm{T}$	0.6134 (0.0471)	0.6079 (0.0503)	0.6116 (0.0472)	0.0669	0.045	0.026	1.000	1
$t_\mathrm{DE}/t_\mathrm{T}$	0.5458 (0.0551)	0.5382 (0.0625)	0.5431 (0.0594)	0.0858	0.093	0.024	1.000	1

Table 5.3.: 3-min average of extracted and derived Parameters. Data are expressed as mean (standard deviation). The notation of mutual timings is $t_\mathrm{xy} = t_\mathrm{y} - t_\mathrm{x}$, where $x, y \in \{S, N, D, E\}$ and S, N, D, E denotes the timing of P_sys, P_notch, P_dwp and the end of the wave, respectively. All timing ratios t' are calculated with respect to the individual total duration of the pulse waves. Column ANOVA comprises the p-value result of the ANOVA itself, whereas the numbered p-value columns contain the result of the post-hoc test, where the numbers indicate which time frames were compared.

frames which is corroborated by their respective boxplots in figures 5.9 -
5.11.
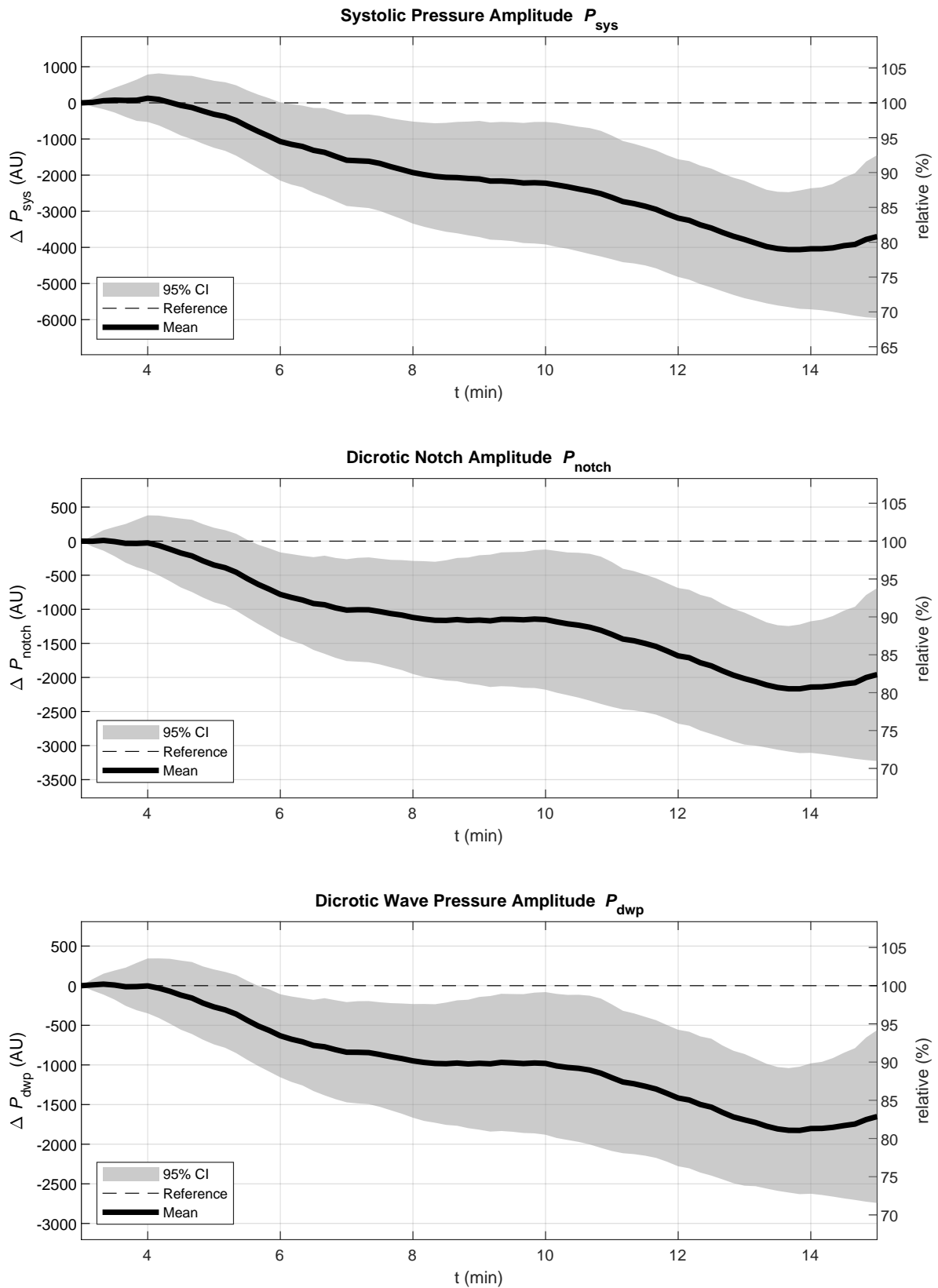
Figure 5.4.: 3-min average of extracted amplitudes.
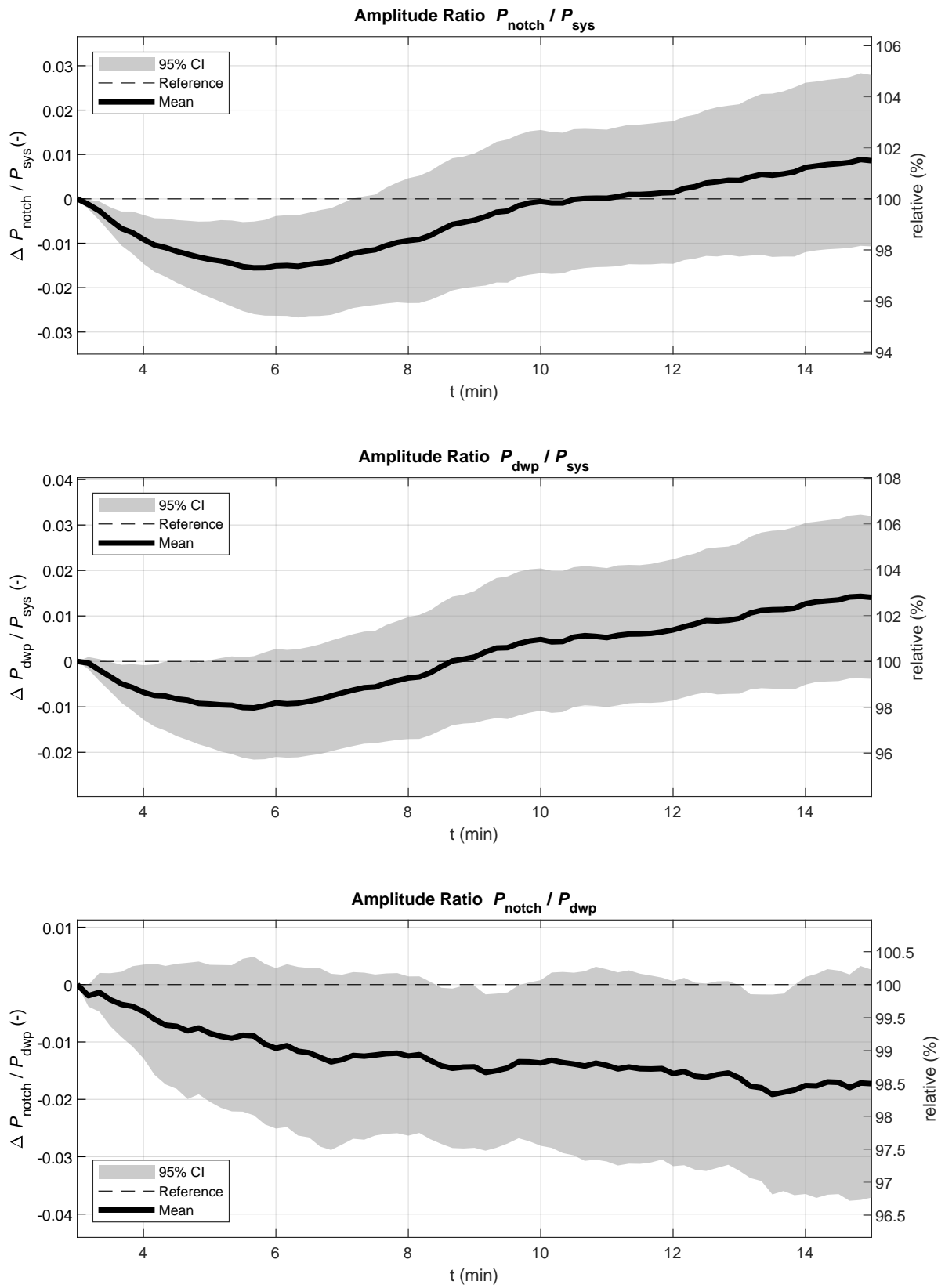
Figure 5.5.: 3-min average of amplitude ratios.
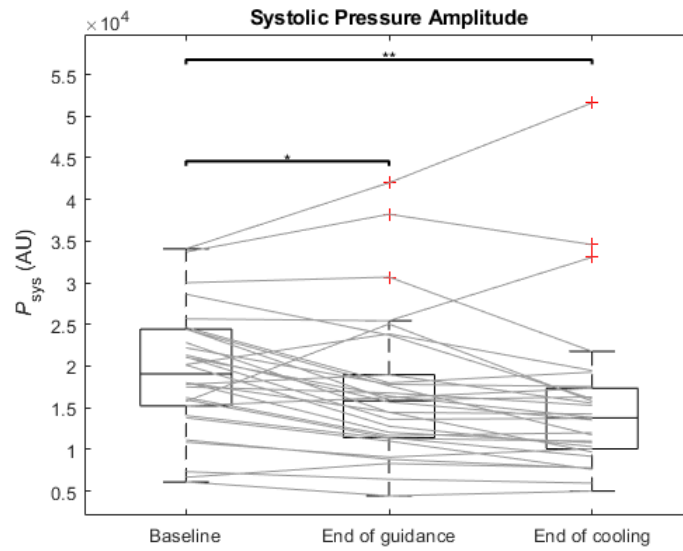
Figure 5.6.: Boxplot of the Systolic Pressure Amplitude. The stars are indicating the level of significance α, where a single star means $p \leq 0.05$ and two stars represent $p \leq 0.01$.
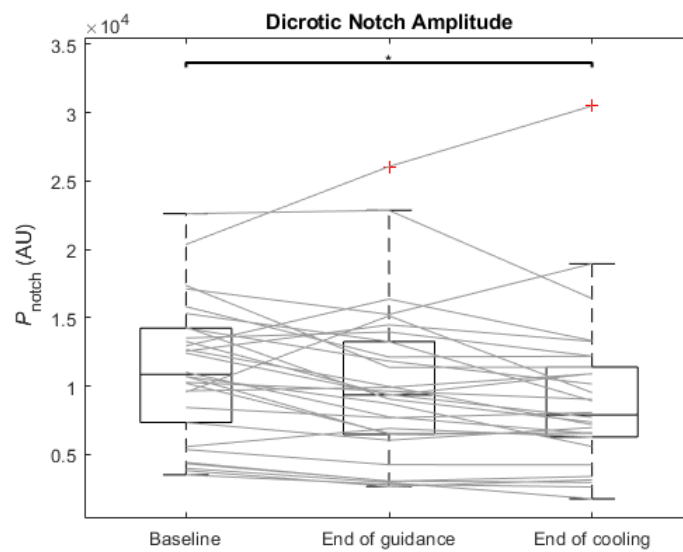
Figure 5.7.: Boxplot of the Dicrotic Notch Amplitude. The star is indicating the level of significance α, where a single star means $p \leq 0.05$.
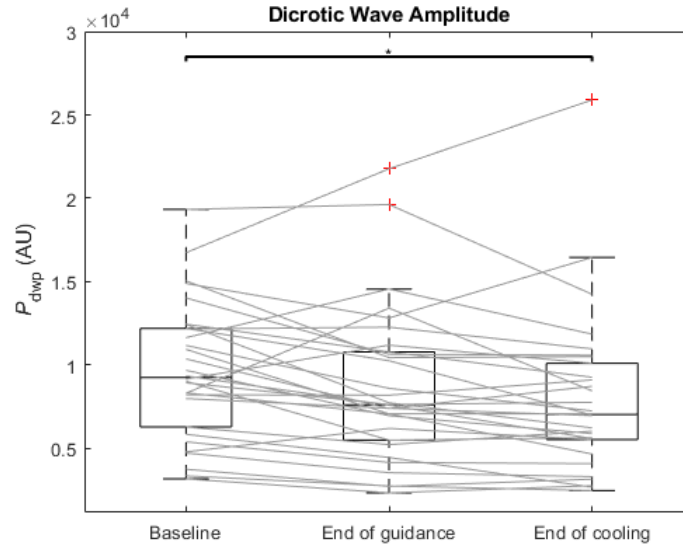
Figure 5.8.: Boxplot of the Dicrotic Wave Amplitude. The star is indicating the level of significance α, where a single star means $p \leq 0.05$.
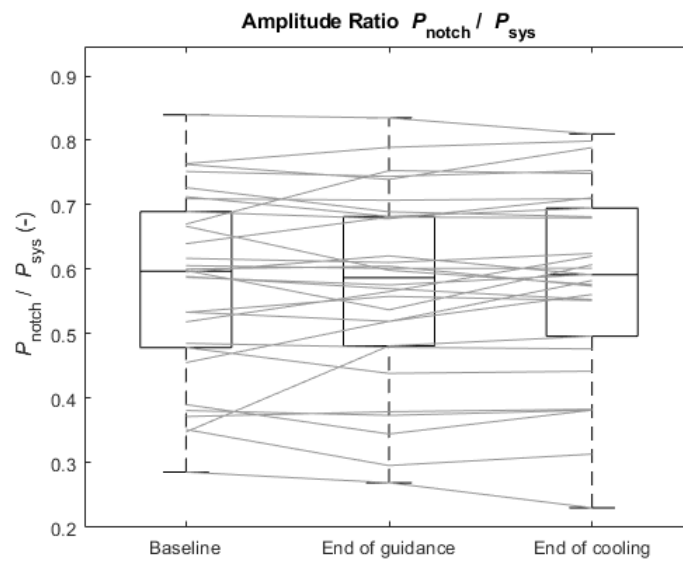
Figure 5.9.: Boxplot of $P'_{\text{notch}} = P_{\text{notch}}/P_{\text{sys}}$.

Amplitude Ratio P_{dwp} / P_{sys}
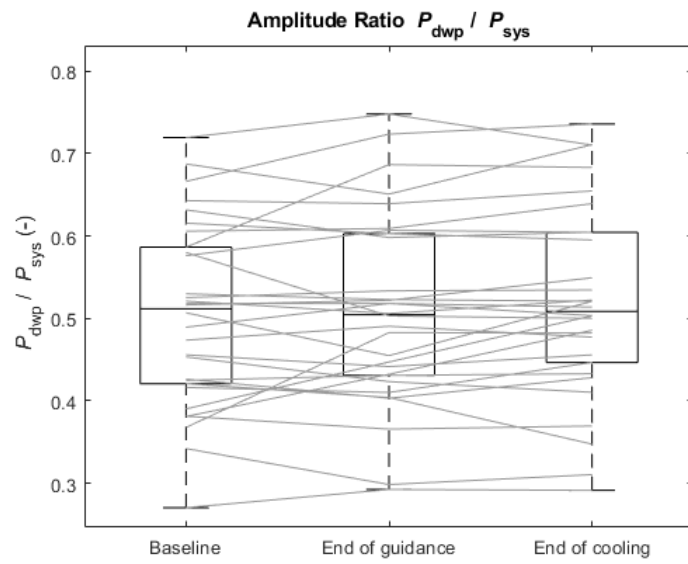
Figure 5.10.: Boxplot of $P'_{dwp} = P_{dwp}/P_{sys}$.

Amplitude Ratio P_{notch} / P_{dwp}
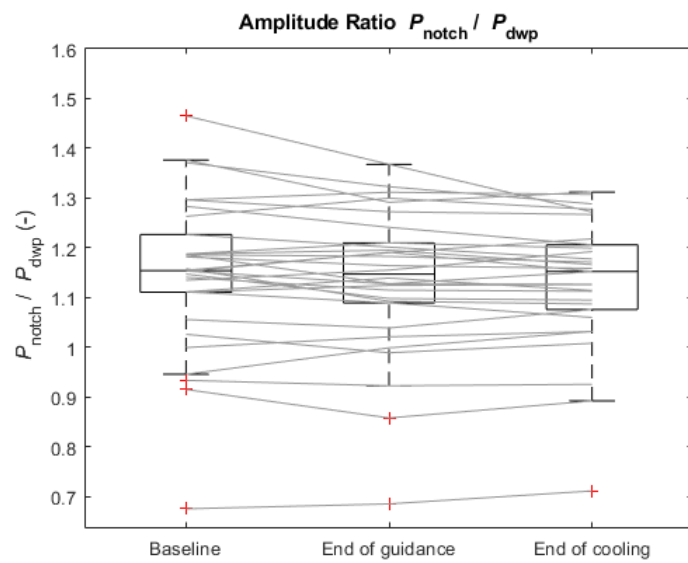
Figure 5.11.: Boxplot of $P'_{ND} = P_{notch}/P_{dwp}$.

5.2.2. Timings and Timing Ratios

Figure 5.14 shows the 3-min average evolution of the total pulse duration t_T and the ejection duration t_{notch}, measured as the interval between P_{notch} and the wave's onset. The total pulse duration and the ejection duration t_{notch} show a significant drop between the first and second window ($p < 0.001$) and between the first and third window ($t_T : p = 0.042$ and $t_{notch} : p = 0.002$), respectively, as depicted in figure 5.12 and 5.13.
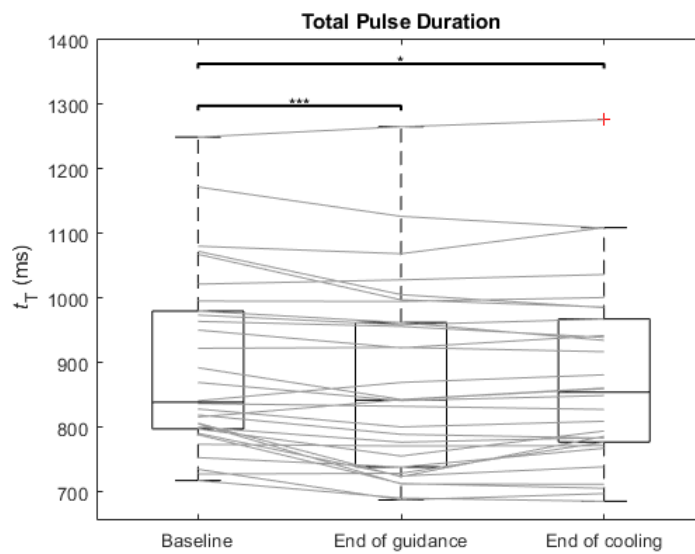
Figure 5.12.: Boxplot of t_T. The stars are indicating the level of significance α, where a single star means $p \leq 0.05$ and three stars represent $p \leq 0.001$.
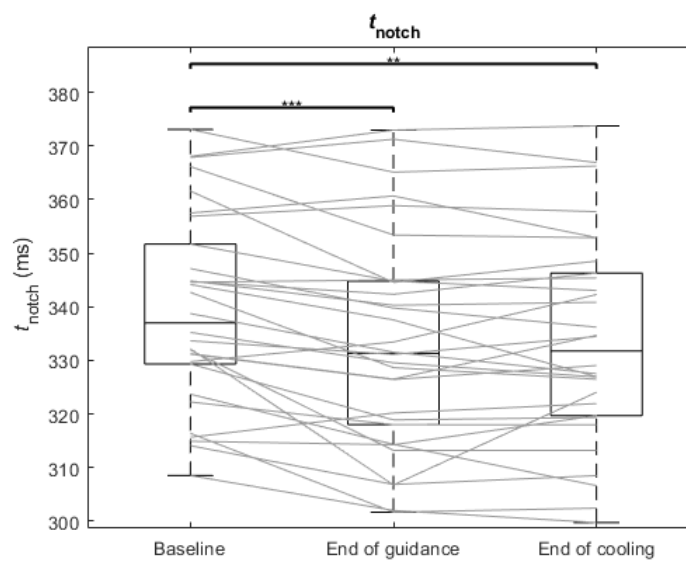
Figure 5.13.: Boxplot of the absolute timing of the Dicrotic Notch. The stars are indicating the level of significance α, where a two star means $p \leq 0.01$ and three stars represent $p \leq 0.001$.
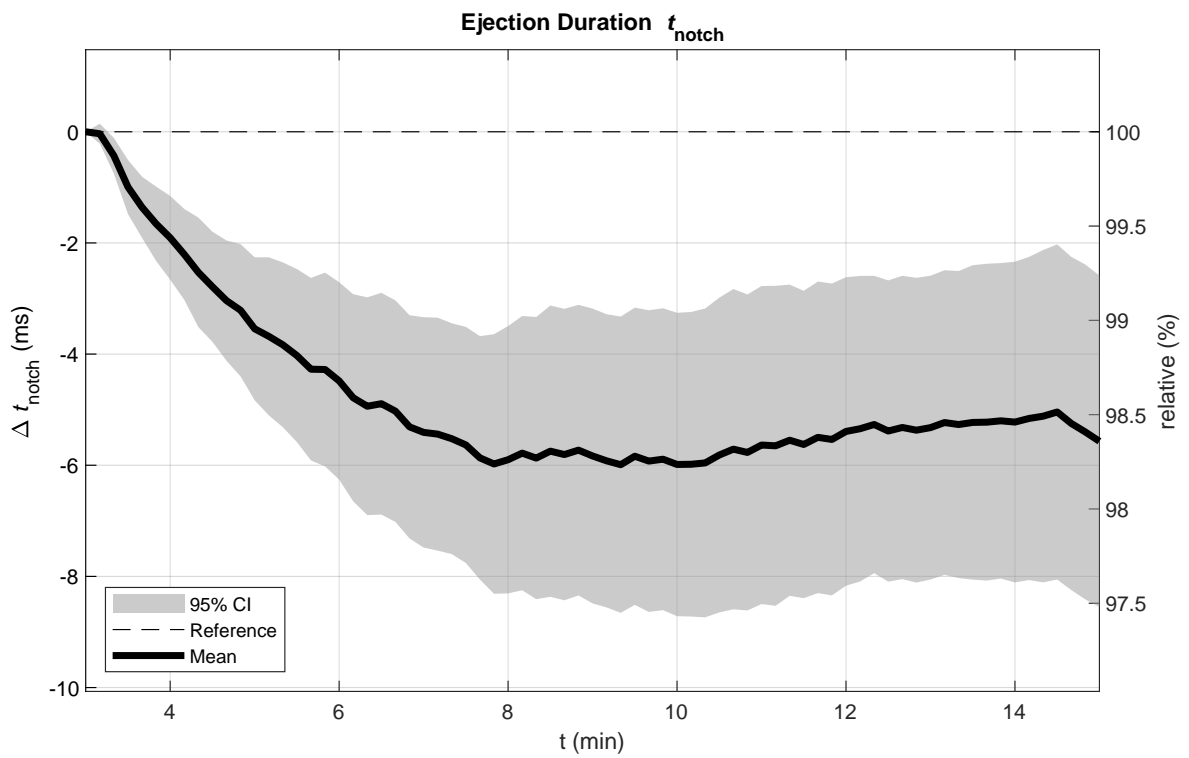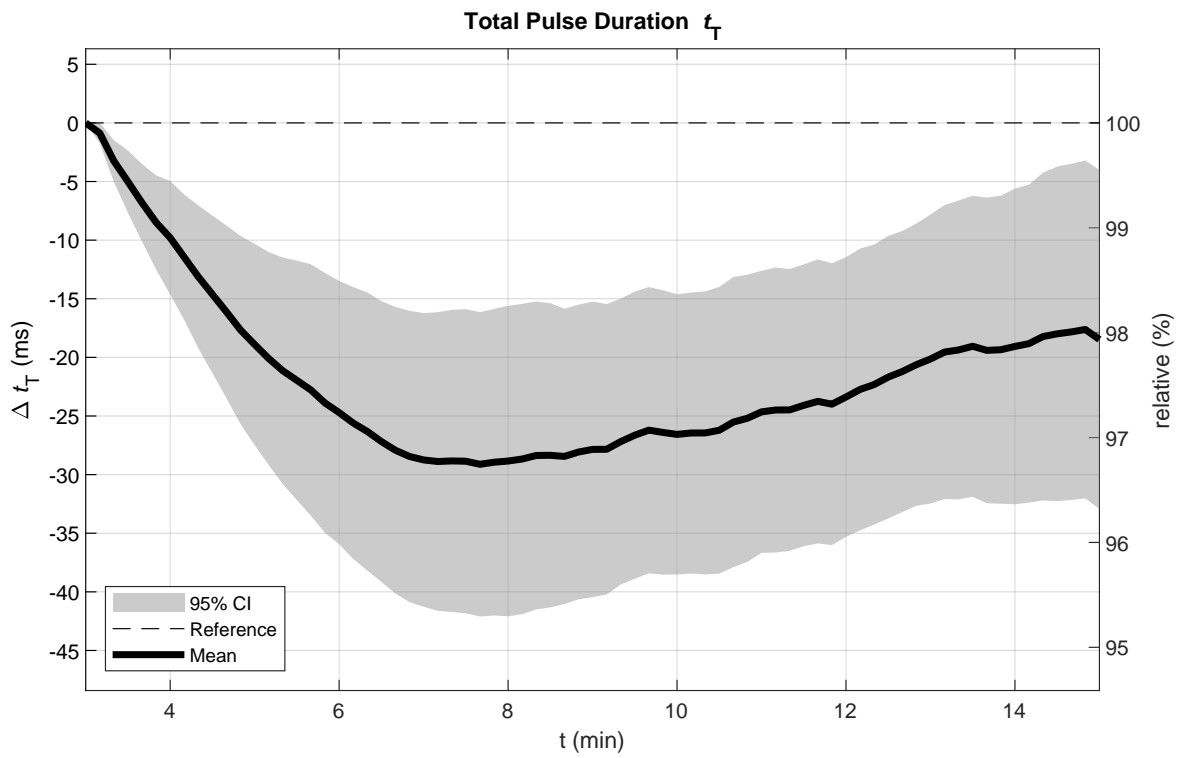
Figure 5.14.: 3-min average of the total pulse duration t_{T} and the ejection duration t_{notch}.

5. Results

The evolution of t'_{sys}, t'_{notch} and t'_{dwp} is depicted in figure 5.15. The timings t'_{notch} and t'_{dwp} show a similar behaviour, an initial increase by a maximum of $+1.91\%$ and $+2.22\%$, followed by a decrease to a final value of $+0.45\%$ and $+0.60\%$ (see table 5.3). Between the first and second window only t'_{notch} shows a significant change ($p = 0.045$), whereas t'_{notch} and t'_{dwp} both display a significant change between the second and third window (t'_{notch} : $p = 0.026$ and t'_{dwp} : $p = 0.024$). The evolution of t'_{sys} in figure 5.15 shows no remarkable change which is also emphasised by the results of the repeated measurement ANOVA with $p = 1$ for all time frames. The boxplots representing the interval-wise results are depicted in figures 5.16 - 5.18.

Furthermore, the points' mutual timings were analysed. Figure 5.19 shows the evolution of the respective intervals between P_{sys}, P_{notch} and P_{dwp} relative to the total pulse duration t_{T}. The three curve shapes display a similar behaviour. Both intervals measured from P_{sys} have their maximum at the seventh minute with an increase of approximately $+4\%$. The initial increase is followed by a decline to roughly the starting value. The interval between P_{notch} and P_{dwp} displays a less pronounced but higher maximum increase of $+4.47\%$ and a final relative value of $+1.42\%$. With p-values between 0.117 and 1, the mutual, relative timings show no significant change between the three intervals which is also underlined by the boxplots 5.20 - 5.22. The remaining boxplots can be found in the appendix A.
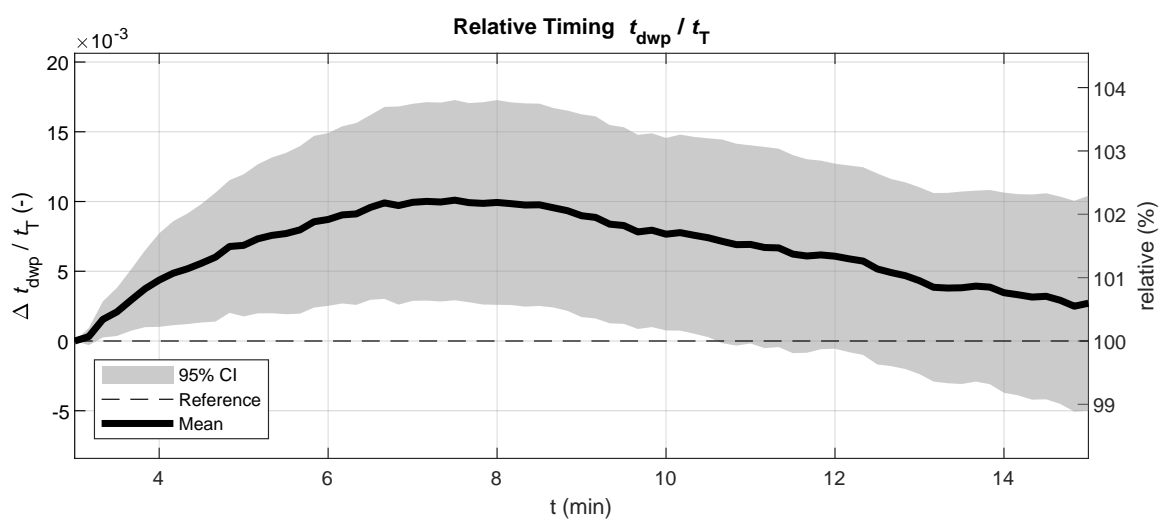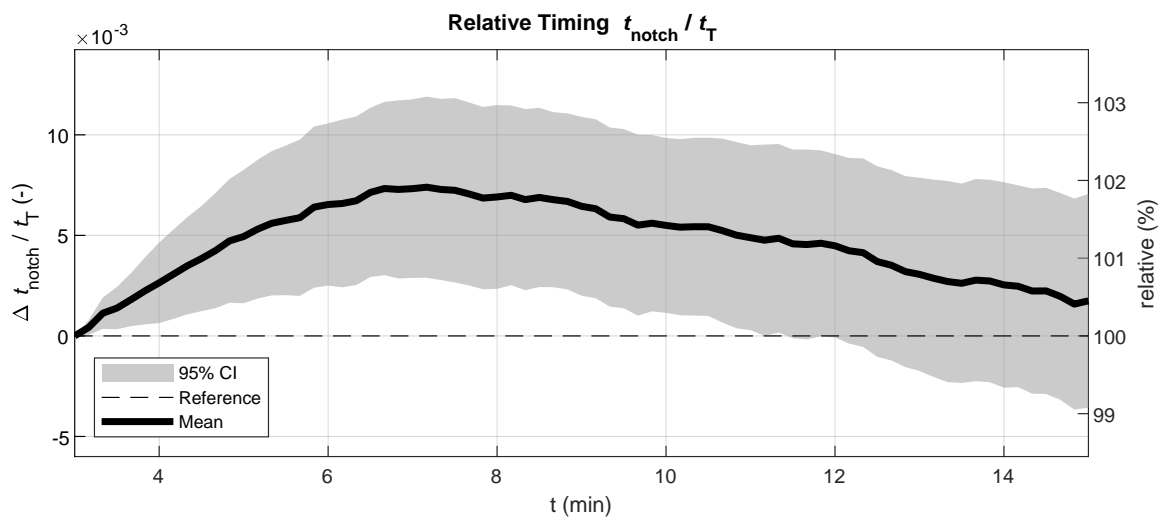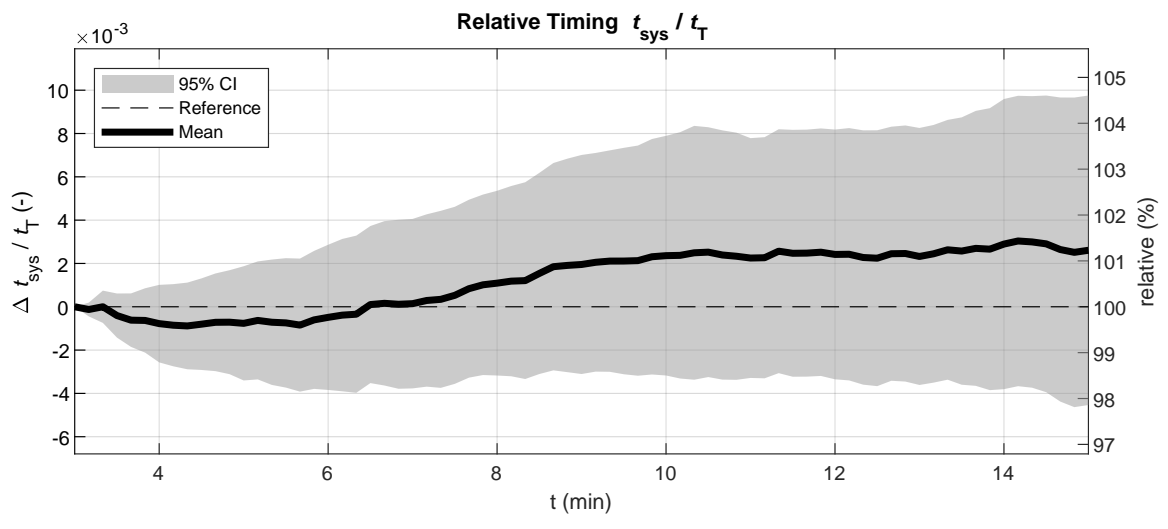
Figure 5.15.: 3-min average of the points' relative timings.

5. Results
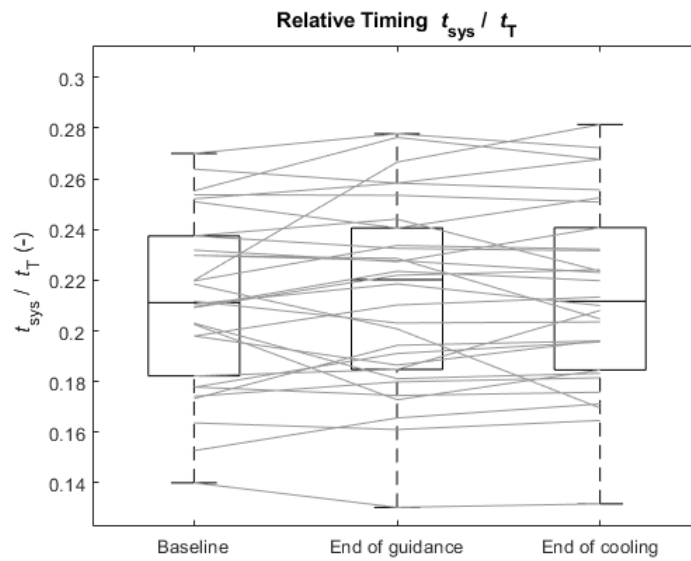
Figure 5.16.: Boxplot of t'_{sys}. The three groups represent the three evaluated time windows.
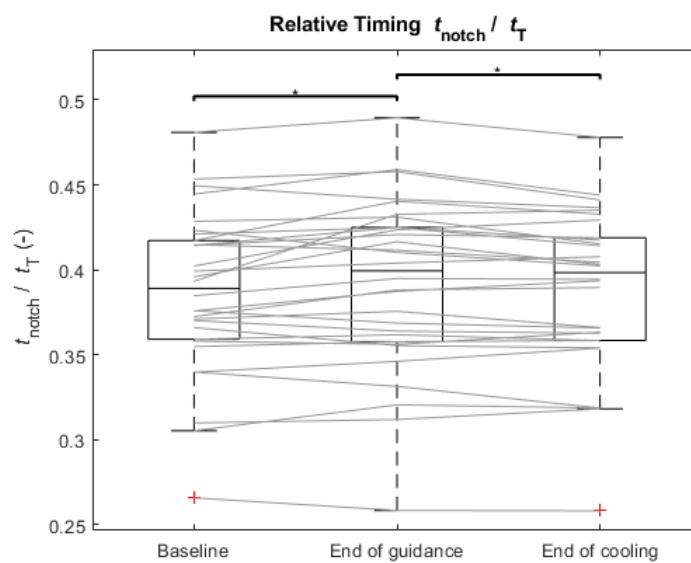
Figure 5.17.: Boxplot of t'_{notch}. The star is indicating the level of significance α, where a single star means $p \leq 0.05$.
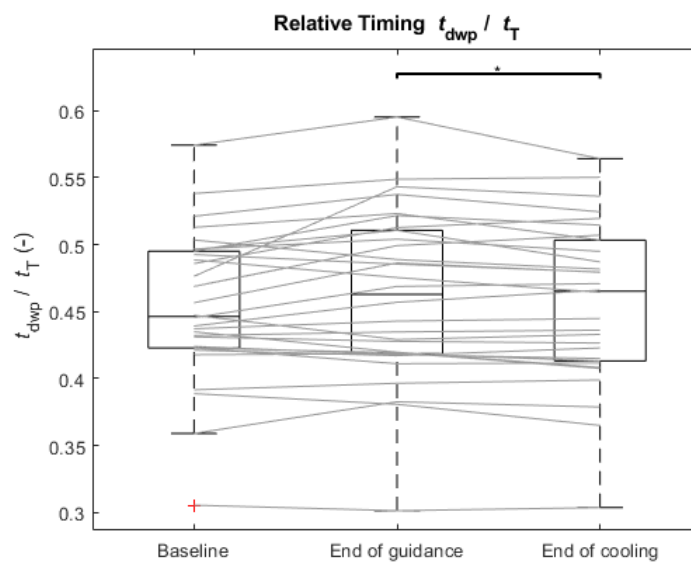
Figure 5.18.: Boxplot of t'_{dwp}. The three groups represent the three evaluated time windows. The star is indicating the level of significance α, where a single star means $p \leq 0.05$.
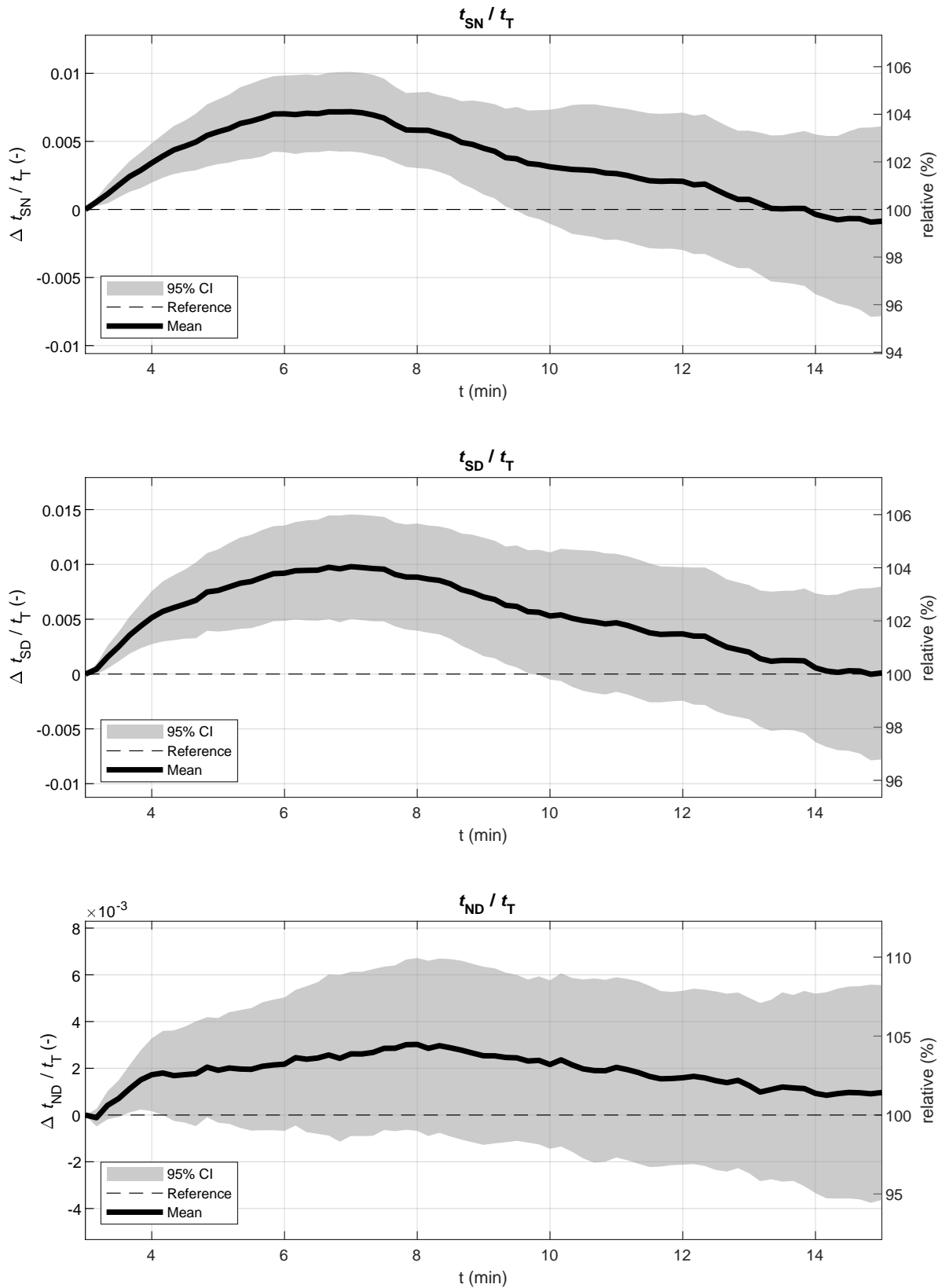
Figure 5.19.: 3-min average of the points' relative mutual timings. The notation of mutual timings is $t_{xy} = t_y - t_x$, where $x, y \in \{S, N, D\}$ and S, N, D denotes the timing of P_{sys}, P_{notch}, P_{dwp}, respectively.
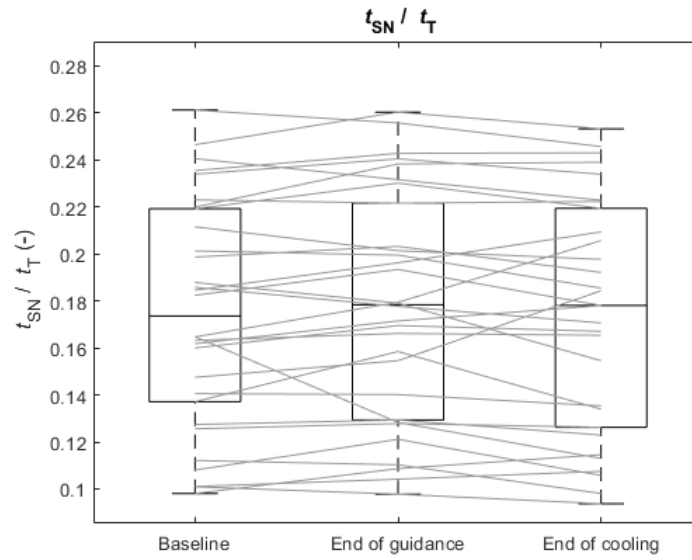
Figure 5.20.: Boxplot of $t'_{\mathrm{SN}} = t'_{\mathrm{notch}} - t'_{\mathrm{sys}}$.
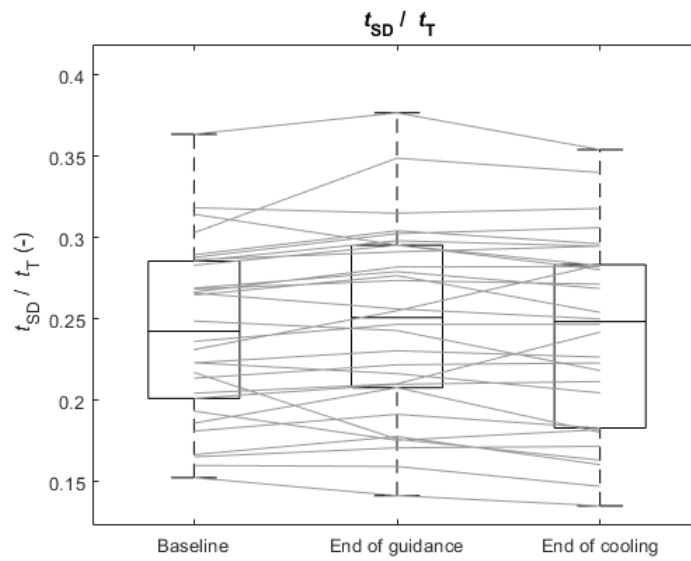
Figure 5.21.: Boxplot of $t'_{\mathrm{SD}} = t'_{\mathrm{dwp}} - t'_{\mathrm{sys}}$.
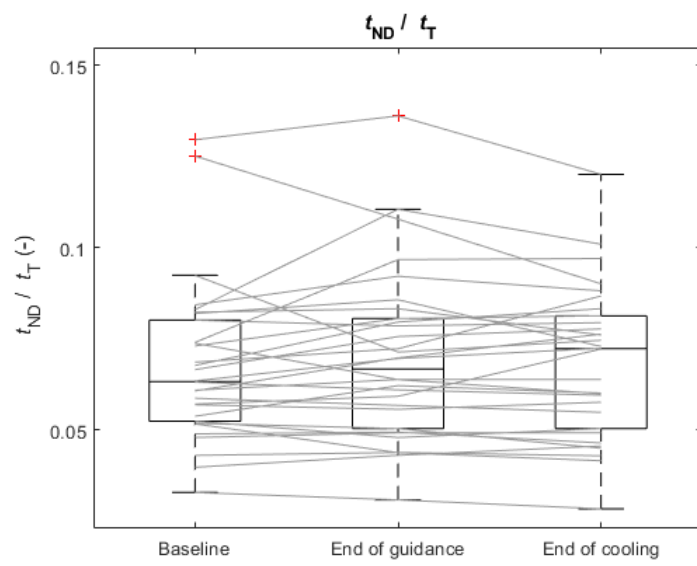
Figure 5.22.: Boxplot of $t'_{\mathrm{ND}} = t'_{\mathrm{dwp}} - t'_{\mathrm{notch}}$.

6. Discussion

The purpose of this thesis was the implementation of an algorithm to quantify and evaluate pulse waves and their evolution over time. The algorithm is furthermore deployed to assess the pulse waves of 30 subjects. Chapter 6 features the discussion of the results provided in chapter 5. Initially, the deployed algorithm will be discussed and compared to already existing algorithms in literature. Finally, the extracted features and their timely evolution will be interpreted.

6.1. Algorithm

To precisely evaluate the algorithm, each point will be discussed shortly. The detection of the Systolic Pressure, by finding the maximum of the wave, proved to be the most simple feature and was robust as well as precise. The visual check yielded no incorrectly annotated points. As a result of the homogeneous definition of the systolic pressure, the implementation of P_{sys} corresponds to those found in literature, for example in [44].

Similarly, the algorithm applied to find the Dicrotic Wave Pressure was readily found in literature [31, 44]. If the wave displays a second local maximum, the maximum coincides with P_{dwp}. Otherwise, P_{dwp} is found to be the point of minimal inclination. While distinct local maxima were rare, they proved to be the most problematic. Sometimes, points were recognized as local maximum due to a slight elevation relative to their neighbouring points. Thus, they displayed a marginal prominence but

were annotated nonetheless. In those cases, visual examination concluded that the actual Dicrotic Wave Pressure would have been no local maximum but rather a point of minimal inclination. As this event occurred rarely compared to the correctly annotated points, this issue was accepted.

Lastly, the implemented method of finding the Dicrotic Notch deviated from existing algorithms. All algorithms found during research deployed the process, that P_{notch} is found as the maximal inflection in the interval $[t_{\mathrm{sys}}; t_{\mathrm{dwp}}]$ or, if P_{dwp} is a local maximum, as local minimum in said interval [31, 44]. Considering the case of P_{dwp} being a local maximum, the implemented algorithm agrees with the process. However, instead of finding the maximal inflection, the algorithm establishes a line between the point of inflection in $[t_{\mathrm{sys}}; t_{\mathrm{dwp}}]$ and P_{dwp}. The Dicrotic Notch is then found to be the point of maximum perpendicular distance to said line. Both algorithms were used on the present data set and the annotated points were visually examined. In comparison, the newly developed method displays an overall superior precision when applied to the present data set, as examplarily seen in figure 6.1. A slight drawback is the dependence on the detection of P_{dwp}, where the aforementioned issue concerning the local maximum affects the placement of P_{notch}.

6.2. Features

All extracted features were averaged within a three minute moving window to eliminate short-term fluctuations as well as outliers and artefacts. The first three minutes were taken as baseline.

The evolution plots of the amplitudes show a significant decline in magnitude. Therefore, the pulse waves undergo a systematic shrinking process. Results of other studies indicate that relaxation techniques can lower blood pressure [63, 62, 64, 65]. The decrease in amplitude could therefore be connected to a decrease in blood pressure. As no blood pressure data was recorded during the present study, no definite statement can be made.

In few sections a sudden, non-physiological change in magnification was

(a) Second derivative of a pulse wave with annotated point of maximum inflection.

(b) Pulse wave with annotated $P_{notch,alt}$, found as point of maximum inflection, and P_{notch}, as found by the novel algorithm.
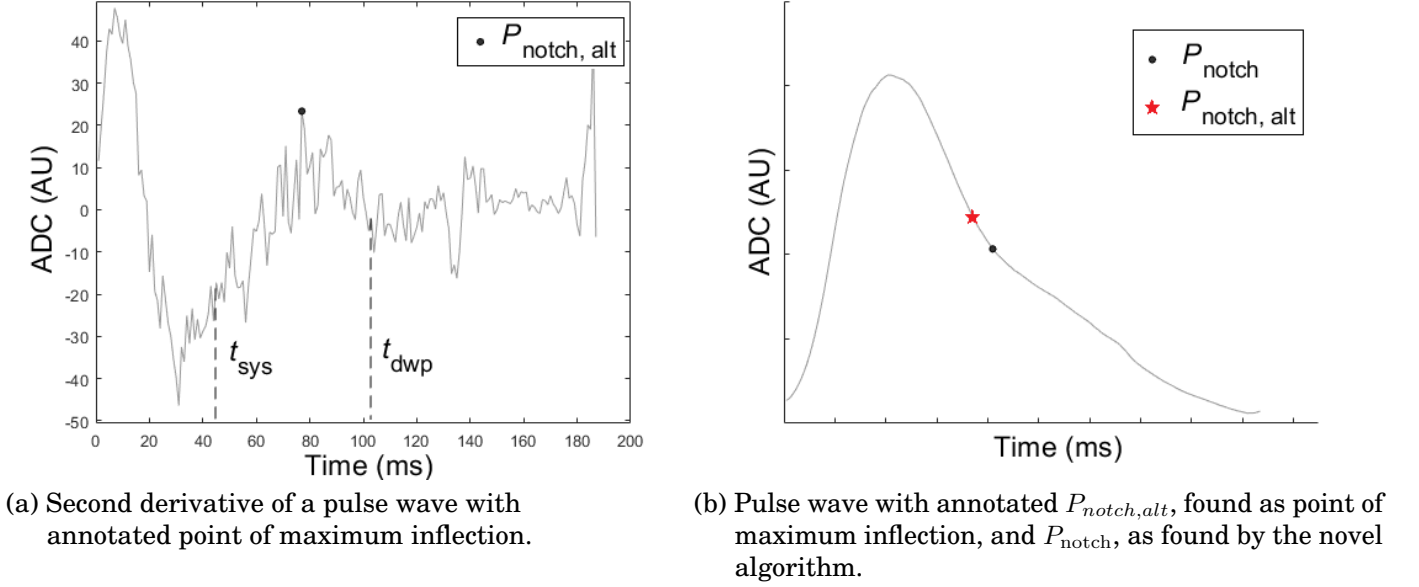
Figure 6.1.: Comparison of existing and novel algorithm for finding P_{notch}.

observed. To eliminate possible malevolent effects on the overall evolution of the amplitudes, ratios were introduced. The evaluation of these amplitude ratios conclude that the shrinking process is not uniform. The ratios P'_{notch} and P'_{dwp} show an initial decrease until minute six, followed by a return to their original ratios at approximately minutes ten and nine. Afterwards, both ratios increase further, ultimately boasting a higher relative prominence compared to their starting values. The ratio of P_{notch} relative to P_{dwp} shows a steady decline, meaning that P_{dwp} is getting more prominent with time compared to P_{notch}.

The Total Pulse Duration t_T decreases during the breathing exercises, reaching a temporarily constant value after approximately seven minutes and climbing again during the cooling phase after ten minutes. This behaviour is corroborated by corresponding changes in the ejection duration t_{notch}. Furthermore, the timing of the Dicrotic Notch, relative to the total pulse duration t_T, shows a significant elevation during the phase of guided breathing. This is explainable because the Systole is virtually constant

with changes in heart rate. Thus, t_{notch}, representing the border between Systole and Diastole, increases with increasing heart rate. Accordingly, an increase in heart rate implies a rightward shift of P_{notch} and P_{dwp} with respect to t_{T} which is shown in Figure 5.15.

6.3. Limitations

While the evolution of the extracted features corroborate the expected outcome and thus seem to validate the algorithm indirectly, an explicit verification is, as of now, not possible. Manual annotation by an expert or a comparison method is necessary to proof the functionality of the algorithm. It is also uncertain, if, respectively how strong, the previously described metrological effect influences the results. Furthermore, the recorded data originated from subjects diagnosed with essential hypertension. The lack of a control group for comparison adds an additional factor of uncertainty.

7. Conclusion and Outlook

To recapitulate, this thesis provided insight regarding the existing quantification methods of pulse waves. The accumulated techniques were summarized and described. To evaluate the evolution of the contour line, three distinct points of the wave were chosen - the Systolic Pressure, the Dictrotic Notch and the Dicrotic Wave Pressure. The devised algorithm adopts existing strategies to locate the Systolic and Dicrotic Wave Pressure and further proposes a novel approach to detect the Dicrotic Notch. While the Systolic Pressure is highly accurate, there is still room for improvement regarding the Dicrotic Wave Pressure and its weakness of detecting local maxima. This improvement may be found in the application of sophisticated machine learning algorithms to an abundance of pulse wave data.

In the course of the thesis, three of the numerous quantification methods of chapter 3 were implemented. To gather further information regarding the evolution of pulse waves, additional methods should be added to the algorithm. For this, the novel method of attractor reconstruction introduced in section 3.8 or the empirical mode decomposition in section 3.7 shows untapped potential.

After gathering and averaging the data points, the displayed plots allow statements regarding the alteration of the contour form. The pulse waves experience a significant shrinking with respect to its amplitudes and a non-significant change in its ratios. Especially interesting with regard to future research is the link between decreasing amplitudes and continuously measured blood pressure which was not recorded in the conducted study. Thus, invasive and continuous blood pressure measurement via

catheterization and the simultaneously recorded pulse wave signal could provide additional insights. Furthermore, apart from hypertensive subjects, future studies should include a control group comprised of healthy individuals.

Aside from already quoted points, a particularly interesting result of the study is the fact that exercised breathing relaxation techniques seem to increase the heart rate instead of lowering it, as seen in figure 5.14. The cause is uncertain.

Appendix A.

Timing Plots

This section contains the remaining evolution plots and boxplots which were not presented in chapter 5. Figure A.1 - A.8 contain the boxplots of the timings of P_{dwp}, P_{notch} and P_{dwp} with respect to the wave's onset as well as the wave's end, absolute and relative to the total wave duration t_{T}. Finally, A.9 - A.12 show the evolution of aforementioned parameters over time.

The stars are indicating the level of significance α, where a single star means $p \leq 0.05$ and two stars represent $p \leq 0.01$.
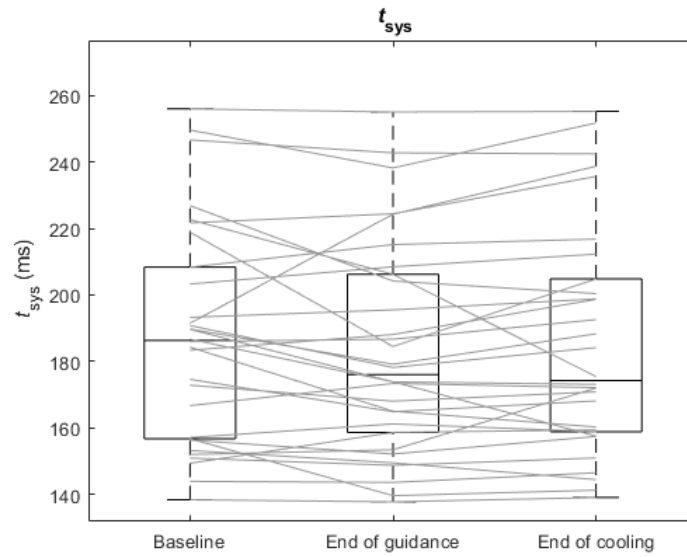
Figure A.1.: Boxplot of the absolute timing of the Systolic Pressure
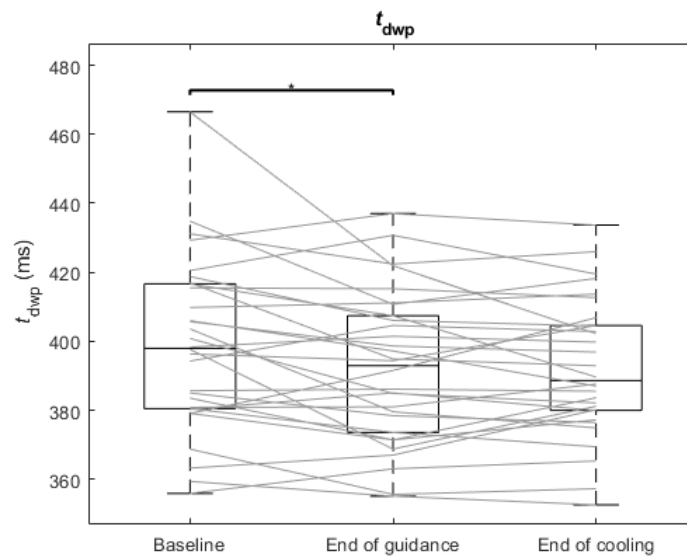
Figure A.2.: Boxplot of the absolute timing of the Dicrotic Wave Pressure. The stars are indicating the level of significance α, where a single star means $p \leq 0.05$
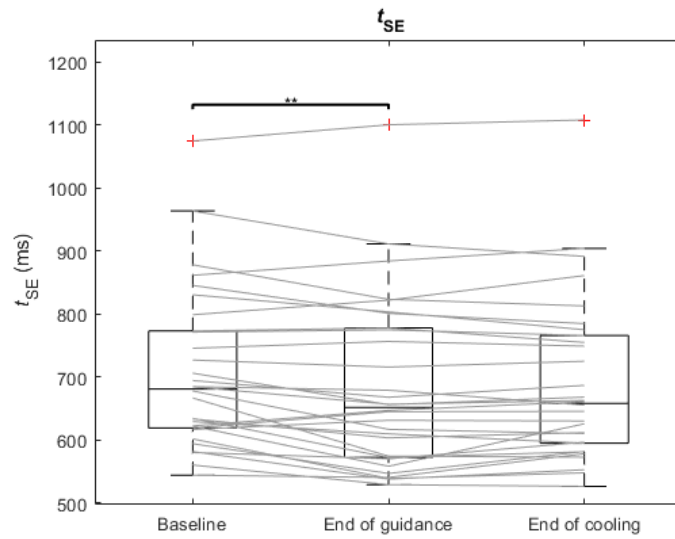
Figure A.3.: Boxplot of the interval between the Systolic Pressure and the wave's end. The stars are indicating the level of significance α, where a two stars means $p \leq 0.01$
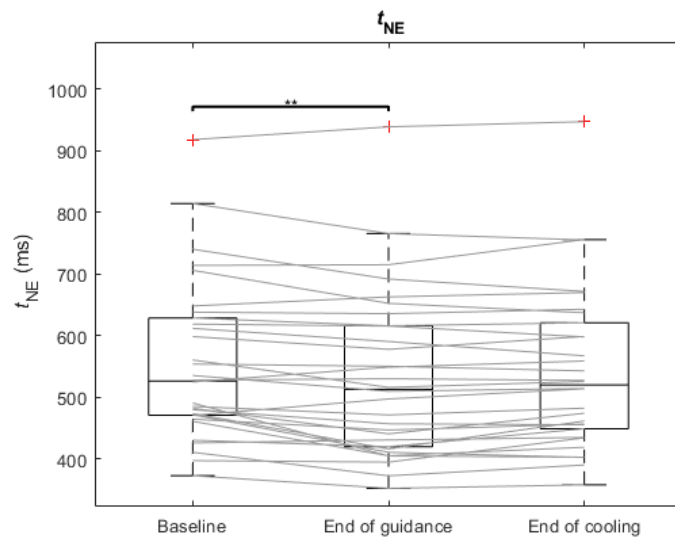
Figure A.4.: Boxplot of the interval between the Dicrotic Notch and the wave's end. The stars are indicating the level of significance α, where a two stars means $p \leq 0.01$
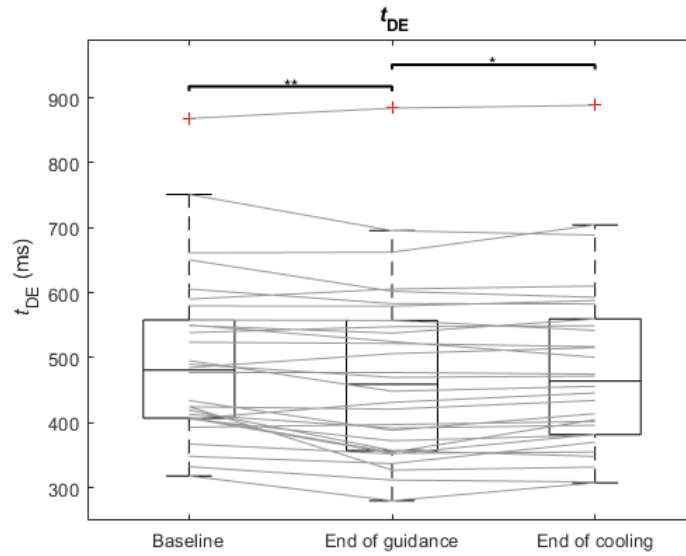
Figure A.5.: Boxplot of the interval between the Dicrotic Wave Pressure and the wave's end. The stars are indicating the level of significance α, where a single star means $p \leq 0.05$ and two stars means $p \leq 0.01$
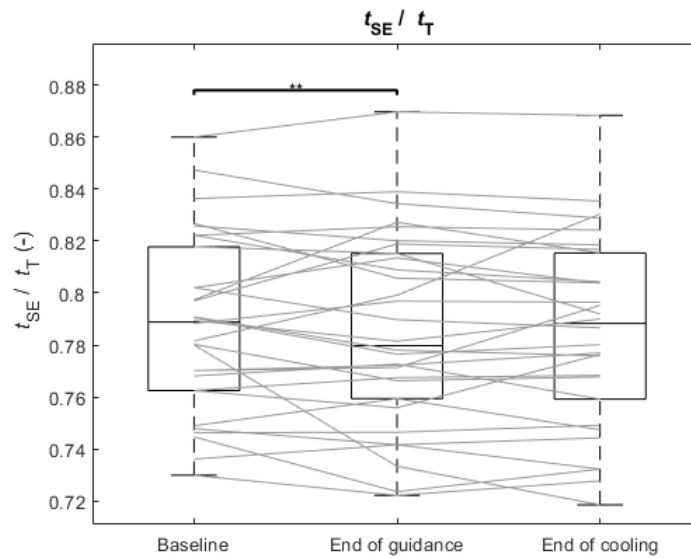
Figure A.6.: Boxplot of the interval between the Systolic Pressure and the wave's end with respect to t_T
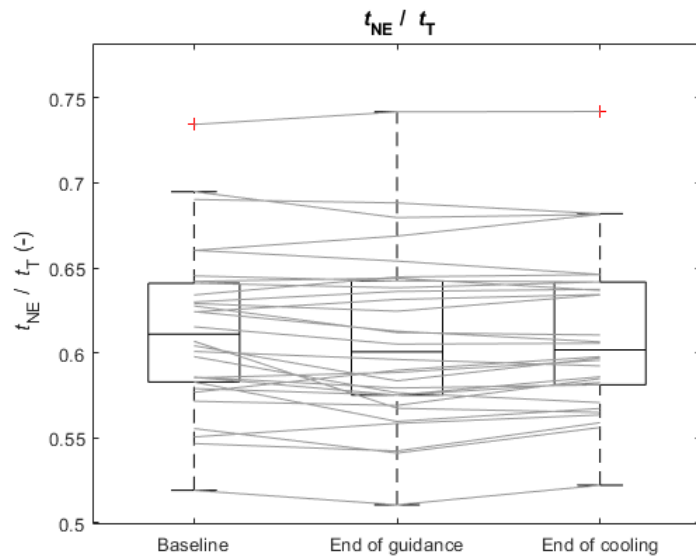
Figure A.7.: Boxplot of the interval between the Dicrotic Notch and the wave's end with respect to t_T.
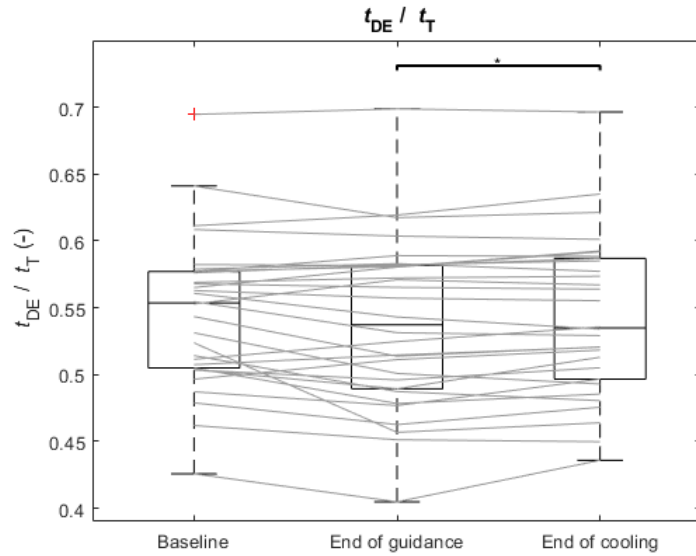
Figure A.8.: Boxplot of the interval between the Dicrotic Wave Pressure and the wave's end with respect to t_T. The stars are indicating the level of significance α, where a single star means $p \leq 0.05$.
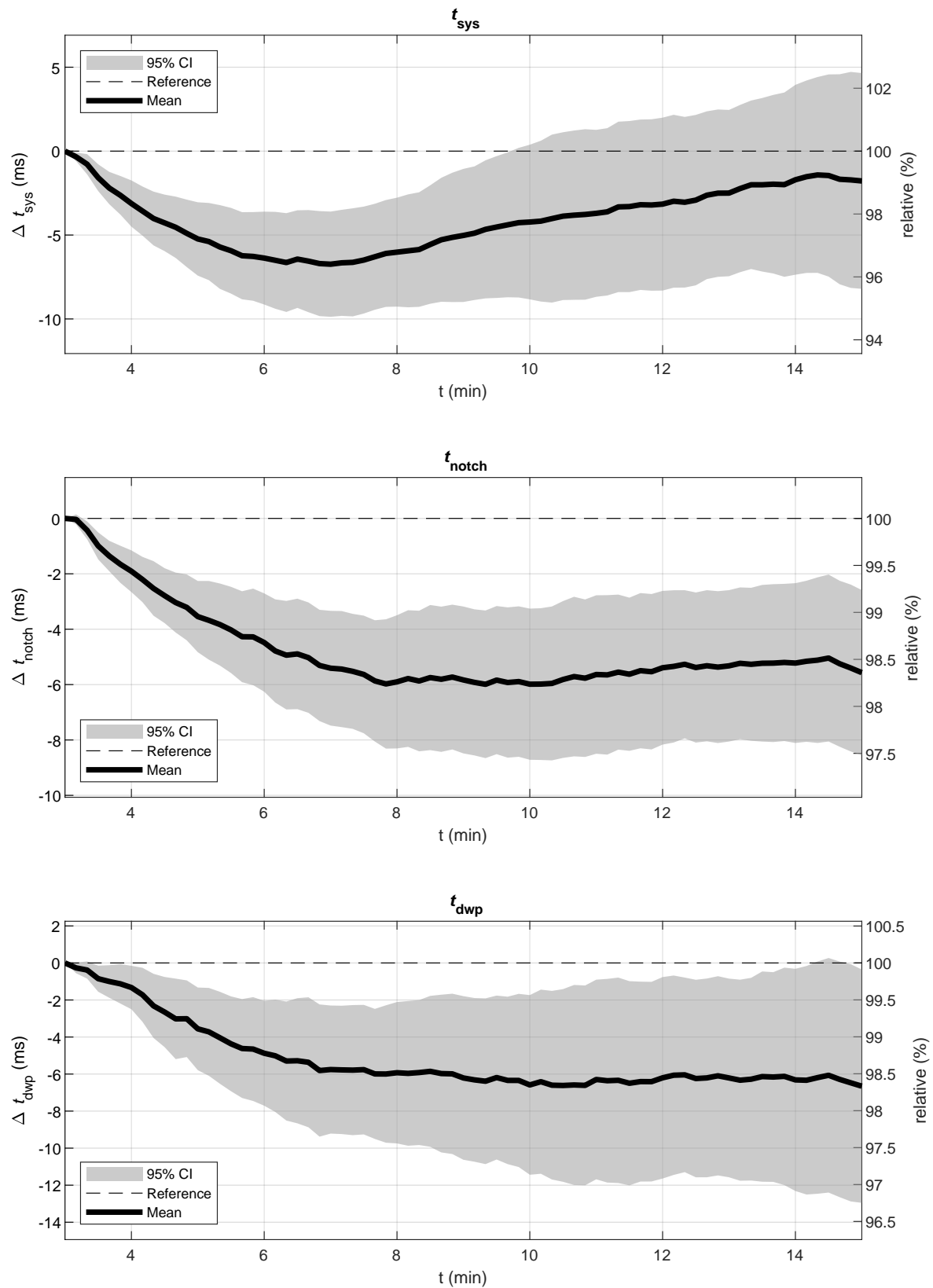
Figure A.9.: Absolute Timings of P_{sys}, P_{notch} and P_{dwp}
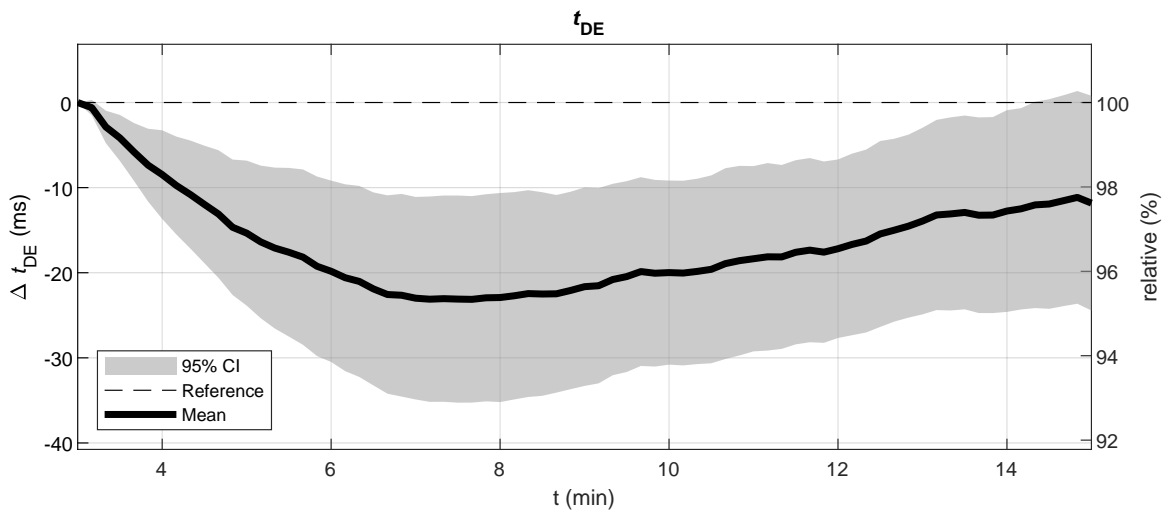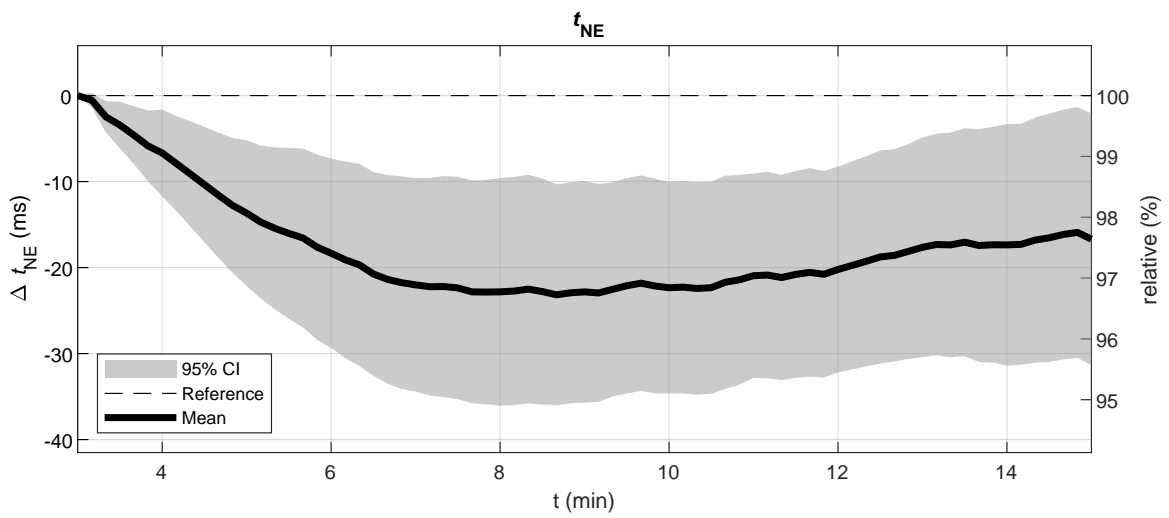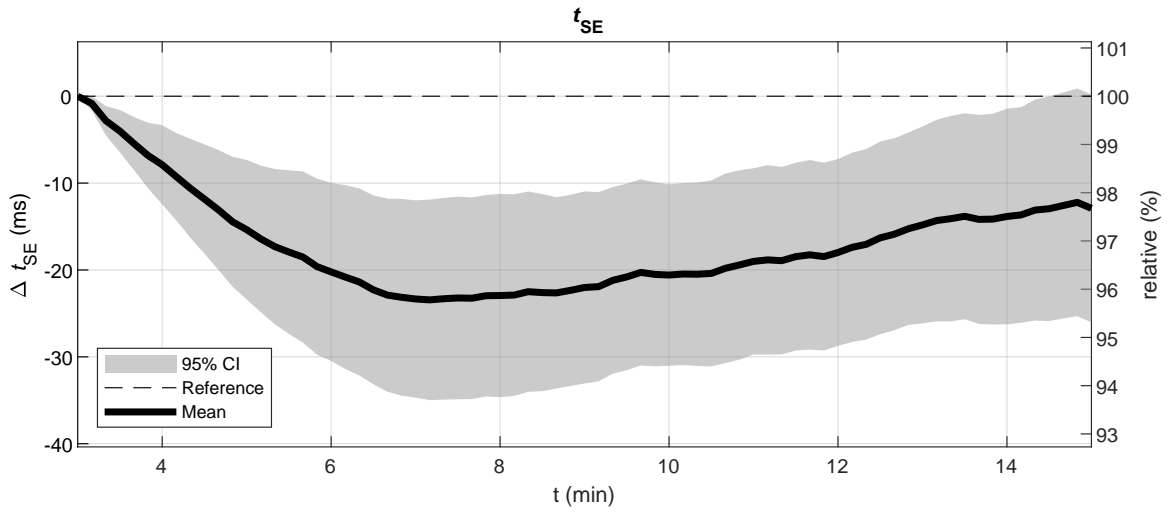
Figure A.10.: Intervals of P_{sys}, P_{notch} and P_{dwp} to the wave's end.
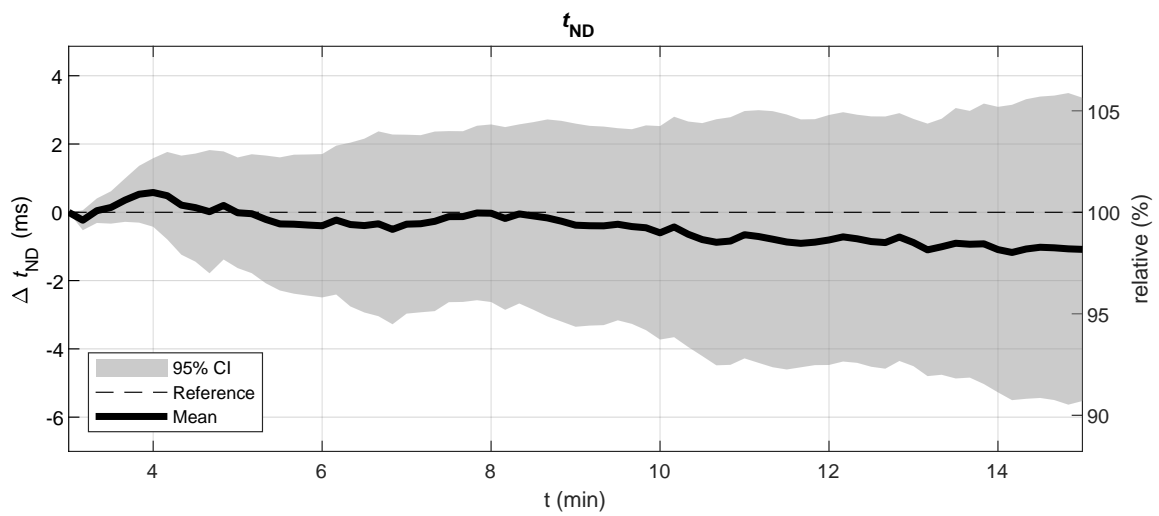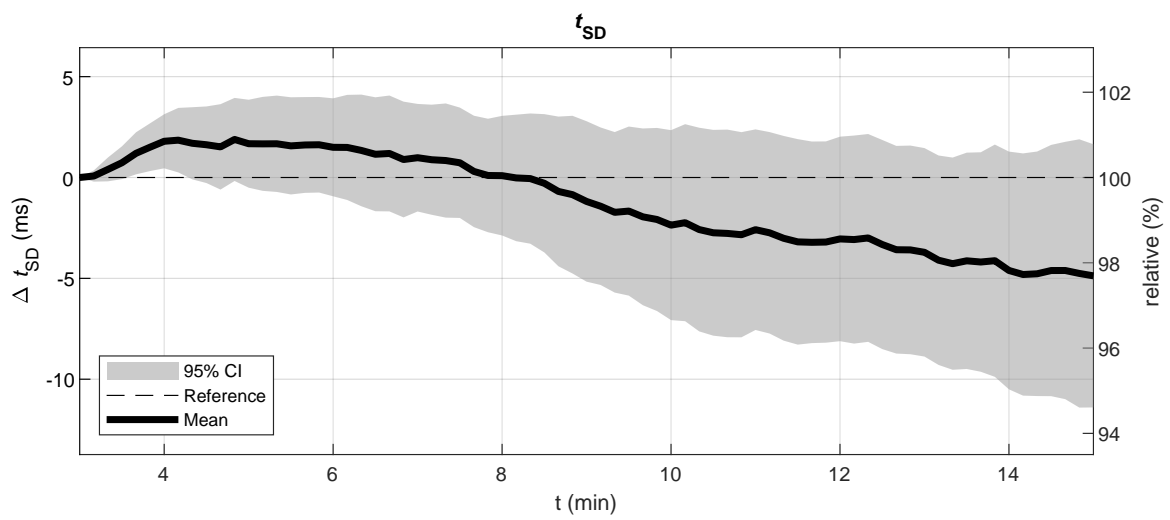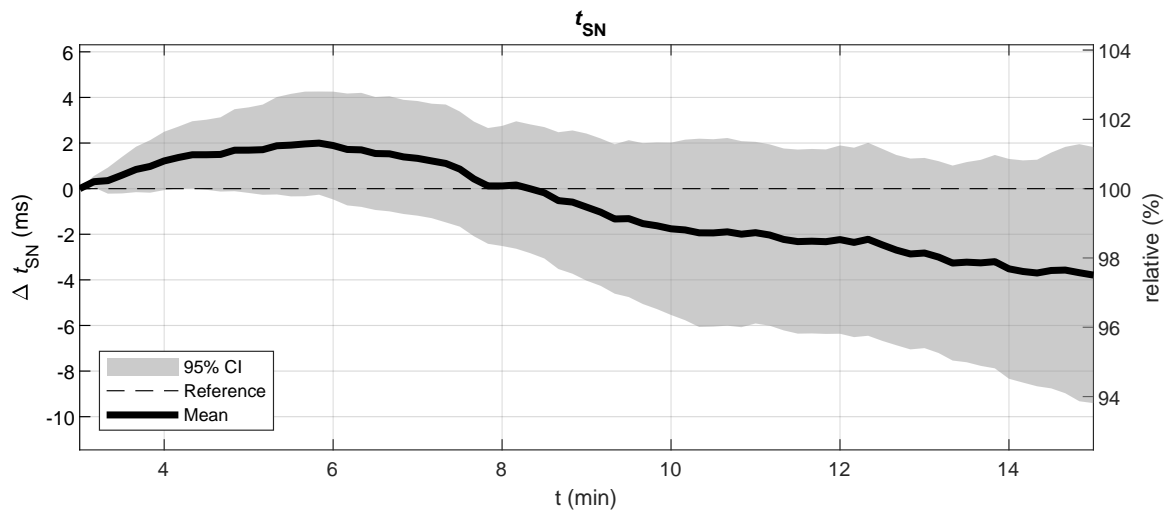
Figure A.11.: Absolute mutual Timings of P_{sys}, P_{notch} and P_{dwp}.
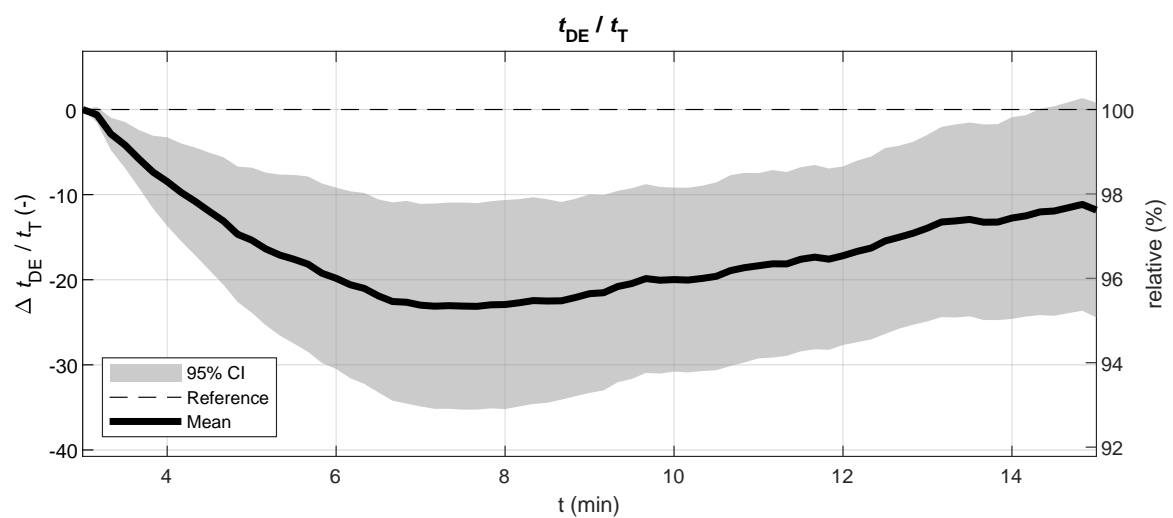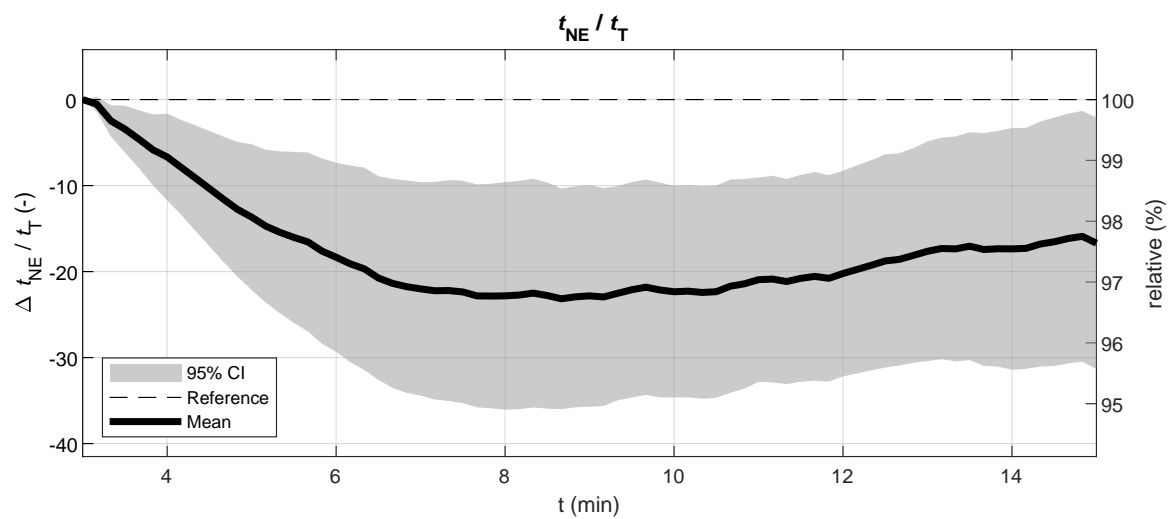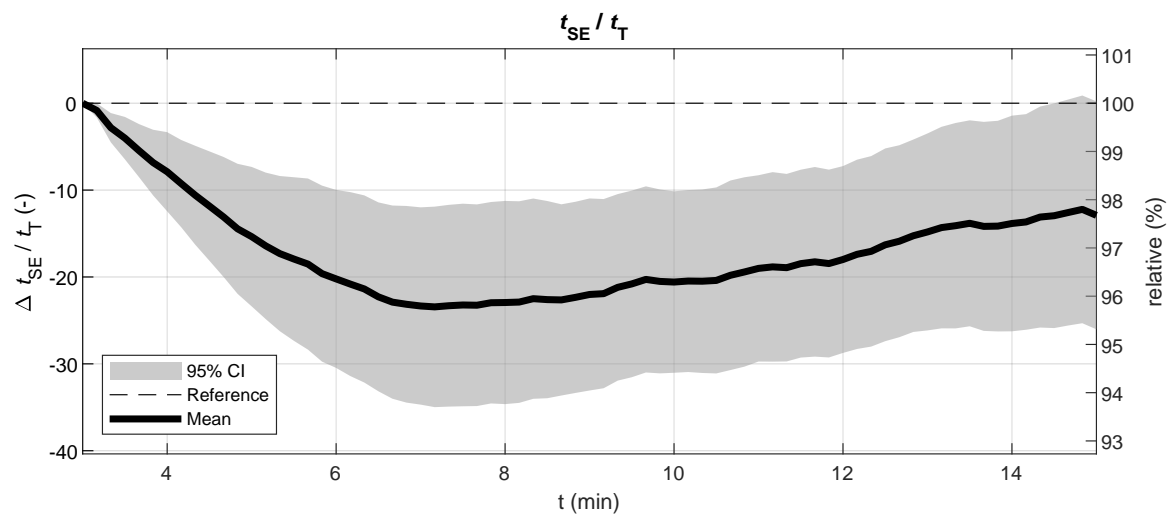
Figure A.12.: Intervals of P_{sys}, P_{notch} and P_{dwp} to the wave's end, with respect to t_{T}.

List of Figures

List of Figures

List of Tables

References

[1] Gregory A Roth et al. "Global and regional patterns in cardiovascular mortality from 1990 to 2013." In: *Circulation* 132.17 (2015), pp. 1667–1678. ISSN: 15244539. DOI: 10.1161/CIRCULATIONAHA.114.008720 (cit. on p. 1).

[2] George Pickering. "Hypertension. Definitions, natural histories and consequences." In: *The American Journal of Medicine* 52.5 (1972), pp. 570–583. ISSN: 00029343. DOI: 10.1016/0002-9343(72)90049-6 (cit. on p. 1).

[3] Beate H McGhee and Elizabeth J Bridges. "Monitoring arterial blood pressure—what you may not know." In: *Crit Care Nurse* 22.2 (2002). ISSN: 0279-5442 (cit. on p. 1).

[4] Ramakrishna Mukkamala et al. "Toward Ubiquitous Blood Pressure Monitoring via Pulse Transit Time: Theory and Practice." In: *IEEE Transactions on Biomedical Engineering* 62.8 (2015), pp. 1879–1901. ISSN: 15582531. DOI: 10.1109/TBME.2015.2441951 (cit. on p. 1).

[5] Shu-Zhen Wang et al. "Effect of Slow Abdominal Breathing Combined with Biofeedback on Blood Pressure and Heart Rate Variability in Prehypertension." In: *The Journal of Alternative and Complementary Medicine* 16.10 (2010), pp. 1039–1045. ISSN: 1075-5535. DOI: 10.1089/acm.2009.0577 (cit. on p. 1).

[6] R Klinke, C Bauer, and S Silbernagl. *Lehrbuch der Physiologie.* Thieme, 2003, p. 842. ISBN: 9783137960041 (cit. on p. 3).

[7] Herbert Lippert. *Lehrbuch Anatomie.* 2006. DOI: 10.1016/j.ostmed.2011.10.003 (cit. on p. 3).

References

[8] J E Guyton, A. C.Hall. *Textbook of Medical Physiology*. 2006 (cit. on pp. 5–8, 11).

[9] M Gabriel Khan. "Blood Pressure." In: ed. by M GABRIEL B T - Encyclopedia of Heart Diseases KHAN. Burlington: Academic Press, 2006, pp. 175–181. ISBN: 978-0-12-406061-6. DOI: `https://doi.org/10.1016/B978-012406061-6/50030-8` (cit. on p. 7).

[10] Toshiyo Tamura and Wenxi Chen. *Seamless Healthcare Monitoring: Advancements in Wearable, Attachable, and Invisible Devices*. 2018. ISBN: 978-3-319-69361-3. DOI: `10.1007/978-3-319-69362-0` (cit. on pp. 8, 11, 13–15).

[11] Wilmer W Nichols. *McDonald's blood flow in arteries : theoretical, experimental, and clinical principles / Wilmer W. Nichols, Michael F. O'Rourke ; with a contribution from Craig Hartley*. Ed. by Michael F O'Rourke, Craig Hartley 1944-, and Donald A Blood flow in arteries McDonald. London : New York: Arnold ; Oxford University Press, 1998. ISBN: 0340646144 (hardback) (cit. on pp. 8, 9, 17, 20, 26, 50).

[12] Bryan Williams et al. "2018 ESC/ESH Guidelines for the management of arterial hypertension." In: *European Heart Journal* 39.33 (Sept. 2018), pp. 3021–3104. ISSN: 0195-668X (cit. on p. 8).

[13] Rhian M Touyz. "Blood Pressure Regulation and Pathology." In: *Cellular and Molecular Pathobiology of Cardiovascular Disease* (2014), pp. 257–275. DOI: `10.1016/B978-0-12-405206-2.00014-4` (cit. on p. 10).

[14] Ethel M Frese, Ann Fick, and H Steven Sadowsky. "Blood pressure measurement guidelines for physical therapists." In: *Cardiopulmonary physical therapy journal* 22.2 (2011), pp. 5–12. ISSN: 2374-8907 (cit. on p. 11).

[15] Yarows SA, S Julius, and Pickering TG. "Home blood pressure monitoring." In: *Archives of Internal Medicine* 160.9 (2000), pp. 1251–1257. ISSN: 0003-9926 (cit. on p. 12).

References

[16] Charles F Babbs. "Oscillometric measurement of systolic and diastolic blood pressures validated in a physiologic mathematical model." In: *BioMedical Engineering Online* 11.1 (2012), p. 1. ISSN: 1475925X. DOI: 10.1186/1475-925X-11-56 (cit. on p. 11).

[17] Gary M Drzewiecki, Julius Melbin, and Abraham Noordergraaf. "Arterial tonometry: Review and analysis." In: *Journal of Biomechanics* 16.2 (1983), pp. 141–152. ISSN: 00219290. DOI: 10.1016/0021-9290(83)90037-4 (cit. on p. 13).

[18] John Allen. "Photoplethysmography and its application in clinical physiological measurement." In: *Physiological Measurement* 28.3 (2007). ISSN: 09673334. DOI: 10.1088/0967-3334/28/3/R01 (cit. on p. 13).

[19] Alexei A Kamshilin et al. "A new look at the essence of the imaging photoplethysmography." In: *Scientific Reports* 5 (2015), pp. 1–9. ISSN: 20452322. DOI: 10.1038/srep10494 (cit. on p. 13).

[20] R Rox Anderson and John A Parrish. "The Optics of Human Skin." In: *Journal of Investigative Dermatology* 77.1 (1981), pp. 13–19. ISSN: 0022-202X. DOI: 10.1111/1523-1747.ep12479191 (cit. on p. 14).

[21] Alexei A Kamshilin and Nikita B Margaryants. "Origin of Photoplethysmographic Waveform at Green Light." In: *Physics Procedia* 86.June 2015 (2017), pp. 72–80. ISSN: 18753892. DOI: 10.1016/j.phpro.2017.01.024 (cit. on p. 15).

[22] Azleena Bt Kamarul Bahrein. "Systolic Amplitude of Photoplethysmogram Among Left Ventricular Hypertrophy Risk and Healthy Individuals." In: *2016 IEEE EMBS Conference on Biomedical Engineering and Sciences (IECBES)* (2016), pp. 499–502 (cit. on p. 17).

[23] Mohamed Elgendi. "On the Analysis of Fingertip Photoplethysmogram Signals." In: *Current Cardiology Reviews* 8.1 (2012), pp. 14–25. ISSN: 1573403X. DOI: 10.2174/157340312801215782 (cit. on pp. 17, 21).

References

[24] Alberto P Avolio Walsh, Mark Butlin, and Andrew. "Arterial blood pressure measurement and pulse wave analysis—their role in enhancing cardiovascular assessment." In: *Physiological Measurement* 31.1 (2010), R1. ISSN: 0967-3334 (cit. on p. 18).

[25] Nicolaas Westerhof, Nikolaos Stergiopulos, and Mark Noble. *Snapshots of Hemodynamics: An Aid for Clinical Research and Graduate Education*. Vol. 37. 2005. DOI: 10.1007/978-1-4419-6363-5 (cit. on pp. 17, 50).

[26] Jingjie Feng et al. "Study of continuous blood pressure estimation based on pulse transit time, heart rate and photoplethysmography-derived hemodynamic covariates." In: *Australasian Physical & Engineering Sciences in Medicine* 0.0 (2018), p. 11. ISSN: 0158-9938. DOI: 10.1007/s13246-018-0637-8 (cit. on pp. 17, 19, 22).

[27] Aymen A Awad et al. "Analysis of the ear pulse oximeter waveform." In: *Journal of Clinical Monitoring and Computing* 20.3 (2006), pp. 175–184. ISSN: 13871307. DOI: 10.1007/s10877-006-9018-z (cit. on pp. 17, 21, 23).

[28] Willie Bosseau Murray and Patrick Anthony Foster. "The peripheral pulse wave: Information overlooked." In: *Journal of Clinical Monitoring* 12.5 (1996), pp. 365–377. ISSN: 1573-2614. DOI: 10.1007/BF02077634 (cit. on p. 19).

[29] Aymen A Alian and Kirk H Shelley. "Photoplethysmography." In: *Best Practice and Research: Clinical Anaesthesiology* 28.4 (2014), pp. 395–406. ISSN: 1532169X. DOI: 10.1016/j.bpa.2014.08.006 (cit. on p. 19).

[30] Tony J Akl et al. "Quantifying tissue mechanical properties using photoplethysmography." In: 5.7 (2014), pp. 1449–1456. DOI: 10.1364/BOE.5.002362 (cit. on p. 19).

[31] Stephen R Alty et al. "Predicting Arterial Stiffness From the Digital Volume Pulse Waveform." In: 54.12 (2007), pp. 2268–2275 (cit. on pp. 19, 20, 23, 82, 83).

[32] S N Zaidi Collins and S M. "Orthostatic stress and area under the curve of photoplethysmography waveform." In: *Biomedical Physics & Engineering Express* 2.4 (2016), p. 45006. ISSN: 2057-1976 (cit. on pp. 19, 22).

[33] S C Millasseau et al. "Determination of age-related increases in large artery stiffness by digital pulse contour analysis." In: 377 (2002), pp. 371–377 (cit. on pp. 20, 21).

[34] D Korpas, J Hálek, and L Doležal. "Parameters describing the pulse wave." In: *Physiological Research* 58.4 (2009), pp. 473–479. ISSN: 08628408 (cit. on pp. 20, 21).

[35] Carmen C Y Poon et al. "Changes in the Photoplethysmogram Waveform After Exercise." In: *Computer Architectures for Machine Perception, 2003 IEEE International Workshop on* (2004), pp. 115–118. DOI: 10.1109/ISSMD.2004.1689576 (cit. on p. 21).

[36] Aymen A Awad et al. "The relationship between the photoplethysmographic waveform and systemic vascular resistance." In: *Journal of Clinical Monitoring and Computing* 21.6 (2007), pp. 365–372. ISSN: 13871307. DOI: 10.1007/s10877-007-9097-5 (cit. on p. 21).

[37] L Wang et al. "Noninvasive cardiac output estimation using a novel photoplethysmogram index." In: *Conference proceedings : ... Annual International Conference of the IEEE Engineering in Medicine and Biology Society. IEEE Engineering in Medicine and Biology Society. Conference* 2009 (2009), pp. 1746–1749. ISSN: 1557-170X. DOI: 10.1109/IEMBS.2009.5333091 (cit. on pp. 22, 27, 28).

[38] M Voelz. "Measurement of the blood-pressure constant k, over a pressure range in the canine radial artery." In: *Medical and Biological Engineering and Computing* 19.5 (1981), pp. 535–537. ISSN: 1741-0444. DOI: 10.1007/BF02442765 (cit. on p. 22).

[39] Yanjun Li et al. "Characters available in photoplethysmogram for blood pressure estimation: Beyond the pulse transit time." In: *Australasian Physical and Engineering Sciences in Medicine* 37.2 (2014), pp. 367–376. ISSN: 18795447. DOI: 10.1007/s13246-014-0269-6 (cit. on p. 23).

[40]   Uldis Rubins. "Finger and ear photoplethysmogram waveform analysis by fitting with Gaussians." In: *Medical and Biological Engineering and Computing* 46.12 (2008), pp. 1271–1276. ISSN: 01400118. DOI: `10.1007/s11517-008-0406-z` (cit. on p. 22).

[41]   Sandrine C Millasseau et al. "The vascular impact of aging and vasoactive drugs: Comparison of two digital volume pulse measurements." In: *American Journal of Hypertension* 16.6 (2003), pp. 467–472. ISSN: 08957061. DOI: `10.1016/S0895-7061(03)00569-7` (cit. on pp. 23, 24).

[42]   Junichiro Hashimoto et al. "Determinants of the second derivative of the finger photoplethysmogram and brachial-ankle pulse-wave velocity: The Ohasama study." In: *American Journal of Hypertension* 18.4 (2005), pp. 477–485. ISSN: 08957061. DOI: `10.1016/j.amjhyper.2004.11.009` (cit. on pp. 24, 25).

[43]   Kenji Takazawa et al. "Assessment of vasoactive agents and vascular aging by the second derivative of photoplethysmogram waveform." In: *Hypertension* 32.2 (1998), pp. 365–370. ISSN: 0194911X. DOI: `10.1161/01.HYP.32.2.365` (cit. on p. 25).

[44]   Peter H Charlton et al. "Assessing mental stress from the photoplethysmogram: a numerical study." In: *Physiological Measurement* 39.5 (2018), p. 54001. ISSN: 1361-6579. DOI: `10.1088/1361-6579/aabe6a` (cit. on pp. 25, 26, 50, 54, 82, 83).

[45]   Christopher S Hayward and Raymond P Kelly. "Gender-Related Differences in the Central Arterial Pressure Waveform." In: *Journal of the American College of Cardiology* 30.7 (1997), pp. 1863–1871. ISSN: 0735-1097. DOI: `https://doi.org/10.1016/S0735-1097(97)00378-1` (cit. on p. 25).

[46]   M H Sherebrin and R Z Sherebrin. "Frequency Analysis of the Peripheral Pulse Wave Detected in the Finger with a Photoplethysmograph." In: *IEEE Transactions on Biomedical Engineering* 37.3 (1990), pp. 313–317. ISSN: 15582531. DOI: `10.1109/10.52332` (cit. on p. 27).

105

References

[47] Oladipupo Olafiranye et al. "Harmonic analysis of noninvasively recorded arterial pressure waveforms in healthy bonnet macaques (Macaca radiata)." In: *Journal of the American Association for Laboratory Animal Science : JAALAS* 50.1 (2011), pp. 79–83. ISSN: 1559-6109 (Print) (cit. on p. 27).

[48] Y S Yan and Y T Zhang. "Noninvasive Estimation of Blood Pressure Using Photoplethysmographic Signals in the Period Domain." In: *2005 IEEE Engineering in Medicine and Biology 27th Annual Conference* 1.1 (2005), pp. 3583–3584. ISSN: 1557-170X. DOI: 10.1109/IEMBS.2005.1617255 (cit. on p. 27).

[49] Chengyu Liu, Lina Zhao, and Changchun Liu. "Effects of blood pressure and sex on the change of wave reflection: Evidence from Gaussian fitting method for radial artery pressure waveform." In: *PLoS ONE* 9.11 (2014). ISSN: 19326203. DOI: 10.1371/journal.pone.0112895 (cit. on pp. 28, 29).

[50] Lu Wang et al. "Multi-Gaussian fitting for pulse waveform using Weighted Least Squares and multi-criteria decision making method." In: *Computers in Biology and Medicine* 43.11 (2013), pp. 1661–1672. ISSN: 00104825. DOI: 10.1016/j.compbiomed.2013.08.004 (cit. on p. 29).

[51] Norden E Huang et al. "The empirical mode decomposition and the Hilbert spectrum for nonlinear and non-stationary time series analysis." In: *Proceedings of the Royal Society of London. Series A: Mathematical, Physical and Engineering Sciences* 454.1971 (Mar. 1998), 903 LP –995 (cit. on p. 30).

[52] Hualou Liang et al. "Empirical mode decomposition: A method for analyzing neural data." In: *Neurocomputing* 65-66.SPEC. ISS. (2005), pp. 801–807. ISSN: 09252312. DOI: 10.1016/j.neucom.2004.10.077 (cit. on p. 31).

[53] Eduardo Rocon de Lima et al. "Empirical mode decomposition: A novel technique for the study of tremor time series." In: *Medical and Biological Engineering and Computing* 44.7 (2006), pp. 569–582. ISSN: 01400118. DOI: 10.1007/s11517-006-0065-x (cit. on p. 31).

References

[54] Yue Liu et al. "A Pulse Wave Based Blood Pressure Monitoring and Analysis Algorithm BT - Artificial Intelligence." In: ed. by Zhi-Hua Zhou et al. Singapore: Springer Singapore, 2018, pp. 211–221. ISBN: 978-981-13-2122-1 (cit. on p. 31).

[55] Geoff Boeing. *Visual Analysis of Nonlinear Dynamical Systems: Chaos, Fractals, Self-Similarity and the Limits of Prediction*. 2016. DOI: `10.3390/systems4040037` (cit. on p. 31).

[56] J M Nichols and J D Nichols. "Attractor reconstruction for nonlinear systems: a methodological note." In: *Mathematical Biosciences* 171.1 (2001), pp. 21–32. ISSN: 0025-5564. DOI: `https://doi.org/10.1016/S0025-5564(01)00053-0` (cit. on p. 31).

[57] Philip J Aston et al. "Beyond HRV: Attractor reconstruction using the entire cardiovascular waveform data for novel feature extraction." In: *Physiological Measurement* 39.2 (2018). ISSN: 13616579. DOI: `10.1088/1361-6579/aaa93d` (cit. on pp. 31, 32, 34).

[58] Manasi Nandi, Jenny Venton, and Philip J Aston. "A novel method to quantify arterial pulse waveform morphology: attractor reconstruction for physiologists and clinicians." In: *Physiological Measurement* (2018). ISSN: 0967-3334. DOI: `10.1088/1361-6579/aae46a` (cit. on pp. 31, 35).

[59] Floris Takens. "Detecting strange attractors in turbulence BT - Dynamical Systems and Turbulence, Warwick 1980." In: ed. by David Rand and Lai-Sang Young. Berlin, Heidelberg: Springer Berlin Heidelberg, 1981, pp. 366–381. ISBN: 978-3-540-38945-3 (cit. on p. 31).

[60] Brook Robert D. et al. "Beyond Medications and Diet: Alternative Approaches to Lowering Blood Pressure." In: *Hypertension* 61.6 (June 2013), pp. 1360–1383. DOI: `10.1161/HYP.0b013e318293645f` (cit. on p. 36).

[61] M J Irvine et al. "Relaxation and stress management in the treatment of essential hypertension." In: *Journal of Psychosomatic Research* 30.4 (1986), pp. 437–450. ISSN: 0022-3999. DOI: `https://doi.org/10.1016/0022-3999(86)90083-8` (cit. on p. 36).

References

[62] Joseph Chacko N. et al. "Slow Breathing Improves Arterial Barore-flex Sensitivity and Decreases Blood Pressure in Essential Hypertension." In: *Hypertension* 46.4 (Oct. 2005), pp. 714–718. DOI: `10.1161/01.HYP.0000179581.68566.7d` (cit. on pp. 36, 83).

[63] Carolyn Buby, Lloyd F Elfner, and Jack G May. "Relaxation pre-training, pulse wave velocity and thermal biofeedback in the treatment of essential hypertension." In: *International Journal of Psychophysiology* 9.3 (1990), pp. 225–230. ISSN: 0167-8760. DOI: `https://doi.org/10.1016/0167-8760(90)90054-H` (cit. on p. 83).

[64] William J Elliott and Joseph L Izzo Jr. "Device-guided breathing to lower blood pressure: case report and clinical overview." In: *MedGenMed : Medscape general medicine* 8.3 (Aug. 2006), p. 23. ISSN: 1531-0132 (cit. on p. 83).

[65] Harald Rau, Michael Bührer, and Rolf Weitkunat. "Biofeedback of R-Wave-to-Pulse Interval Normalizes Blood Pressure." In: *Applied Psychophysiology and Biofeedback* 28.1 (2003), pp. 37–46. ISSN: 1573-3270. DOI: `10.1023/A:1022352631988` (cit. on p. 83).